MARKUS AICHHORN

Charge Order and Optical Conductivity of NaV_2O_5

DIPLOMARBEIT

zur Erlangung des akademischen Grades Diplomingenieur der
Studienrichtung Technische Physik

Technische Universität Graz

Betreuer:

O.Univ.-Prof. Dr. Wolfgang von der Linden
Institut für Theoretische Physik
Technische Universität Graz

Dr. Peter Horsch
Max-Planck-Institut für Festkörperforschung
D-70569 Stuttgart

Jänner 2002

Abstract

Low dimensional transition metal oxides like α'-NaV_2O_5 can adopt several types of charge order: zig-zag order, inline order or valence fluctuations. We present a mean field phase diagram which gives a simple picture of the transition between the different phases dependent on parameter ratios. Furthermore we investigate the charge order by calculating the optical conductivity in the frame of both the t-J-V and the t-U-V model, because this observable gives the main excitations of the system and one can determine the charge order by considering these excitations.

The integrated optical conductivity (IOC) and its temperature dependence reflects the changes of the kinetic energy. It provides a unique way to explore experimentally the kinetic properties of strongly correlated systems. Numerical calculations by finite temperature Lanczos method showed quite good agreement with experimental data. The strong low temperature dependence of the IOC can be explained by the destruction of short range spin correlations, which can be studied by considering a small system. Charge excitations that where attributed to the low temperature decrease of the IOC can only explain the high temperature behavior of the system.

Zusammenfassung

Niedrigdimensionale Übergangsmetalloxide, wie z.B. α'-NaV_2O_5 können prinzipiell mehrere verschiedene Typen von Ladungsordnung annehmen: zickzack Ordnung, inline Ordnung oder Valenzfluktuationen. Wir berechnen ein Mean-Field Phasendiagramm, das die einzelnen Phasen zu Parameterverhältnissen in Beziehung setzt. Darüber hinaus untersuchen wir die Ladungsordnung über die optische Leitfähigkeit im Rahmen des t-J-V und des t-U-V Modells. Die optische Leitfähigkeit enthält Informationen über die Ladungsordnung sowie über elementare Anregungen.

Die integrierte optische Leitfähigkeit (IOC) und deren Temperaturabhängigkeit zeigt Änderungen der kinetischen Energie und gibt somit die Möglichkeit, kinetische Eigneschaften von stark korrelierten Systemen experimentell zu untersuchen. Numerische Rechnungen mittels des Lanczos Algorithmus zeigen gute Übereinstimmung mit den experimentellen Daten. Die starke Abhängigkeit bei niedrigen Temperaturen kann durch die Abnahme von kurzreichweitigen antiferromagnetischen Spinkorrelationen erklärt werden, die durch Betrachtung eines kleinen Systems untersucht werden können. Ladungsanregungen, die auch als Grund für diese starke Abnahme der IOC bei niedrigen Temperaturen diskutiert wurde, können nur das Verhalten des Systems bei sehr hohen Temperaturen erklären.

Contents

1 Introduction **1**

2 Theoretical Preliminaries **3**
2.1 Current Operator 3
2.2 Linear Response Theory 5
2.3 Conductivity 7
2.4 f-sum Rule 10

3 Exact Diagonalisation **13**
3.1 Theoretical Background, Krylov-Space 13
3.2 Lanczos-Algorithm 15
3.3 Dynamical correlations at T=0 17
3.4 Lanczos Method at Finite Temperatures 19
3.4.1 Static Expectation Values 19
3.4.2 Dynamical Correlations 22

4 Charge order in NaV_2O_5 **25**
4.1 Structure of NaV_2O_5 25
4.2 Model 29
4.3 Mean-field Phase Diagram 31
4.3.1 Zig-Zag Charge Order 33
4.3.2 Inline Charge Order 34
4.3.3 Results and Phase Diagram 35
4.4 Results from Exact Diagonalisation 39
4.4.1 No Diagonal Hopping 39
4.4.2 Including Diagonal Hopping 44
4.4.3 Results for Finite Temperature 46

5 Temperature dependence of Spectra **49**
5.1 Experimental Results 49
5.2 Numerical Results for the Optical Conductivity 52

5.3 Ising Model in a Transverse Field (IMTF) 55
5.3.1 Hamiltonian of the IMTF 57
5.3.2 Jordan-Wigner Transformation 58
5.3.3 Application to the IMTF 60
5.3.4 Bogoliubov Transformation 62
5.3.5 Magnetization and Kinetic Energy 65
5.3.6 Correlation Functions 70
5.4 Influence of Spin Correlations 75
5.4.1 Two Rung Model 75
5.4.2 Optical Conductivity 81

6 Conclusion **87**

Chapter 1

Introduction

One main object of theoretical solid state physics is the description and analysis of phenomenons found in experiments. As physician one is faced by severe problems because one has to solve the Schrödinger equation, which is in fact a many body problem. An exact solution is only in few cases possible and hence one has to apply approximations, but the realistic description of electron correlations is still very difficult.

One has to distinguish between weakly and strongly correlated electronic systems. For weakly correlated systems there is a famous approximation based on the introduction of an effective potential that describes the influence of all other electrons on a single one and has to be calculated self-consistently. In other words one has a one electron Schrödinger equation where the correlations are included in the effective potential. The local density approximation (LDA) is a further development of this idea of a self consistent effective potential. This method leads to very satisfactory results for weakly correlated systems.

Starting point of the LDA is the homogeneous electron gas without correlations, which means that one can use LDA only when correlations are weak. Correlated systems for which the LDA does not work any more are called strongly correlated. In solids the coulomb repulsions can get very strong, if the distances between electrons or the electron density gets small. The Hubbard model for instance shows a splitting of the energy band into two bands, if the interaction is large enough. Application of standard methods of quantum theory like perturbation theory is not possible in this case, because the coulomb repulsion cannot be treated as small perturbation. Therefore very often numerical methods like exact diagonalisation or quantum monte carlo (QMC) methods are used.

This work deals with the charge order and the optical conductivity of the low dimensional transition metal oxide α'-NaV_2O_5. This compound attracted attention from experimental and theoretical point of view because of its very interesting properties. Starting point was the observation that α'-NaV_2O_5 can be described in a very wide temperature range by a one dimensional Heisenberg chain. Moreover there is a phase transition at 34 K, which was identified as Spin-Peierls transition but is still under discussion. If one wants to study the kinetic properties of the system one can do that by calculating the integrated optical conductivity (IOC) because it is proportional to the kinetic energy of the system.

In the following chapter we introduce some basic theoretical elements like the current operator, linear response theory and the optical conductivity, which is a special case of the electric conductivity.

The calculations of the optical conductivity is done by exact diagonalisation of finite systems for both zero and finite temperature. The algorithm that is used for this purpose is called Lanczos algorithm and is presented in chapter 3.

In chapter 4 we investigate the charge order of ladder systems. By mean field calculations we derive a phase diagram dependent on two parameter ratios. In a next step we study the influence of the parameters on the charge order of α'-NaV_2O_5 by exact diagonalisation. We calculated the optical conductivity for zero temperature and studied the shifting of the peaks in the spectrum when the parameters are varied.

Chapter 5 deals with the temperature dependence of the optical conductivity, where we first compare experimental and numerical results. Then we introduce a pseudo spin model in order to investigate the influence of the charge excitations on the temperature dependence. In the frame of this model it is possible to calculate the kinetic energy of the system, which can be compared to the IOC. In order to explain the low temperature dependence of the IOC it is necessary to include spin correlations in the model. By studying these spin correlations on a small two rung system it is possible to get an analytic expression for the IOC, that can then be fitted to the numerical results for the extended system.

In chapter 6 a conclusion is added summarizing all the results of our studies.

Some aspects of this work have already been published [1].

Chapter 2

Theoretical Preliminaries

In this chapter we first introduce the current operator in many-particle physics, which will be needed in many aspects of this work. The connection between the electrical current in the system and the outer electrical field will be defined next and is known as conductivity. The optical conductivity, of which we want to investigate the thermal behavior in this work, is then a special case of that conductivity. Furthermore we will derive the so called f-sum rule, which connects the optical conductivity with the kinetic energy of the system.

2.1 Current Operator

We want to derive the current operator for the tight binding model, that will be used throughout this work. The derivation starts from the definition of the polarization operator [2]

$$\mathbf{P} = \int d^3r \ \mathbf{r}\rho(\mathbf{r}) \tag{2.1}$$

where $\rho(\mathbf{r})$ denotes the density operator, which is the sum over the positions of all particles

$$\rho(\mathbf{r}) = \sum_i \delta(\mathbf{r} - \mathbf{r}_i) \tag{2.2}$$

The polarization operator is therefore again a sum over all particles and their positions. It is now easy to prove that the time derivative of the polarization

operator is just the particle current. First we differentiate equation (2.1) with respect to time and get

$$\frac{\partial}{\partial t}\mathbf{P} = \int d^3r \ \mathbf{r}\frac{\partial}{\partial t}\rho(\mathbf{r},t) \tag{2.3}$$

The time derivative of the density operator can be calculated using the continuity equation, which is well known from electrodynamics. It says that the divergence of the current gives the negative time derivative of the density

$$\frac{\partial}{\partial t}\rho(\mathbf{r},t) = -\nabla\cdot\mathbf{j}(\mathbf{r},t),$$

where $\mathbf{j}(\mathbf{r},t)$ denotes the current operator. Inserting this equation in equation (2.3) and integrating by parts yields

$$\begin{aligned}\frac{\partial}{\partial t}\mathbf{P} &= -\int d^3r \ \mathbf{r}(\nabla\cdot\mathbf{j}(\mathbf{r},t)) \\ &= \int d^3r \ \mathbf{j}(\mathbf{r},t)(\nabla\cdot\mathbf{r}) = \int d^3r \ \mathbf{j}(\mathbf{r},t)\end{aligned}$$

where we have used $\nabla\cdot\mathbf{r} = 1$ which is known from vector analysis.

Let us now turn to the tight binding model. In this case the polarization operator (2.1) is given by

$$\mathbf{P} = \sum_i \mathbf{R}_i n_i, \tag{2.4}$$

where $\mathbf{R}_i$ is the space coordinate of site i and $n_i = c_i^\dagger c_i$ is the density operator at site i. The current operator, i.e. the time derivative of the polarization operator, can then be written using the Heisenberg equation for time evolution of an operator

$$\mathbf{j} = \frac{\partial}{\partial t}\mathbf{P} = i[\mathcal{H},\mathbf{P}] \tag{2.5}$$

In the tight binding model the Hamiltonian has the form

$$\mathcal{H} = -\sum_{\langle ij\rangle,\sigma} t_{ij}(c_{i\sigma}^\dagger c_{j\sigma} + \text{h.c.}) + V,$$

where V denotes an operator which consist only of terms of the density operator. Therefore we have $[V,\mathbf{P}] = 0$. The commutator of the hopping term of the Hamiltonian and the polarization operator can be calculated using the commutation relations

$$\begin{aligned}[n_i, c_j^\dagger] &= \delta_{ij}c_j^\dagger \\ [n_i, c_j] &= -\delta_{ij}c_j\end{aligned}$$

The different sign of these two commutation relations gives now a different sign for hopping to the left and right in the current operator, which was expected. The current operator is therefore given by

$$j_\alpha = i \sum_{\langle ij \rangle, \sigma} t_{ij} R_\alpha^{ij} (c_{i\sigma}^\dagger c_{j\sigma} - \text{h.c.}), \tag{2.6}$$

where R_α^{ij} denotes the α-th component of the vector connecting neighboring sites i and j. One has to be careful we choosing periodic boundary conditions. In this case one has to set the correct value for the lattice vector when hopping across the boundary, in other words one must set $R_\alpha^{N1} = R_\alpha^{12} = a$ with a the lattice constant in α direction.

2.2 Linear Response Theory

The linear response theory [3] is a commonly used concept in both theoretical and experimental physics. The main idea is that the response to a weak external perturbation is proportional to the perturbation itself. The physical question is now, what is the influence of this perturbation in linear order to an observable A. In this section we will derive a general formula that gives the connection between the change of the observable A and the perturbation H'.

The Hamiltonian we have to consider is

$$\mathcal{H} = H + H'$$

where H is the Hamiltonian of the unperturbed system. Let us now assume that the perturbation H' is switched on adiabatically

$$H' = \tilde{H}' e^{\eta t},$$

which means the perturbation is switched on at $t = -\infty$, rises slowly and reaches it full strength at $t = 0$ with η a small real positive quantity. The expectation value of an observable A is given by

$$\langle A \rangle = \text{Tr}(\rho A), \tag{2.7}$$

where $\rho = \frac{1}{Z} e^{-\beta \mathcal{H}}$ is the statistical operator and $Z = \text{Tr}(e^{-\beta \mathcal{H}})$ the partition function.

We now turn to the interaction picture which is very useful when dealing with perturbation. It is similar to the Heisenberg picture with the difference

that for the transformation only the unperturbed Hamiltonian H is used. The transformation for an operator O is therefore

$$O^I = e^{iHt} O e^{-iHt}$$

The equation for the time evolution of the statistical operator in this picture reads

$$\dot{\rho}^I(t) = -i \left[H'^I, \rho^I(t) \right].$$

The initial condition for this differential equation can be readily obtained. Without perturbation we have

$$\rho(-\infty) = \rho_0 = \frac{1}{Z} e^{-\beta H}.$$

This gives in the interaction picture

$$\rho^I(-\infty) = e^{iHt} \frac{1}{Z} e^{-\beta H} e^{-iHt} = \frac{1}{Z} e^{-\beta H} = \rho_0.$$

We now define the Liouville operator for the perturbation by $\mathcal{L}'(t)O = \left[H'^I, O \right]$. With this definition we can write

$$\dot{\rho}'(t) = -i \mathcal{L}'(t) \rho^I(t).$$

This differential equation is formally solvable. We get

$$\rho^I(t) = \rho_0 \exp\left(-i \int_{-\infty}^{t} d\tau \mathcal{L}'(\tau) \right) = \rho_0 - i \int_{-\infty}^{t} d\tau \mathcal{L}'(\tau) \rho_0 + \cdots$$

Taking into account only terms up to first order and inserting the definition of the Liouville operator one can write for the expectation value (2.7)

$$\begin{aligned} \langle A \rangle_t &= \mathrm{Tr}(\rho_0 A^I) - i \int_{-\infty}^{t} d\tau \mathrm{Tr}\left(\left[H'^I(\tau), \rho_0 \right] A^I(t) \right) \\ &= \langle A \rangle_0 - i \int_{-\infty}^{t} d\tau \left\langle \left[A^I(t), H'^I(\tau) \right] \right\rangle_0 \end{aligned} \tag{2.8}$$

This is already the general formula which gives the expectation value of A when a weak perturbation H' is present. This equation is also known as Kubo formula. All expectation values in the above formula are calculated for the unperturbed Hamiltonian H, which allows us to drop the index I and to regard the above equation as formulated in the Heisenberg picture.

2.3 Conductivity

The conductivity tensor gives the response of a system to an external electric field [2, 4], i.e.

$$\langle J_\mu(\mathbf{q})\rangle(\omega) = \sum_\nu \sigma_{\mu\nu}(\mathbf{q},\omega) E_\nu(\mathbf{q},\omega),$$

where J_μ is one component of the electrical current density. When applying an electric field one has

$$\begin{aligned}\mathbf{J}(\mathbf{r},t) &= -e\sum_\alpha \mathbf{v}_\alpha = \frac{-e}{m}\sum_a \left(\mathbf{p}_\alpha + \frac{e}{\sqrt{\varepsilon_0\mu_0}}\mathbf{A}(\mathbf{r}_\alpha,t)\right)\\ &= (-e)\mathbf{j}(\mathbf{r}) - \sum_\alpha \frac{e^2}{m\sqrt{\varepsilon_0\mu_0}}\mathbf{A}(\mathbf{r}_\alpha,t)\end{aligned}$$

with the paramagnetic current density $\mathbf{j}(\mathbf{r}) = \sum_\alpha \frac{1}{m}\mathbf{p}_\alpha$. The electromagnetic field is determined by the scalar potential Φ and the vector potential $\mathbf{A}$ by

$$\mathbf{E}(\mathbf{r},t) = -\frac{1}{\sqrt{\varepsilon_0\mu_0}}\frac{\partial \mathbf{A}(\mathbf{r},t)}{\partial t} - \mathrm{grad}\Phi(\mathbf{r},t) \tag{2.9}$$

Without magnetic field it is always possible to choose a convenient gauge such that $\Phi \neq 0$ and $\mathbf{A} = 0$. Therefore we get

$$\langle -e j_\mu(\mathbf{q})\rangle(\omega) = \sum_\nu \sigma_{\mu\nu}(\mathbf{q},\omega) E_\nu(\mathbf{q},\omega) \tag{2.10}$$

With this gauge the Hamiltonian of the system is given by

$$\mathcal{H}(t) = \underbrace{\sum_\alpha \left(\frac{1}{2m}\mathbf{p}_\alpha^2 + V(\mathbf{r}_\alpha)\right)}_{H} \underbrace{-e\sum_\alpha \Phi(\mathbf{r}_\alpha,t)}_{\tilde{H}'}.$$

By applying Fourier transformation one obtains for the perturbation

$$H'(t) = -\frac{e}{\Omega}\sum_{\mathbf{q}} \Phi(\mathbf{q},t) n_{-\mathbf{q}}(t) e^{\eta t},$$

where $n_{-\mathbf{q}}(t)$ is the charge density operator. We insert the perturbation into equation (2.8) and get

$$\langle j_\mu(\mathbf{q})\rangle_t = i\frac{e}{\Omega}\sum_{\mathbf{q}'}\int_{-\infty}^{t} d\tau \Phi(\mathbf{q}',\tau)\,\langle [j_\mu(\mathbf{q},t), n_{-\mathbf{q}'}(\tau)]\rangle\, e^{\eta\tau}, \tag{2.11}$$

where we have used $\langle j_\mu(\mathbf{q})\rangle = 0$ without perturbation. Assuming translation invariance of the system we get only contributions from the sum for $\mathbf{q}' = \mathbf{q}$. In order to evaluate the expectation value of the commutator in equation (2.11) we use the Mori product [4], which is defined by

$$(A|B) = \int_0^\beta d\lambda \frac{1}{Z}\mathrm{Tr}\left(e^{-\beta H}A^\dagger e^{-\lambda H}Be^{\lambda H}\right). \tag{2.12}$$

Defining the Liouville operator for the unperturbed system by $\mathcal{L}O = [H, O]$ one gets

$$(A|\mathcal{L}B) = -\int_0^\beta d\lambda \frac{1}{Z}\mathrm{Tr}\left(e^{-\beta H}A^\dagger \frac{d}{d\lambda}\left[e^{-\lambda H}Be^{\lambda H}\right]\right).$$

The integral in the above formula can be evaluated and leads to the Kubo identity

$$(A|\mathcal{L}B) = \left\langle \left[A^\dagger, B\right]\right\rangle.$$

Using this identity equation (2.11) reads

$$\langle j_\mu(\mathbf{q})\rangle_t = i\frac{e}{\Omega}\int_{-\infty}^t d\tau \Phi(\mathbf{q},\tau)\left(j_\mu^\dagger(\mathbf{q},t)\middle|\mathcal{L}n_{-\mathbf{q}}(\tau)\right)e^{\eta t}.$$

In the Heisenberg picture one has

$$\dot{n}_\mathbf{q} = i\left[H, n_\mathbf{q}\right] = i\mathcal{L}n_\mathbf{q}.$$

In connection with the continuity equation $\nabla\mathbf{j}(\mathbf{r},t) = \dot{n}(\mathbf{r},t)$ a Fourier transformation yields

$$\mathcal{L}n_{-\mathbf{q}}(\tau) = \sum_\nu q_\nu j_\nu(-\mathbf{q},\tau).$$

Thus one has

$$\langle j_\mu(\mathbf{q})\rangle_t = i\frac{e}{\Omega}\sum_\nu \int_{-\infty}^t d\tau q_\nu \Phi(\mathbf{q},\tau)\left(j_\mu(-\mathbf{q},t)\middle|j_\nu(-\mathbf{q},\tau)\right)e^{\eta\tau},$$

where we have used $j_\mu^\dagger(\mathbf{q}) = j_\mu(-\mathbf{q})$. In order to replace the scalar potential Φ by the electric field $\mathbf{E}$ we apply a Fourier transformation to equation (2.9) and obtain

$$\mathbf{E}(\mathbf{q},t) = -i\sum_\nu q_\nu \Phi(\mathbf{q},t).$$

Therefore we can write

$$\langle -ej_\mu(\mathbf{q})\rangle_t = \frac{e^2}{\Omega}\sum_\nu \int_{-\infty}^{t} d\tau E_\nu(\mathbf{q},\tau)\left(j_\mu(-\mathbf{q},t)\middle|j_\nu(-\mathbf{q},\tau)\right)e^{\eta\tau}$$
$$= \int \frac{d\omega}{2\pi}\frac{e^2}{\Omega}\sum_\nu E_\nu(\mathbf{q},\omega)\int_{-\infty}^{t} d\tau\left(j_\mu(-\mathbf{q},t)\middle|j_\nu(-\mathbf{q},\tau)\right)e^{-i(\omega+i\eta)\tau}$$

The Mori product is only dependent on the time difference $t-\tau$. Setting $\tau = t-\tau$ we have

$$\langle -ej_\mu(\mathbf{q})\rangle_t = \int \frac{d\omega}{2\pi} e^{-i(\omega+i\eta)t}\sum_\nu E_\nu(\mathbf{q},\omega)\times$$
$$\times\frac{e^2}{\Omega}\int_0^{\infty} d\tau\left(j_\mu(-\mathbf{q},\tau)\middle|j_\nu(-\mathbf{q})\right)e^{+i(\omega+i\eta)\tau} \qquad (2.13)$$

Comparing equations (2.10) and (2.13) one can see that the conductivity is given by

$$\sigma_{\mu\nu}(\mathbf{q},\omega) = \frac{e^2}{\Omega}\int_0^{\infty} d\tau\left(j_\mu(-\mathbf{q},\tau)\middle|j_\nu(-\mathbf{q})\right)e^{+i(\omega+i\eta)\tau}.$$

Inserting the definition of the Mori product (2.12) and interchanging the order of integration one gets

$$\sigma_{\mu\nu}(\mathbf{q},\omega) = \frac{e^2}{\Omega}\int_0^{\beta} d\lambda \frac{1}{Z}\sum_n \langle n|e^{-\beta H}j_\mu(\mathbf{q})\frac{i}{w^+-(H-E_n)}e^{-\lambda H}j_\nu(-\mathbf{q})e^{\lambda H}|n\rangle$$

where $|n\rangle$ and E_n are Eigenvectors and Eigenvalues of H and $\omega^+ = \omega + i\eta$. Inserting a complete set of Eigenvectors $|m\rangle$ behind the fraction and using

$$\frac{1}{\omega+i\eta} = P\frac{1}{\omega} - i\pi\delta(\omega)$$

we finally obtain

$$\sigma_{\mu\nu}(\mathbf{q},\omega) = \pi\frac{e^2}{\Omega}\frac{1-e^{-\beta\omega}}{\omega}\frac{1}{Z}\sum_{n,m} e^{-\beta E_n}\langle n|j_\mu(\mathbf{q})|m\rangle\langle m|j_\nu(-\mathbf{q})|n\rangle\delta\left(\omega-(E_m-E_n)\right) \qquad (2.14)$$

Using the representation of the δ-function

$$\delta(\omega) = \frac{1}{\pi}\mathrm{Re}\int_0^\infty dt e^{-i(\omega+i\eta)t}$$

one gets the final result

$$\sigma_{\mu\nu}(\mathbf{q},\omega) = \frac{e^2}{\Omega}\frac{1-e^{-\beta\omega}}{\omega}\mathrm{Re}\int_0^\infty dt e^{i\omega^+ t}\langle j_\mu(\mathbf{q},t) j_\nu(-\mathbf{q})\rangle.$$

The optical conductivity is defined in the following way: One does not consider the current perpendicular to $\mathbf{q}$ and takes the limit $\mathbf{q} \to 0$. Thus it is given by

$$\sigma_\mu(\omega) = \frac{e^2}{\Omega}\frac{1-e^{-\beta\omega}}{\omega}\mathrm{Re}\int_0^\infty dt e^{i\omega^+ t}\langle j_\mu(t) j_\mu\rangle \tag{2.15}$$

For completeness we give in addition the spectral representation of the optical conductivity. Starting from equation (2.14) one can write

$$\sigma_\mu(\omega) = \pi\frac{e^2}{\Omega}\frac{1}{Z}\frac{1-e^{-\beta\omega}}{\omega}\sum_{n,m} e^{-\beta E_n}|\langle n|j_\mu|m\rangle|^2\delta\left(\omega-(E_m-E_n)\right). \tag{2.16}$$

2.4 f-sum Rule

Starting from the spectral representation we will derive the f-sum rule [5, 6] which connects the optical conductivity with the kinetic energy of the system. From equation (2.16) one gets

$$\int_0^\infty d\omega\sigma_\mu(\omega) = \pi\frac{e^2}{\Omega}\frac{1}{Z}\sum_{n,m}\frac{e^{-\beta E_n}-e^{-\beta E_m}}{E_m-E_n}|\langle n|j_\mu|m\rangle|^2.$$

Inserting the definition of the current operator (2.5) the matrix elements read as

$$\begin{aligned}\langle n|j_\mu|m\rangle\langle m|j_\mu|n\rangle &= \frac{1}{2}i\Big(\langle n|j_\mu|m\rangle\langle m|[H,P_\mu]|n\rangle + \langle n|[H,P_\mu]|m\rangle\langle m|j|n\rangle\Big)\\ &= \frac{1}{2}i(E_m-E_n)\Big(\langle n|j_\mu|m\rangle\langle m|P_\mu|n\rangle - \langle n|P_\mu|m\rangle\langle m|j_\mu|n\rangle\Big)\end{aligned}$$

Inserting these matrix elements again in the above equation we get

$$\int_0^\infty d\omega \sigma_\mu(\omega) = \frac{i}{2}\frac{\pi e^2}{\Omega}\frac{1}{Z}\sum_{n,m}\left(e^{-\beta E_n} - e^{-\beta E_m}\right)\Big(\langle n|j_\mu|m\rangle\langle m|P_\mu|n\rangle - \langle n|P_\mu|m\rangle\langle m|j_\mu|n\rangle\Big)$$

We can apply now the distributive law to the first bracket in the sum, from which we get two terms. In the second one we interchange now n and m and can therefore write

$$\begin{aligned}\int_0^\infty d\omega \sigma_\mu(\omega) &= i\frac{\pi e^2}{\Omega}\frac{1}{Z}\sum_{n,m} e^{-\beta E_n}\Big(\langle n|j_\mu|m\rangle\langle m|P_\mu|n\rangle - \langle n|P_\mu|m\rangle\langle m|j_\mu|n\rangle\Big) \\ &= i\frac{\pi e^2}{\Omega}\frac{1}{Z}\sum_n \langle n|e^{-\beta H}[j_\mu, P_\mu]|n\rangle\end{aligned}$$

Using the definitions (2.6) and (2.4) for the current operator and the polarization operator one can calculate the commutator which leads to

$$\int_0^\infty d\omega \sigma_\mu(\omega) = \frac{\pi e^2 a^2}{\Omega}\frac{1}{Z}\sum_n \langle n|e^{-\beta H}\sum_{\langle ij\rangle_\mu,\sigma}(-t_{ij})(c^\dagger_{i\sigma}c_{j\sigma} + c^\dagger_{j\sigma}c_{i\sigma})|n\rangle$$

where we introduced the lattice constant $a = R^{ij}_\mu$ and $\langle ij\rangle_\mu$ connects neighboring sites only in μ direction. In other words, we have a direct connection of the kinetic energy in a certain direction with the integral over the optical conductivity in this direction, i.e.

$$\int_0^\infty d\omega \sigma_\mu(\omega) \propto \langle H_{kin,\mu}\rangle \tag{2.17}$$

Chapter 3

Exact Diagonalisation

In the last few years many numerical methods for dealing with strongly correlated many-particle systems have been developed, for example the (quantum)-monte-carlo methods or renormalization group methods. One very powerful numerical technique is the exact diagonalisation (ED)[4, 7, 8] of finite systems. This method is based on a very simple idea: By choosing a suitable basis we can transfer the Hamiltonian of the systems into a Hamilton matrix, which has to be diagonalised.

This shows already one of the big disadvantages of the ED, because if we enlarge the system the basis and Hamilton matrix will blow up in size,[1] and therefore the ED is limited to rather small (up to 25 sites) systems. But even for dealing this small systems we need powerful numerical algorithms like the Lanczos-method, which will be presented in the sequel.

3.1 Theoretical Background, Krylov-Space

Let us assume we have chosen a basis and created the Hamilton matrix as matrix elements of the Hamiltonian within this special basis. To understand the way the Lanczos-method works we have to consider invariant subspaces of the Hamilton-matrix.

Assuming the Hamilton-matrix is a $(N \times N)$-matrix $\mathcal{H}$, then a M-dimensional subspace $\mathcal{G}$ defined as the linear span of the vectors $|\gamma_1\rangle, |\gamma_2\rangle, \ldots, |\gamma_M\rangle$ with

[1] The number of basis states is given by $\binom{N}{n_\uparrow}\binom{N}{n_\downarrow}$ which yields for example 784 basis states for 2 spin up and 2 spin down electrons on 8 sites but already 3312400 basis states for 4 spin up and 4 spin down electrons on 16 sites.

$M < N$ is called an invariant subspace, if

$$|\phi\rangle \in \mathcal{G} \Longrightarrow \mathcal{H}|\phi\rangle \in \mathcal{G} \tag{3.1}$$

for every element $|\phi\rangle$ of $\mathcal{G}$. This definition implies, that every eigenstate of $\mathcal{H}$ spans a one-dimensional invariant subspace. If we use an arbitrary basis $|\gamma_1\rangle, \ldots, |\gamma_M\rangle$ we can write $\mathcal{G}$ as a $(N \times M)$-matrix, where the columns $|\gamma_i\rangle$ of this matrix are the basis vectors of the subspace. If $\mathcal{G}$ is an invariant subspace of the Hamilton-matrix $\mathcal{H}$, then the matrix product $\mathcal{H}\mathcal{G}$ is again a $(N \times M)$-matrix, where the columns are linear combinations of the $|\gamma_i\rangle$. Now we can define a $(M \times M)$-matrix $\mathcal{H}_M$ by

$$\mathcal{H}\mathcal{G} = \mathcal{G}\mathcal{H}_M \tag{3.2}$$

Suppose we can find a solution of the eigenvalue problem

$$\mathcal{H}_M|\psi\rangle = \varepsilon|\psi\rangle \tag{3.3}$$

of $\mathcal{H}_M$, then a solution of the eigenvalue problem of $\mathcal{H}$ can be constructed. If we use (3.3) in (3.2) we get

$$\mathcal{H}[\mathcal{G}|\psi\rangle] = \varepsilon[\mathcal{G}|\psi\rangle]. \tag{3.4}$$

This means, that we can find eigenvectors and eigenvalues of the very high dimensional Hamilton matrix $\mathcal{H}$ by solving the eigenvalue problem of the smaller matrix $\mathcal{H}_M$, if $\mathcal{G}$ is an invariant subspace.

Let us now turn back to the discussion of the Lanczos-method. The idea of this algorithm is to construct iteratively an approximately invariant subspace of $\mathcal{H}$, the so called Krylov-space

$$K_M = \text{linspan}\left\{|\phi_0\rangle, \mathcal{H}|\phi_0\rangle, \mathcal{H}^2|\phi_0\rangle, \ldots, \mathcal{H}^{M-1}|\phi_0\rangle\right\}, \qquad M < N, \tag{3.5}$$

where $|\phi_0\rangle$ is a normalized random vector. It has to be verified, that the Krylov-space has the above mentioned properties, which can be seen as follows:

If we apply the Hamiltonian $\mathcal{H}$ to the basis vectors of the Krylov-space (3.5), we get the set

$$\left\{\mathcal{H}|\phi_0\rangle, \mathcal{H}^2|\phi_0\rangle, \ldots, \mathcal{H}^M|\phi_0\rangle\right\}, \tag{3.6}$$

which are elements of K_M except the last vector. If we consider now a large value for M, we find the following convergence behavior:

$$\begin{aligned}\mathcal{H}^{M-1}|\phi_0\rangle &= \mathcal{H}^{M-1}\sum_{l=0}^{N} c_l|\psi_l\rangle \\ &= \sum_{l=0}^{N} c_l\varepsilon_l^{M-1}|\psi_l\rangle \\ &= c_0\varepsilon_0^{M-1}\left(|\psi_0\rangle + \sum_{l=1}^{N}\frac{c_l}{c_0}\left(\frac{\varepsilon_l}{\varepsilon_0}\right)^{M-1}|\psi_l\rangle\right), \end{aligned} \tag{3.7}$$

where ε_l and $|\psi_l\rangle$ are eigenvalues and eigenvectors of $\mathcal{H}$. Provided

$$|\varepsilon_0| > |\varepsilon_l|, \qquad l > 0, \tag{3.8}$$

one can see that for large M the iteration $\mathcal{H}^{M-1}|\phi_0\rangle$ converges to the ground state $|\psi_0\rangle$. In other words, for large M the vector $\mathcal{H}^{M-1}|\phi_0\rangle$ is dominated by the eigenvectors of $\mathcal{H}$ with the largest eigenvalues, which implies that $\mathcal{H}^{M-1}|\phi_0\rangle$ is approximately proportional to $\mathcal{H}^{M}|\phi_0\rangle$ and consequently an approximately invariant subspace.

3.2 Lanczos-Algorithm

Starting point of the Lanczos procedure is a normalized vector $|\phi_0\rangle$, which can be chosen at random. The corresponding expectation value of the energy is

$$\varepsilon_0 = \langle\phi_0|\mathcal{H}|\phi_0\rangle. \tag{3.9}$$

We now calculate the first new vector

$$|\tilde{\phi}_1\rangle = \mathcal{H}|\phi_0\rangle - \varepsilon_0|\phi_0\rangle. \tag{3.10}$$

It is readily verified that $|\tilde{\phi}_1\rangle$ and $|\phi_0\rangle$ are orthogonal:

$$\begin{aligned}\langle\phi_0|\tilde{\phi}_1\rangle &= \langle\phi_0|\mathcal{H}|\phi_0\rangle - \varepsilon_0\langle\phi_0|\phi_0\rangle \\ &= \varepsilon_0 - \varepsilon_0 = 0 \end{aligned} \tag{3.11}$$

After having normalized the new vector, the next iteration reads

$$|\tilde{\phi}_2\rangle = \mathcal{H}|\phi_1\rangle - \varepsilon_1|\phi_1\rangle - k_1|\phi_0\rangle. \tag{3.12}$$

If we choose

$$\varepsilon_1 = \langle\phi_1|\mathcal{H}|\phi_1\rangle \tag{3.13}$$
$$k_1 = \langle\phi_0|\mathcal{H}|\phi_1\rangle \tag{3.14}$$

the new vector $|\tilde{\phi}_2\rangle$ is orthogonal to the first two vectors. Moreover k_1 is real:

$$k_1^* = \langle\phi_1|\mathcal{H}|\phi_0\rangle = \langle\phi_1|\tilde{\phi}_1\rangle + \varepsilon_0 \underbrace{\langle\phi_1|\phi_0\rangle}_{=0} = \| \phi_1 \| \in \mathbb{R}. \tag{3.15}$$

Finally, we got the iteration rule:

$$|\tilde{\phi}_{n+1}\rangle = \mathcal{H}|\phi_n\rangle - \varepsilon_n|\phi_n\rangle - k_n|\phi_{n-1}\rangle \tag{3.16}$$
$$\varepsilon_n = \langle\phi_n|\mathcal{H}|\phi_n\rangle \tag{3.17}$$
$$k_n = \langle\phi_{n-1}|\mathcal{H}|\phi_n\rangle = \| \tilde{\phi}_n \| \tag{3.18}$$
$$|\phi_{n+1}\rangle = \frac{|\tilde{\phi}_{n+1}\rangle}{\| \tilde{\phi}_{n+1} \|} \tag{3.19}$$

This set of vectors is orthogonal, which can be proved by induction:

$|\phi_0\rangle$, $|\phi_1\rangle$ and $|\phi_2\rangle$ are orthogonal, as calculated above. Let us now assume that the set of vectors up to the n-th step is orthogonal. If we take into account the iteration rules (3.16)-(3.19) we get

$$\begin{aligned}
\langle\phi_n|\tilde{\phi}_{n+1}\rangle &= \underbrace{\langle\phi_n|\mathcal{H}|\phi_n\rangle}_{=\varepsilon_n} - \varepsilon_n \underbrace{\langle\phi_n|\phi_n\rangle}_{=1} - k_n \underbrace{\langle\phi_n|\phi_{n-1}\rangle}_{=0} = 0 \\
\langle\phi_{n-1}|\tilde{\phi}_{n+1}\rangle &= \underbrace{\langle\phi_{n-1}|\mathcal{H}|\phi_n\rangle}_{=k_n} - \varepsilon_n \underbrace{\langle\phi_{n-1}|\phi_n\rangle}_{=0} - k_n \underbrace{\langle\phi_{n-1}|\phi_{n-1}\rangle}_{=1} = 0 \\
\langle\phi_i|\tilde{\phi}_{n+1}\rangle &= \langle\phi_i|\mathcal{H}|\phi_n\rangle - \varepsilon_n \underbrace{\langle\phi_i|\phi_n\rangle}_{=0} - k_n \underbrace{\langle\phi_i|\phi_{n-1}\rangle}_{=0} \\
&= \left(\langle\phi_n|\mathcal{H}|\phi_i\rangle\right)^* \\
&= \Big(\langle\phi_n|\tilde{\phi}_{i+1}\rangle + \varepsilon_i\langle\phi_n|\phi_i\rangle + k_i\langle\phi_n|\phi_{i-1}\rangle\Big)^* \\
&= 0,
\end{aligned}$$

where $i < n-1$. This completes the proof. □

Therefore the Hamilton matrix represented in the Krylov basis is tridiagonal

and has the form

$$\mathcal{H}_{ij} = \begin{pmatrix} \varepsilon_0 & k_1 & 0 & \cdot & \cdot & \cdot \\ k_1 & \varepsilon_1 & k_2 & 0 & \cdot & \cdot \\ 0 & k_2 & \varepsilon_2 & k_3 & 0 & \cdot \\ \cdot & 0 & k_3 & \varepsilon_3 & k_4 & \ddots \\ \cdot & \cdot & 0 & k_4 & \varepsilon_4 & \ddots \\ \cdot & \cdot & \cdot & \ddots & \ddots & \ddots \end{pmatrix} \tag{3.20}$$

As discussed in section 3.1 the eigenvalues of this matrix converge to the eigenvalues of the original Hamilton matrix when M becomes large, especially those at the edges of the spectrum. The ground state of the original Hamilton matrix can be calculated by

$$|\Psi\rangle = \mathcal{G}|\psi\rangle, \tag{3.21}$$

where the columns of $\mathcal{G}$ consist of the basis vectors of the Krylov space and $|\psi\rangle$ is the eigenvector with lowest energy of the matrix in Krylov-representation. With this ground state one can – at $T = 0$ – calculate the static expectation value $\langle\Psi|A|\Psi\rangle$ of an observable A.

There is one thing left to be mentioned. The above procedure is based on the fact, that the vectors in the Krylov space are exactly orthogonal. But after a few iterations due to numerical limitations the vectors are not orthogonal any more and have to be re-orthogonalized, which is numerically rather exhaustive. For a detailed analysis of the influence of the loss of orthogonality on the results see [7].

3.3 Dynamical correlations at T=0

The Lanczos algorithm allows us not only to calculate the ground state and static expectation values and correlations but also dynamic correlation. To every dynamical correlation function there exists a retarded Green´s function [2, 3], which is defined for an operator O as follows

$$\begin{aligned} \ll O(t), O^\dagger \gg &:= -i\Theta(t)\langle [O(t), O^\dagger]_\eta \rangle \\ &= -i\Theta(t)\left(\langle O(t)O^\dagger\rangle + \eta\langle O^\dagger O(t)\rangle\right), \end{aligned} \tag{3.22}$$

where $\eta = +1(-1)$ for bosons (fermions).

After inserting the Heisenberg time evolution and applying Fourier transformation the Green´s function can be written as [8]

$$\begin{aligned} \ll O, O^\dagger \gg_\omega = & -i \left\langle O \left[\int_0^\infty e^{i(\omega^+ - (\mathcal{H}-E_0))t} dt \right] O^\dagger \right\rangle \\ & - i\eta \left\langle O^\dagger \left[\int_0^\infty e^{i(\omega^+ + (\mathcal{H}-E_0))t} dt \right] O \right\rangle, \end{aligned} \tag{3.23}$$

where E_0 is the ground state energy and $\omega^+ = \omega + i\delta$ and δ a small real quantity. The integration can be done using the spectral theorem and leads to

$$\begin{aligned} \ll O, O^\dagger \gg_\omega = & \langle \psi_0 \mid O \frac{1}{\omega^+ - (\mathcal{H} - E_0)} O^\dagger \mid \psi_0 \rangle \\ & + \eta \langle \psi_0 \mid O^\dagger \frac{1}{\omega^+ + (\mathcal{H} - E_0)} O \mid \psi_0 \rangle, \end{aligned} \tag{3.24}$$

where $|\psi_0\rangle$ is the ground state. For the further calculation let us now consider the first term of the right hand side of equation (3.24). At each side of the fraction we insert a complete set of eigenvectors $|\psi_\nu\rangle$ of $\mathcal{H}$. It is now possible to replace the Hamiltonian by its eigenvalues which leads to the following formula for the first term of equation (3.24)

$$\langle \psi_0 \mid O \frac{1}{\omega^+ - (\mathcal{H} - E_0)} O^\dagger \mid \psi_0 \rangle = \sum_\nu \frac{|\langle \psi_\nu | O^\dagger | \psi_0 \rangle|^2}{\omega^+ - (E_\nu - E_0)} \tag{3.25}$$

We can now expand the eigenvectors $|\psi_\nu\rangle$ in a Lanczos basis $|\phi_i\rangle$

$$|\psi_\nu\rangle = \sum_i c_i^{(\nu)} |\phi_i\rangle, \qquad c_i^{(\nu)} = \langle \phi_i | \psi_\nu \rangle,$$

where $|\phi_o\rangle = \frac{1}{\| O^\dagger \psi_0 \|} O^\dagger |\psi_0\rangle$ is the initial vector of the procedure. Thus we get for the numerator of equation (3.25)

$$\langle \psi_\nu | O^\dagger | \psi_0 \rangle = \sum_i \left(c_i^{(\nu)} \right)^* \langle \phi_i | O^\dagger | \psi_0 \rangle = \sum_i \left(c_i^{(\nu)} \right)^* \| O^\dagger \psi_0 \| \underbrace{\langle \phi_i | \phi_0 \rangle}_{\delta_{i,0}}$$

One can see from this formula that only the first term of the sum contributes, whereas all other terms vanish. Therefore we have

$$\langle \psi_\nu | O^\dagger | \psi_0 \rangle = \left(c_0^{(\nu)} \right)^* \| O^\dagger \psi_0 \| .$$

With this result we can write for equation (3.25)

$$\langle\psi_0 \mid O\frac{1}{\omega^+ - (\mathcal{H} - E_0)}O^\dagger \mid \psi_0\rangle = \parallel O^\dagger\psi_0 \parallel \sum_\nu \frac{|c_0^{(\nu)}|^2}{\omega^+ - (E_\nu - E_0)}, \qquad (3.26)$$

using only the first components $c_0^{(\nu)}$ of the expansion of the eigenvectors $|\psi_\nu\rangle$. This method, that we presented in this section is called *spectral decoding method.*

3.4 Lanczos Method at Finite Temperatures

A major disadvantage of the method for calculating dynamical correlation functions as presented in section 3.3 is the limitation to $T = 0$. Often there is need to calculate dynamical correlations at finite temperatures, for example if one wants to investigate phase transitions. This limitation can, however, be overcome by calculating the thermodynamic trace by random sampling [9]. The matrix elements which are needed in this procedure are again calculated using the Lanczos algorithm.

3.4.1 Static Expectation Values

The thermodynamic expectation value of an observable O is given by

$$\langle O\rangle_\beta = \frac{1}{Z}\sum_{n=1}^{N}\langle n|e^{-\beta\mathcal{H}}O|n\rangle \qquad (3.27)$$

$$Z = \sum_{n=1}^{N}\langle n|e^{-\beta\mathcal{H}}|n\rangle \qquad (3.28)$$

where $\beta = 1/T$ denotes the inverse temperature and the sum runs over a complete basis set of orthonormal vectors. Because it is quite impossible to find all eigenstates and eigenvectors another approach is employed.

For calculating the matrix elements we first expand the exponential function into its power series which is equivalent to the high temperature expansion

$$\langle O\rangle_\beta = \frac{1}{Z}\sum_{n=1}^{N}\sum_{k=0}^{\infty}\frac{(-\beta)^k}{k!}\langle n|\mathcal{H}^k O|n\rangle \qquad (3.29)$$

$$Z = \sum_{n=1}^{N}\sum_{k=0}^{\infty}\frac{(-\beta)^k}{k!}\langle n|\mathcal{H}^k|n\rangle \qquad (3.30)$$

In the next step we use the Lanczos algorithm to evaluate the matrix elements. Therefore we start a Lanczos procedure with the initial vector $|\phi_0^{(n)}\rangle = |n\rangle$ up to the order M. This leads to a tridiagonal representation of $\mathcal{H}$ defined in the $(M+1)$-dimensional space spanned by the Krylov basis functions $|\phi_i^{(n)}\rangle, i = 0 \ldots M$. Let us assume this tridiagonal matrix has the eigenvectors $|\psi_j^{(n)}\rangle$ and eigenvalues $\epsilon_j^{(n)}$. Using the Krylov basis $|\phi_i^{(n)}\rangle$ we can define projection operators

$$P_m^{(n)} = \sum_{n=0}^{m} |\phi_i^{(n)}\rangle\langle\phi_i^{(n)}|, m < M \tag{3.31}$$

which project on a Krylov subspace. Let us now consider the product of such an projection operator with the Hamiltonian. We get

$$P_m^{(n)}\mathcal{H} = \sum_{i=1}^{m} |\phi_i^{(n)}\rangle\langle\phi_i^{(n)}|\mathcal{H} = \sum_{i=1}^{m} |\phi_i^{(n)}\rangle \left(k_{i+1}^{(n)}\langle\phi_{i+1}^{(n)}| + \varepsilon_i^{(n)}\langle\phi_i^{(n)}| + k_i^{(n)}\langle\phi_{i-1}^{(n)}|\right),$$

where we have used the hermitian conjugate of the Lanczos iteration formula (3.16). This formula shows, that the product $P_m^{(n)}\mathcal{H}$ consists only of Lanczos vectors up to the order $m+1$. Therefore we can write

$$P_m^{(n)}\mathcal{H} = P_m^{(n)}\mathcal{H}P_{m+1}^{(n)} = P_m^{(n)}\mathcal{H}P_M^{(n)}, \qquad m < M. \tag{3.32}$$

The last step can be done, because the operator $P_M^{(n)}$ projects onto the whole Krylov space and naturally preserves all the states up to order $m+1$.

With (3.32) and the fact that $\langle n| = \langle\phi_0^{(n)}| = \langle\phi_0^{(n)}|P_0^{(n)}$ holds we can write for the matrix element in equation (3.29) for $k < M$

$$\begin{aligned}\langle n|\mathcal{H}^k O|n\rangle &= \langle\phi_0^{(n)}|P_0^{(n)}\mathcal{H}^k O|\phi_0^{(n)}\rangle \\ &= \langle\phi_0^{(n)}|P_0^{(n)}\mathcal{H}P_1^{(n)}\mathcal{H}\cdots\mathcal{H}P_k^{(n)}O|\phi_0^{(n)}\rangle \\ &= \langle\phi_0^{(n)}|P_M^{(n)}\mathcal{H}P_M^{(n)}\mathcal{H}\cdots\mathcal{H}P_M^{(n)}O|\phi_0^{(n)}\rangle \end{aligned} \tag{3.33}$$

The only projection operator used in this formula is $P_M^{(n)}$, which can be seen as the identity operator in the Krylov space. The projection operators can therefore be constructed by the eigenvectors $|\psi_j^{(n)}\rangle$. Inserting the projection operators in equation (3.33) yields

$$\langle n|\mathcal{H}^k O|n\rangle = \sum_{i=0}^{M} \left(\epsilon_i^{(n)}\right)^k \langle n|\psi_i^{(n)}\rangle\langle\psi_i^{(n)}|O|n\rangle, \qquad k < M. \tag{3.34}$$

This shows that we can calculate the matrix elements in (3.29) exactly using the Lanczos algorithm provided $k < M$. But we want to extend the power series to infinity, i.e. $k \to \infty$. For this case we use equation (3.34) as approximation also for $k > M$ and thus we can write for the expectation value (3.29)

$$\langle O \rangle_\beta \approx \frac{1}{Z} \sum_{n=1}^{N} \sum_{i=0}^{M} e^{-\beta \epsilon_i^{(n)}} \langle n|\psi_i^{(n)}\rangle \langle \psi_i^{(n)}|O|n\rangle \tag{3.35}$$

$$Z \approx \sum_{n=1}^{N} \sum_{i=0}^{M} e^{-\beta \epsilon_i^{(n)}} \langle n|\psi_i^{(n)}\rangle \langle \psi_i^{(n)}|n\rangle \tag{3.36}$$

In equation (3.35 the trace still runs over all basis states $|n\rangle$ which is a huge number of states and it is therefore impossible to evaluate the sum in this form. In this approach [9] we evaluate the trace stochastically upon summing over suitable random vectors defined by

$$|r\rangle = \sum_{n=1}^{N} \alpha_n^{(r)} |n\rangle, \tag{3.37}$$

where the $\alpha_n^{(r)}$ are random variables with zero mean and diagonal variance

$$\overline{\alpha_{n_1}^{(r_1)} \alpha_{n_2}^{(r_2)}} = \delta_{n_1 n_2} \delta_{r_1 r_2} \tag{3.38}$$

We estimate the trace $\mathrm{Tr}(O)$ of an operator O by

$$T := \mathrm{Tr}(O) = \frac{1}{N_r} \sum_{r=1}^{N_r} \langle r|O|r\rangle, \tag{3.39}$$

where N_r is the number of random vectors. The expectation value of the random variable T reads

$$\begin{aligned} \overline{T} &= \frac{1}{N_r} \sum_{r=1}^{N_r} \sum_{n_1=1}^{N} \sum_{n_2=1}^{N} \overline{\alpha_{n_1}^{(r_1)} \alpha_{n_2}^{(r_2)}} \langle n_1|O|n_2\rangle \\ &= \frac{1}{N_r} \sum_{n_1=1}^{N} \langle n_1|O|n_1\rangle \sum_{r=1}^{N_r} 1 = \sum_{n_1=1}^{N} \langle n_1|O|n_1\rangle \end{aligned} \tag{3.40}$$

Therefore (3.39) represents an unbiased estimator. The variance of the random variable T is given by $\mathrm{var}(T) := \overline{(\Delta T)^2} = \mathrm{Tr}(O^2)/N_r$. If the operator O is represented by a sparse band like matrix the trace of this operator is of the

order of the dimension of the matrix, $\mathrm{Tr}(O) \propto O(N)$. When squaring such matrices the band like structure is conserved, i.e. $\mathrm{Tr}(O^2) \propto O(N)$. Therefore the relative error reads

$$\frac{\sqrt{\mathrm{var}(T)}}{\mathrm{Tr}(O)} \propto \frac{1}{\sqrt{NN_r}},$$

which means that for large N it suffices in general to use a quite small number N_r of random variables.

If we use equation (3.39) in equation (3.35) we get

$$\langle O \rangle_\beta \approx \frac{1}{N_r Z} \sum_{r=1}^{N_r} \sum_{i=0}^{M} e^{-\beta \epsilon_i^{(r)}} \langle r|\psi_i^{(r)}\rangle \langle \psi_i^{(r)}|O|r\rangle \tag{3.41}$$

$$Z \approx \frac{1}{N_r} \sum_{r=1}^{N_r} \sum_{i=0}^{M} e^{-\beta \epsilon_i^{(r)}} \langle r|\psi_i^{(r)}\rangle \langle \psi_i^{(r)}|r\rangle \tag{3.42}$$

In conclusion we have achieved to evaluate the expectation value (3.29) numerically, because it is no longer needed to calculate the sum over all basis states but only over a smaller number of random states.

3.4.2 Dynamical Correlations

By using the same approximations as in the previous section it is possible to calculate dynamical correlation functions. They are defined as

$$\langle A(t)B \rangle = \frac{1}{Z} \sum_{n=1}^{N} \langle n|e^{-\beta \mathcal{H}} e^{i\mathcal{H}t} A e^{-i\mathcal{H}t} B|n\rangle \tag{3.43}$$

with Z from equation (3.28). Similar to the procedure for evaluating the matrix elements for the static expectation values we insert again projection operators which are built by eigenvectors of $\mathcal{H}$ calculated by the Lanczos algorithm. One difference is that in this case we need a double sum over these eigenstates, since we expand the exponentials $e^{-(\beta - it)\mathcal{H}}$ and $e^{-i\mathcal{H}t}$. Thus we get

$$\langle A(t)B \rangle = \frac{1}{Z} \sum_{n=1}^{N} \sum_{k=0}^{M} \sum_{l=0}^{M} e^{(-\beta \epsilon_k^{(n)})} e^{i(\epsilon_k^{(n)} - \epsilon_l^{(\tilde{n})})t} \langle n|\psi_k^{(n)}\rangle \langle \psi_k^{(n)}|A|\psi_l^{(\tilde{n})}\rangle \langle \psi_l^{(\tilde{n})}|B|n\rangle, \tag{3.44}$$

where $\epsilon_l^{(\tilde{n})}$ and $|\psi_l^{(\tilde{n})}\rangle$ are eigenvalues and eigenvectors from a Lanczos run starting with the initial vector $|\tilde{n}\rangle = B|n\rangle$. Now we again replace the sum

over all basis vectors by a sum over random vectors which leads to the final formula

$$\langle A(t)B\rangle \approx \frac{1}{N_r Z}\sum_{r=1}^{N_r}\sum_{k=0}^{M}\sum_{l=0}^{M} e^{(-\beta\epsilon_k^{(r)})} e^{i(\epsilon_k^{(r)}-\epsilon_l^{(\tilde{r})})t}\langle r|\psi_k^{(r)}\rangle\langle\psi_k^{(r)}|A|\psi_l^{(\tilde{r})}\rangle\langle\psi_l^{(\tilde{r})}|B|r\rangle \tag{3.45}$$

with Z from equation (3.42).

Chapter 4

Charge order in NaV_2O_5 and Ladder Systems in general

In this chapter we introduce the compound α'-NaV_2O_5. It is part of the very interesting family AV_2O_5 with A = Na, Li, Ca, Mg, ... of low-dimensional strongly correlated electron systems. In the last few years there were many experimental and theoretical studies in order to investigate and understand the fascinating properties of this class of compounds, especially the unconventional spin and charge excitation spectra. We studied the features of NaV_2O_5 using numerical techniques. The experimental results are very important for the correct understanding of this material.

In particular we investigate the charge order in ladder systems as NaV_2O_5 depending on the different values for the hopping parameter and the coulomb interaction. Mean field calculations were done and lead to a very simple phase diagram, that shows the change form charge order to valence fluctuation.

4.1 Structure of NaV_2O_5

The first crystallographic structure analysis were done in the sixties and seventies of the last century by means of x-ray scattering [10]. Several different phases could be identified, which have in common the $V^{4+}O_5$ pyramids as basic element of the structure and only differ on the amount of rare earth atoms inserted in the compound.

Depending upon doping of the system $Na_xV_2O_5$ one has the following phases:

- α-phase: $0 < x \leq 0.02$
- β-phase: $0.22 \leq x \leq 0.4$
- α'-phase: $0.70 \leq x \leq 1.00$
- η-phase: $1.28 \leq x \leq 1.45$
- λ-phase: $1.68 \leq x \leq 1.82$

In our studies we investigated the properties of the α'-phase, in other words at doping $x = 1$. Besides studies were done on the β-phase, showing quasi one-dimensional electronic properties. Throughout this work we concentrate on the α' phase and therefore we drop the identification of the phase.

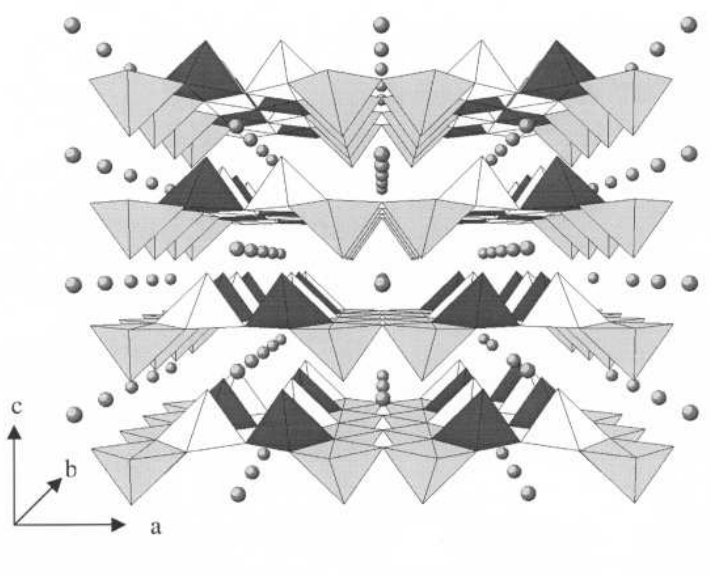

Figure 4.1: Crystallographic structure of NaV_2O_5. The pyramids are built by oxygen atoms around a central vanadium site. The sodium atoms are lying between the V_20_5 layers.

The crystallographic structure of NaV_2O_5 is schematically depicted in figure 4.1. It is mainly determined by the layers formed by the V_2O_5 pyramids. The sodium atoms, which are mainly acting as charge reservoir, form chains that are lying between the layers. The coupling c direction, i.e. between the single layers, is very weak, and the properties of this compound are therefore mainly determined by the quasi two-dimensional V_2O_5 layers, shown in figure 4.2. The black circles indicate the vanadium atoms and the yellow ones the

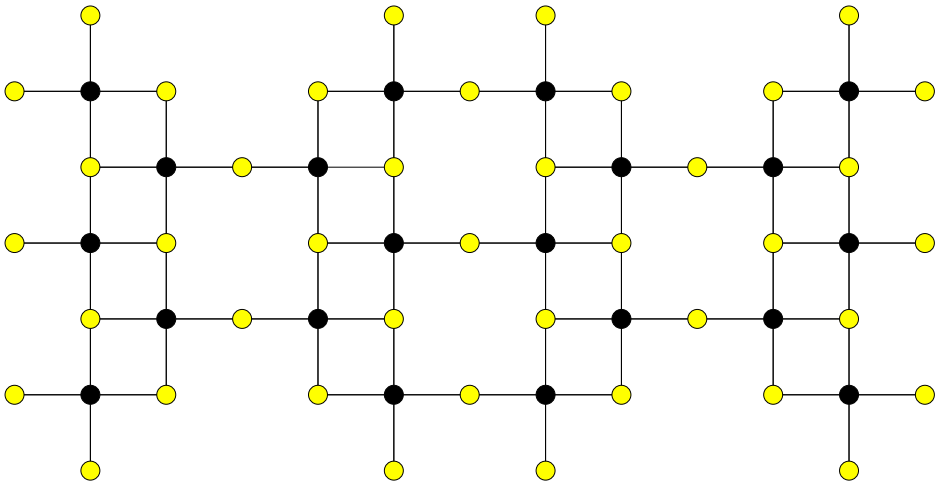

Figure 4.2: One V_2O_5 layer, where only the oxygen atoms of the ground plane of the pyramids are displayed. Yellow circles indicate oxygen atoms and black circles vanadium atoms.

oxygen atoms of the ground plane of the pyramids. The oxygen on top of the pyramids is not important, because it does not couple two vanadium atoms.

The first x-ray studies indicated a non-centrosymmetric structure $P2_1mn$ [10] with two different vanadium atoms in the unit cell, forming chains of two kinds of VO_5 pyramids. Analysis of the V-O bond length and of the Na-V distance showed that these chains are possibly $V^{4+}O_5$ and $V^{5+}O_5$ chains, resp. Therefore this compound should behave like a quasi one-dimensional spin system, because the magnetic V^{4+} ions are well separated by the non-magnetic V^{5+} ions.

Measurements of the magnetic susceptibility by Isobe and Ueda (figure 4.3) [11] brought a first insight in this system. They found that NaV_2O_5 behaves like a $S = \frac{1}{2}$ 1-D antiferromagnetic Heisenberg linear chain. The coupling constant was determined to $J = 560K$ by fitting the experimental results to the theoretical formula. In addition they found a phase transition at $T_c = 34K$ with a rapid decrease of the magnetic susceptibility, a spin gap with $\Delta \approx 10$ meV opens and the unit cell is doubled in a- and b-direction and quadrupled in c-direction. They supposed that this could take place due to a Spin-Peierls transition, where the linear chain dimerises below a critical temperature. This dimerisation produces two different coupling constants and the ground state energy can therefore be lowered by establishing coupled spin-singlets. Hence NaV_2O_5 would be the second inorganic compound beside

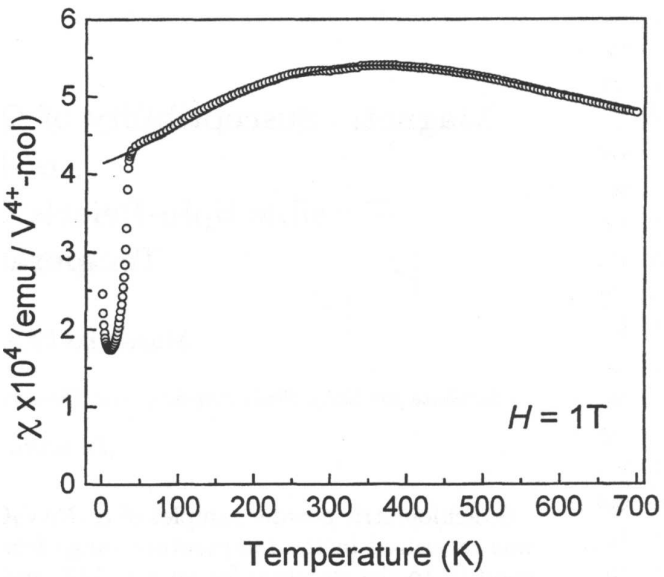

Figure 4.3: Magnetic susceptibility of NaV_2O_5 measured in a field of $H = 1T$. Solid line is the fit to the formula for the $S = \frac{1}{2}$ 1-D Heisenberg model. Figure taken from reference [11].

$CuGeO_3$, where this phase transition occurs.

But there were few hints, that this phase transition is no real Spin-Peierls transition: The ratio between spin gap and critical temperature $\frac{2\Delta}{k_b T} \approx 6.5$ is approximately twice as large as the BCS mean-field value of 3.52 for a Spin-Peierls transition. Furthermore the changes at T_c of the dielectric constant and the thermal conductivity differ significantly from the case of $CuGeO_3$, and the magnetic field dependence $\Delta T_c \propto H^2$ is only one fifth of what could be expected for a Spin Peierls transition.

Recent x-ray studies [12, 13, 14] showed, that the crystallographic structure of NaV_2O_5 at room temperature is the centrosymmetric structure $Pmmn$, indicating that all vanadium sites are equivalent with valence 4.5. The insulating properties where therefore rather astonishing, but Horsch and Mack could explain this behavior by taking the molecular orbital state of one electron on a rung as key element of the electronic structure [15]. NMR studies [16] revealed that below the phase transition temperature $T_c = 34K$ again two different vanadium sites show up, which indicates that this phase transition is not of Spin-Peierls type but rather driven by charge ordering.

The low temperature phase is still under discussion. It is not yet justified whether there is an inline charge order, i.e. V^{4+} ions forming chains, or

zig-zag charge order. A new crystallographic measurement even found three different vanadium sites identified as space group $Fmm2$ [17]. It was assumed that this could occur due to three different valence states V^{4+}, $V^{4.5+}$ and V^{5+}, resp. But this assumption is not compatible with the NMR measurements and therefore the discussion about the charge order in the low temperature phase and the driving mechanism for the phase transition is still going on [18, 19, 20].

4.2 Model

The question is now, how to describe all these features found in experimental studies by a theoretical model. Band structure calculations showed that the density of states at the Fermi edge is mainly determined by the $3d_{xy}$ orbitals of the vanadium atoms. Therefore it is obvious to choose a one orbital model on the vanadium lattice. As mentioned before the single V_2O_5 layers are only weakly coupled and the model is therefore chosen to be two dimensional.

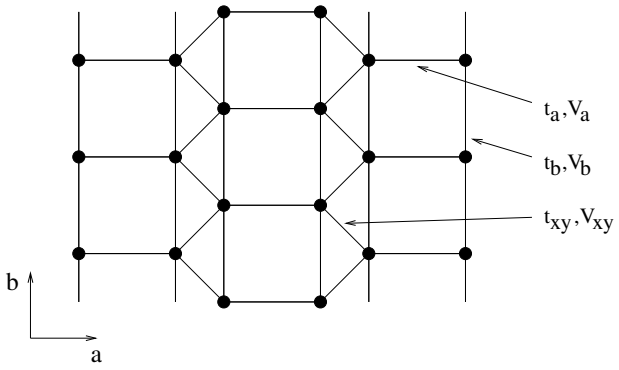

Figure 4.4: Lattice of the vanadium atoms in NaV_2O_5.

The lattice is shown in figure 4.4. It consists of ladders that are shifted in b-direction with respect to the neighboring ladders. Many studies focus on a quarter filled Hubbard-like model, specifically the t-U-V model

$$\mathcal{H} = -\sum_{\langle ij\rangle,\sigma} t_{ij}\left(c^{\dagger}_{i\sigma}c_{j\sigma} + \text{h.c.}\right) + \sum_{\langle ij\rangle} V_{ij}n_i n_j + U\sum_i n_{i\uparrow}n_{i\downarrow} \qquad (4.1)$$

where U is the intrasite Hubbard repulsion and V_{ij} is the intersite Coulomb interaction. The density operators are given by $n_{i\sigma} = c^{\dagger}_{i\sigma}c_{i\sigma}$ and $n_i = n_{i\uparrow}+n_{i\downarrow}$. The sum over all next neighbor pairs is indicated by $\langle ij\rangle$.

In our model several different parameters are used. As one can see from figure 4.4 three different hopping matrix elements t_a, t_b, t_{xy}, three coulomb interactions V_a, V_b, V_{xy} and the Hubbard intrasite repulsion U occur. The values for these parameters are still controversially discussed in the literature.

The estimated values for the hopping matrix elements within one single ladder, i.e. t_a and t_b, agree in the different studies. Density functional theory calculations (DFT) lead to a value of $t_a = 0.38$[1] and $t_b = 0.17$ [13], which is similar to the value estimated by empirical rules of $t_a = 0.35$ and $t_b = 0.15$ [15]. The values for the hopping between the ladders differ. The DFT calculations found a relatively small value of $t_{xy} = 0.012$, whereas from empirical rules the value $t_{xy} = 0.3$ was estimated. We will take a closer look on this interladder hopping later on.

The values for the Coulomb interactions are quite unsure and differ in the different studies. If one takes as starting point the bare coulomb interaction

$$V_{ij} = \frac{1}{4\pi\varepsilon_0\varepsilon_r}\frac{e^2}{d_{ij}},$$

where d_{ij} denotes the distance between two sites, the Coulomb interaction depends on the choice of the anisotropic dielectric constant ε_r. If one takes the isotropic value of $\varepsilon_r \approx 11$ from susceptibility measurements one gets $V_a = 0.37$, $V_b = 0.10$ and $V_{xy} = 0.43$, which is quite small. By comparing EELS-experiments and optical conductivity one can find $\varepsilon_r = 7$ for a-direction and $\varepsilon_r = 5$ for b-direction [21], which leads to $V_a = 0.8$, $V_b = 0.6$ and $V_{xy} = 0.9$. In this work we chose the values $V_a = V_b = 0.8$ and $V_{xy} = 0.9$. The value for the intrasite Hubbard repulsion was chosen as $U = 4.0$.

Due to the rather large ratio $\frac{U}{|t_{ij}|}$ double occupancies are strongly suppressed and we use a different representation of Hamiltonian (4.1), which is defined in the subspace of the Hilbert space with no double occupancies. This leads to the t-J-V model

$$\mathcal{H} = -\sum_{\langle ij\rangle,\sigma} t_{ij}\left(\tilde{c}^\dagger_{i\sigma}\tilde{c}_{j\sigma} + \text{h.c.}\right) + \sum_{\langle ij\rangle} J_{ij}\left(\mathbf{S}_i\cdot\mathbf{S}_j - \frac{1}{4}n_i n_j\right) + \sum_{\langle ij\rangle} V_{ij} n_i n_j, \tag{4.2}$$

where $\tilde{c}^\dagger_{i\sigma} = c^\dagger_{i\sigma}(1 - n_{i,-\sigma})$ are constrained electron creation operators, that forbid double occupancy of a site. The density operator $n_{i\sigma}$ is defined equivalently as for the Hubbard Hamiltonian (4.1). The exchange term in the t-J-V model is given by

$$J_{ij} = \frac{4t_{ij}^2}{U}.$$

[1] From now on all energies are given in eV

The advantage of the t-J-V model is that the Hilbert space is smaller than it is for the full t-U-V model and therefore exact diagonalisation is a bit easier to implement. The main disadvantage is that one cannot study any weight transfer to high energy, because all these high energy states are projected out.

4.3 Mean-field Phase Diagram

To get a first insight in the behavior and the nature of charge ordering in ladder systems we study the simplified problem of one electron per rung. This means that any interladder and interrung hopping in equation (4.1) is set to zero, i.e. $t_b = t_{xy} = 0$. In addition no double occupancy of a site or a rung can occur, therefore the Hubbard interaction term proportional to U and the coulomb interaction term proportional to V_a can be omitted. Furthermore we can drop the spin index because we deal with one electron per rung. The Hamiltonian for our simplified problem reads therefore

$$\mathcal{H} = -t_a \left(c_l^\dagger c_r + c_r^\dagger c_l \right) + \sum_{\langle ij \rangle} V_{ij} n_i n_j \tag{4.3}$$

where l and r denote the left and right position within a rung. We apply now the Hartree-Fock(HF)-approximation to the interaction term in order to decouple the density operators:

$$(A - \langle A \rangle)(B - \langle B \rangle) = AB - \langle A \rangle B - A\langle B \rangle + \langle A \rangle \langle B \rangle.$$

The HF-approximation consists of approximating the left hand side by zero, in other words correlated fluctuations are neglected. This leads to

$$AB = \langle A \rangle B + A\langle B \rangle - \langle A \rangle \langle B \rangle \tag{4.4}$$

Applied to the interaction term of our Hamiltonian (4.3) we get

$$\mathcal{H} = -t_a \left(c_l^\dagger c_r + c_r^\dagger c_l \right) + \sum_{\langle ij \rangle} V_{ij} \left(\langle n_i \rangle n_j + n_i \langle n_j \rangle - \langle n_i \rangle \langle n_j \rangle \right) \tag{4.5}$$

The last term in the brackets of equation (4.5) presents only an energy shift and can be neglected during the calculation. For calculating the ground state energy it has to be included again afterwards. We now turn to the notation

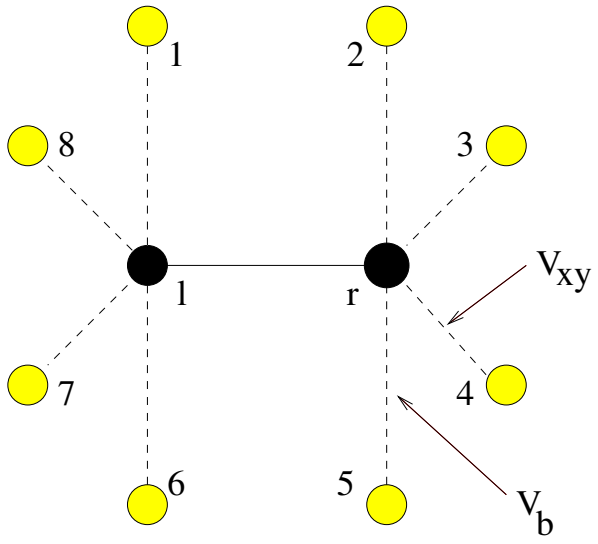

Figure 4.5: Structure of the single rung problem. The yellow circles indicate the mean field - see equation (4.6).

shown in figure 4.5. The Hamiltonian (4.5) reads

$$\begin{aligned}\mathcal{H} = &- t_a \left(c_l^\dagger c_r + c_r^\dagger c_l \right) \\ &+ V_b \left[n_l (\langle n_1 \rangle + \langle n_6 \rangle) + n_r (\langle n_2 \rangle + \langle n_5 \rangle) \right] \\ &+ V_{xy} \left[n_l (\langle n_7 \rangle + \langle n_8 \rangle) + n_r (\langle n_3 \rangle + \langle n_4 \rangle) \right] \end{aligned} \tag{4.6}$$

At this point one can see why the HF-approximation is also called mean-field approximation. One solves the eigenvalue problem of the Hamiltonian for a very small system, which is connected by the interactions to a mean field. After solving the eigenvalue problem one inserts the solutions as new mean-field values in equation (4.5) and solves the eigenvalue problem again. This procedure has to be iterated until the calculated solutions are in agreement with the given mean-field values. One can now determine the charge order of the system by choosing the proper mean-field starting values and by setting the right iteration rules from one step to the next. After simulating different charge order patterns, in our case zig-zag and inline order, one can identify the true ground state by comparing the different ground state energies.

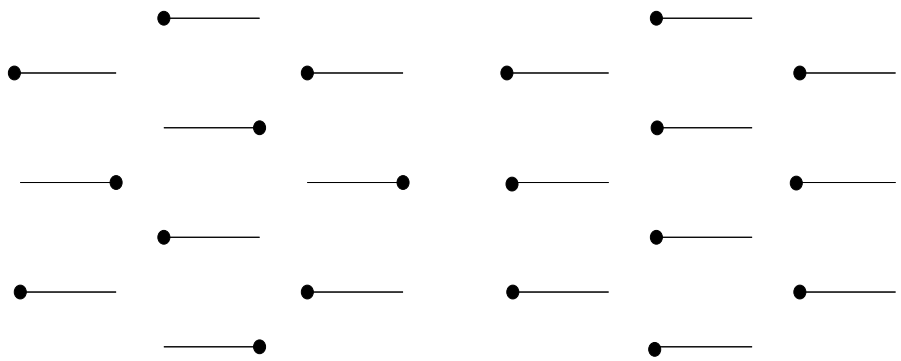

Figure 4.6: Zig-zag (left) and inline (right) charge order pattern simulated in mean field.

4.3.1 Zig-Zag Charge Order

In order to get a zig-zag charge order (see figure 4.6 on the left) we choose the following starting values for our HF-iteration:

$$\langle n_1 \rangle = \langle n_3 \rangle = \langle n_6 \rangle = \langle n_7 \rangle = 1$$
$$\langle n_2 \rangle = \langle n_4 \rangle = \langle n_5 \rangle = \langle n_8 \rangle = 0$$

One has to be careful to put the right number of electrons into the system, that means in our case

$$\sum_{i=1}^{8} n_i = 4$$

Let us now assume we have solved the eigenvalue problem for (4.6). From the ground state one can now calculate the densities $\langle n_l \rangle$ and $\langle n_r \rangle$ on the left and right position of the rung. We define now

$$n_{max} = \mathrm{Max}(\langle n_l \rangle, \langle n_r \rangle) \tag{4.7a}$$
$$n_{min} = \mathrm{Min}(\langle n_l \rangle, \langle n_r \rangle) \tag{4.7b}$$

It is obvious that $n_{max} + n_{min} = 1$ holds, because we have one electron on the rung. The iteration rules for zig-zag charge order are now

$$\langle n_1 \rangle = \langle n_3 \rangle = \langle n_6 \rangle = \langle n_7 \rangle = n_{max} \tag{4.8a}$$
$$\langle n_2 \rangle = \langle n_4 \rangle = \langle n_5 \rangle = \langle n_8 \rangle = n_{min} \tag{4.8b}$$

With this definitions one can rewrite the Hamiltonian (4.6) as matrix for this small system with only two states according to the left and right position of

the electron on the rung

$$H = \begin{pmatrix} 2V_b n_{max} + V_{xy}(n_{max} + n_{min}) & -t_a \\ -t_a & 2V_b n_{min} + V_{xy}(n_{max} + n_{min} \end{pmatrix}$$
$$= \begin{pmatrix} 2V_b n_{max} + V_{xy} & -t_a \\ -t_a & 2V_b n_{min} + V_{xy} \end{pmatrix} \tag{4.9}$$

The eigenvalue equation which has to be solved is

$$H\mathbf{x} = \varepsilon\mathbf{x}, \tag{4.10}$$

with $\mathbf{x} = (x_l, x_r)$. The densities for the left and right position on the rung can then be calculated using the ground state vector by $n_l = x_l^2$ and $n_r = x_r^2$. After choosing the right n_{max} and n_{min} one inserts them again in equation (4.9) and starts the procedure again. We observe that V_{xy} is irrelevant in zig-zag charge order. As one can see from equation (4.9) it causes merely a constant shift in energy. The physical reason for that is frustration (see figure 4.6).

4.3.2 Inline Charge Order

The same procedure can be performed for inline charge order (see figure 4.6 on the right). The initial values for this iteration are

$$\langle n_1\rangle = \langle n_3\rangle = \langle n_4\rangle = \langle n_6\rangle = 1$$
$$\langle n_2\rangle = \langle n_5\rangle = \langle n_7\rangle = \langle n_8\rangle = 0$$

Again we solve the eigenvalue problem for (4.6) and calculate the densities $\langle n_l\rangle$ and $\langle n_r\rangle$. The iteration rules for inline charge order read

$$\langle n_1\rangle = \langle n_3\rangle = \langle n_4\rangle = \langle n_6\rangle = n_{max} \tag{4.11a}$$
$$\langle n_2\rangle = \langle n_5\rangle = \langle n_7\rangle = \langle n_8\rangle = n_{min} \tag{4.11b}$$

The matrix for the Hamiltonian (4.6) reads therefore

$$H = \begin{pmatrix} 2V_b n_{max} + 2V_{xy} n_{min} & -t_a \\ -t_a & 2V_b n_{min} + 2V_{xy} n_{max} \end{pmatrix} \tag{4.12}$$

The eigenvalue problem for this Hamiltonian is again solved iteratively.

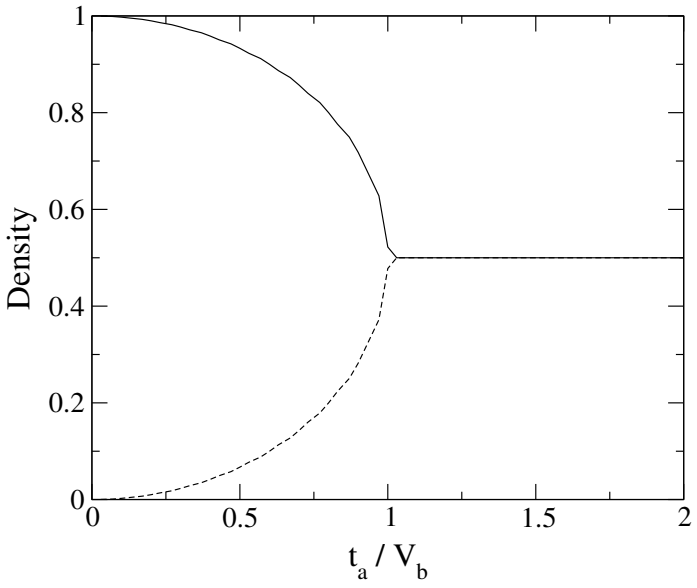

Figure 4.7: Charge density n_r (solid line) and n_l (dashed line) on the left and right position on the rung (see figure 4.5) calculated by HF-approximation in zig-zag order.

4.3.3 Results and Phase Diagram

In a first step we want to find out for which values of $\frac{t_a}{V_b}$ the zig-zag charge order is stable. For this purpose we set $V_b = 1$ and vary the parameter t_a. The ratio $\frac{V_{xy}}{V_b}$ is not important, because the coulomb interaction V_{xy} is frustrated in zig-zag order, that means that V_{xy} only contributes to the ground state energy but does not produce any preference of the left or right position.

The results of this calculation are shown in figure 4.7. One can see, that the zig-zag charge order is stable up to a value of $\frac{t_a}{V_b} = 1$, whereas for larger values no charge order occurs. In this region the ground state is determined by charge fluctuations where the valence of the left and right position on the rung is equal to 0.5.

Whether zig-zag or inline charge order appears depends on the ratio of $\frac{V_{xy}}{V_b}$. As one can see from figure 4.6 for large values of $\frac{V_{xy}}{V_b}$ inline order should occur, because in this case the large interladder coulomb interaction V_{xy} does not give any contribution to the energy, whereas in zig-zag order it does. In order to determine the critical value for $\frac{V_{xy}}{V_b}$ we perform the HF-iteration for fixed $V_b = 1$ and several but fixed t_a and vary the parameter V_{xy}. By comparing the ground state energy, where the constant term in equation (4.5) is included,

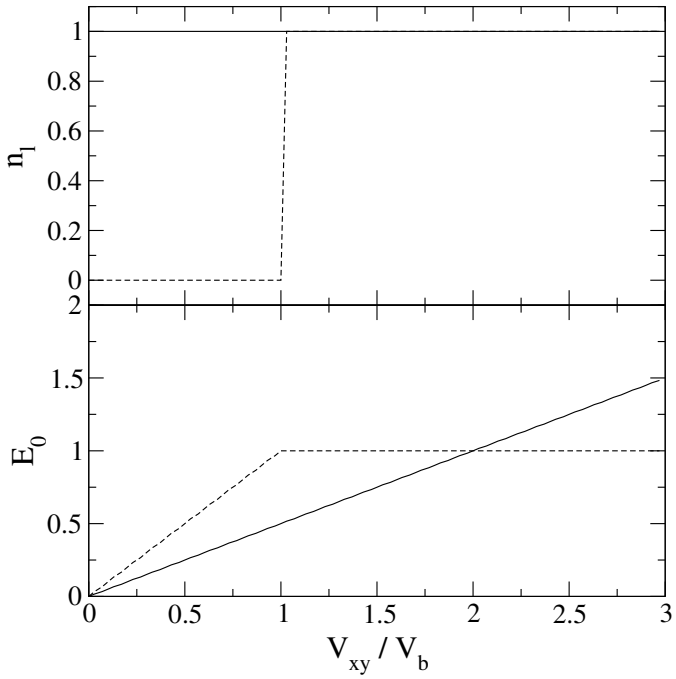

Figure 4.8: Comparison of the ground state energy E_0 of zig-zag (solid line) and inline charge order (dashed line) in the atomic limit, i.e. $\frac{t_a}{V_b} = 0$. Charge density of the left position on the rung is shown in the upper panel for zig-zag and inline order, resp.

one can find the ground state, i.e. zig-zag or inline charge order.

Let us first consider the atomic limit, i.e. $\frac{t_a}{V_b} = 0$. As we have mentioned above zig-zag order is not influenced by the ratio of $\frac{V_{xy}}{V_b}$ as one can see in figure 4.8. When simulating inline order the situation is different. Up to value of $\frac{V_{xy}}{V_b} = 1$ there exists no perfect inline order. The charge densities in the upper panel in figure 4.8 show, that below that value the electron on the central rung wants to avoid the inline order and sits on the wrong position in the rung, in other words if we have started with charge density $n_l = 1$ on the left position of the rungs in the mean field, the electrons on the central rung is on the right position and vice versa. If the ratio $\frac{V_{xy}}{V_b}$ is larger then one perfect inline order is stable but lies energetically above the zig-zag order (see figure 4.8). Only when $\frac{V_{xy}}{V_b}$ gets larger than two zig-zag order breaks down and inline order is established.

For $0 < \frac{t_a}{V_b} < 1$ the situation is similar (see figure 4.9), but with the difference that due to the finite t_a valence fluctuations are possible. One can see this in the charge density of the inline charge order. At small values of $\frac{V_{xy}}{V_b}$ the

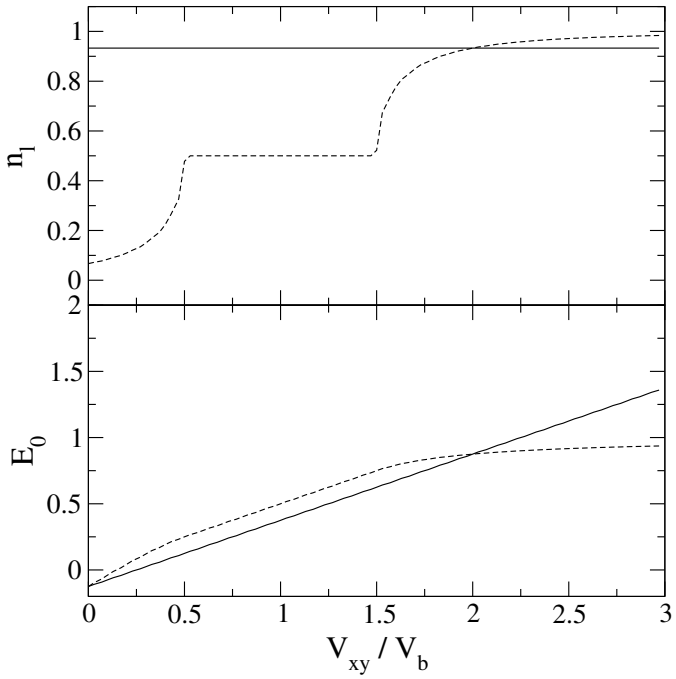

Figure 4.9: Ground state energy and charge densities on the left position on the rung for $\frac{t_a}{V_b} = 0.5$ for zig-zag (solid line) and inline charge order (dashed line).

electron is at the wrong position on the rung, similar to the atomic limit. But here we have no jump of the electron from one position to the other at $\frac{V_{xy}}{V_b} = 1$ but this transition into the perfect inline order is rather smooth. In the region $\left|\frac{V_{xy}}{V_b} - 1\right| < \frac{t_a}{V_b}$ we have valence fluctuations, because the energy difference between the left and right position on the rung due to the coulomb interaction is too small to induce charge order and the electron fluctuates. Physically this is not really important, because for $\frac{V_{xy}}{V_b} < 2$ zig-zag order is lower in energy and therefore the ground state, and in zig-zag order these features do not occur.

The case $\frac{t_a}{V_b} > 1$ is different. One can see from figure 4.10 that for low values of $\frac{V_{xy}}{V_b}$ no charge order can be found and the ground state is determined by valence fluctuations. But for large values of $\frac{V_{xy}}{V_b}$ inline order again occurs, more precisely in the region $\frac{V_{xy}}{V_b} - 1 > \frac{t_a}{V_b}$. In this region the energy difference between the left and the right position on the rung is again large enough to induce charge order, namely inline order. In contrast to the case of $0 < \frac{t_a}{V_b} < 1$ this is now relevant, because in this region inline order is the ground state.

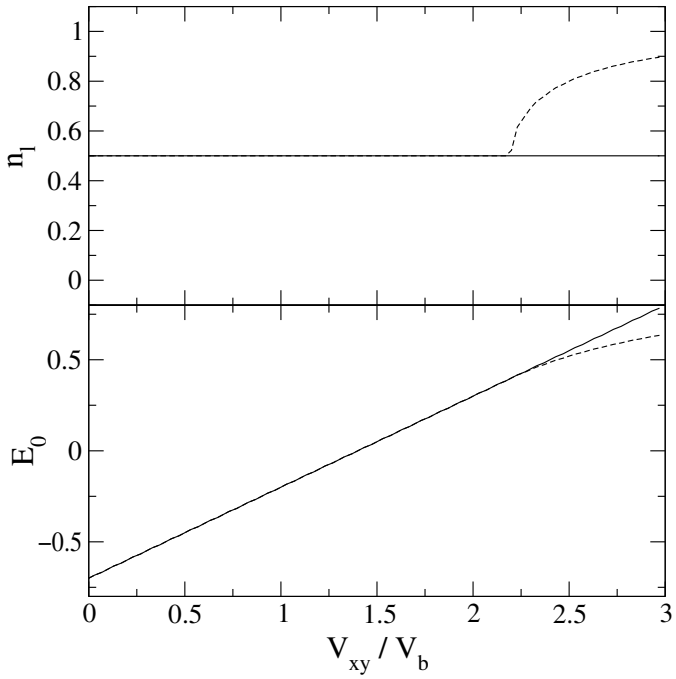

Figure 4.10: Ground state energy and charge densities on the left position on the rung for $\frac{t_a}{V_b} = 1.2$ for zig-zag (solid line) and inline charge order (dashed line).

Summarizing all our results one can obtain the mean-field phase diagram for the single rung problem shown in figure 4.11. The parameter on the x-axis is denoted as $\frac{2t_a}{V_b}$ and not as $\frac{t_a}{V_b}$ as before, because later on when studying the Ising model in a transverse field we will see, that this is the relevant parameter for the system. One point should be mentioned. By transforming the Hubbard-like Hamiltonian to a pseudo-spin Hamiltonian, which will be done in a later section, one can obtain the exact solution of the problem of one electron per rung, which is solved here in mean field approximation only. In this solution one finds the value of $\frac{t_a}{V_b} = 0.5$ as critical point for the phase transition from the ordered state to the disordered state.

In recent studies an onsite energy has been added, which differentiates between the two positions on the rung. This onsite energy is not independent of the interladder coulomb interaction V_{xy}. One can therefore set $V_{xy} = 0$ and control the charge order by varying the onsite energy.

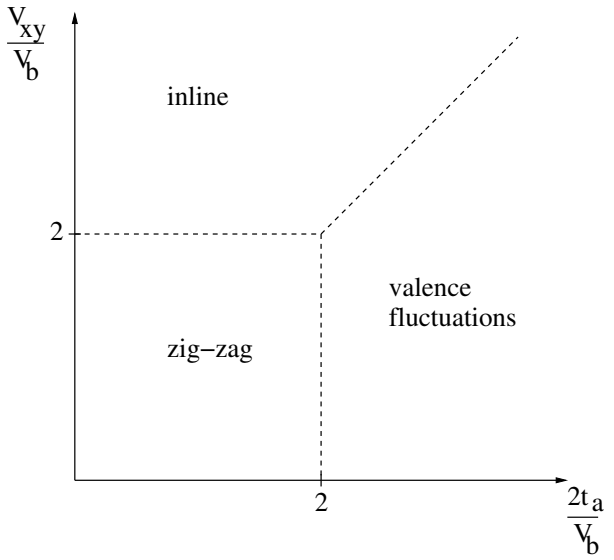

Figure 4.11: Mean-field phase diagram for the single rung problem.

4.4 Results from Exact Diagonalisation

In the previous section we investigated the charge order of ladder systems by means of the Hartree-Fock approximation in the simplified model of one electron per rung. Here we want to determine the charge order of the special ladder system NaV_2O_5 by exact diagonalisation presented in section 3. Even without calculating the charge correlation function of the system one can get information about the charge order by studying the optical conductivity, because this quantity shows the elementary excitations of the system. The calculations in this sections were mainly done by means of the Lanczos method for zero temperature, because the calculation for finite temperature need much more computer power. It is therefore not very practicable to do parameter studies with the finite temperature method.

4.4.1 No Diagonal Hopping

Starting point of our calculations for zero temperature is the full t-U-V Hamiltonian (4.1) introduced in section 4.2. At this point we exclude diagonal hopping within the ladders, in other words we have only three hopping matrix elements t_a, t_b and t_{xy}. We use the following parameter set:

- hopping matrix elements: $t_a = 0.4$, $t_b = 0.2$

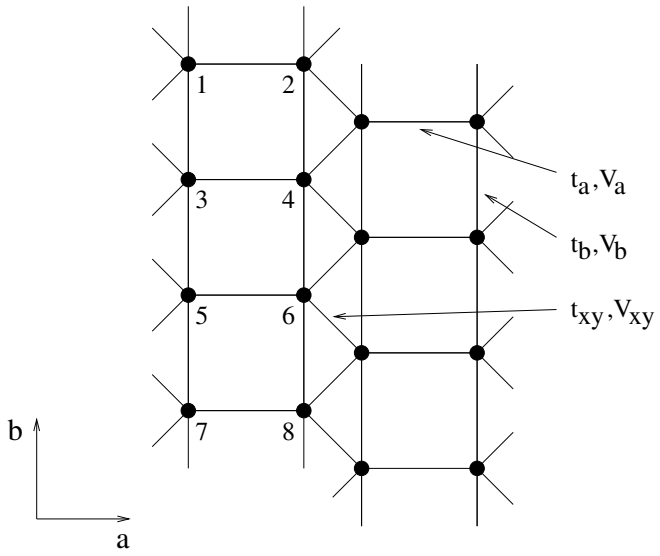

Figure 4.12: Shape of cluster simulated in exact diagonalisation.

- coulomb interactions: $V_a = 0.8$, $V_b = 0.8$
- intrasite Hubbard repulsion: $U = 4.0$

whereas the other parameters t_{xy} and V_{xy} are varied to study their influence on the optical conductivity and the charge order. The simulations were done on a 16-site cluster consisting of two ladders with four rungs each, and periodic boundary conditions were chosen. This cluster is shown in figure 4.12.

To begin with we investigate the influence of the interladder coulomb interaction V_{xy} on the optical conductivity. For this purpose t_{xy} is set equal to zero and V_{xy} is varied. The results are shown in figure 4.13. One can see, that the peak in the spectrum for b direction is almost independent of V_{xy}, whereas the peak in the spectrum for a direction shows a dramatic downward shift. If the system was in a simple zig-zag charge order without valence fluctuations, which should occur regarding our mean field phase diagram 4.11, this behavior cannot be understood. In this case the interaction V_{xy} was frustrated (see figure 4.6) and there should be no energy shift at all, because flipping one electron from the left to the right does not change the number of frustrated bonds with energy $\sim V_{xy}$ and the excitation energy is $2V_b$. Let us now assume we have valence fluctuations in the system. This means that there are many defects of the perfect zig-zag charge order, i.e. the electron

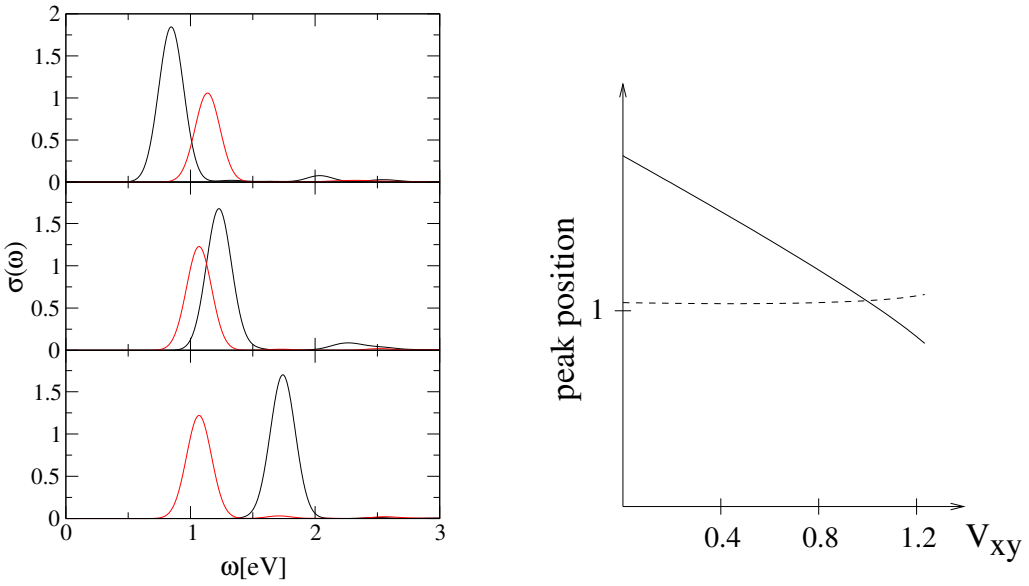

Figure 4.13: Left panel: Optical conductivity in a (black line) and b direction (red line). Parameters are $t_a = 0.4$, $t_b = 0.2$, $t_{xy} = 0$, $V_a = V_b = 0.8$ at $T = 0\,\mathrm{K}$. From bottom to top: $V_{xy} = 0.0,\ 0.8,\ 1.2$. Right panel: Peak position of the peaks in a (solid line) and b direction (dashed line).

is on the wrong position on the rung. This defects lead to a reduction of the frustrated bonds with energy $\sim V_{xy}$ and the peak position of the optical conductivity in a direction becomes dependent on V_{xy} with excitation energy approximately $2V_b - V_{xy}$. If the system was in inline charge order this behavior cannot be explained. In inline order the excitation energy is given by $\kappa V_{xy} - 2V_b$ with $1 < \kappa < 2$ depending on the amount of defects in the system. This means that the peaks should be shifted to higher energies, when V_{xy} is increased, which is not observed in our calculations. In order to investigate the charge order of the ground state directly we calculated the density correlation function $\langle n_1 n_i \rangle$ (see table 4.1), which clearly indicates zig-zag charge order with many defects, in agreement with our assumptions above. With increasing interladder coulomb interaction V_{xy} the zig-zag correlations $\langle n_1 n_4 \rangle$ and $\langle n_1 n_5 \rangle$ decrease, whereas the inline correlations $\langle n_1 n_3 \rangle$ and $\langle n_1 n_6 \rangle$ increase. This means that due to the defects the ground state is influenced by V_{xy} favouring inline charge order.

The conductivity in b direction connects to excitation with two and zero electrons on a rung, which is not influenced by valence fluctuations and by V_{xy} since this interaction is still frustrated. In conclusion on can argue that there must be many defects of the perfect zig-zag charge order in the system

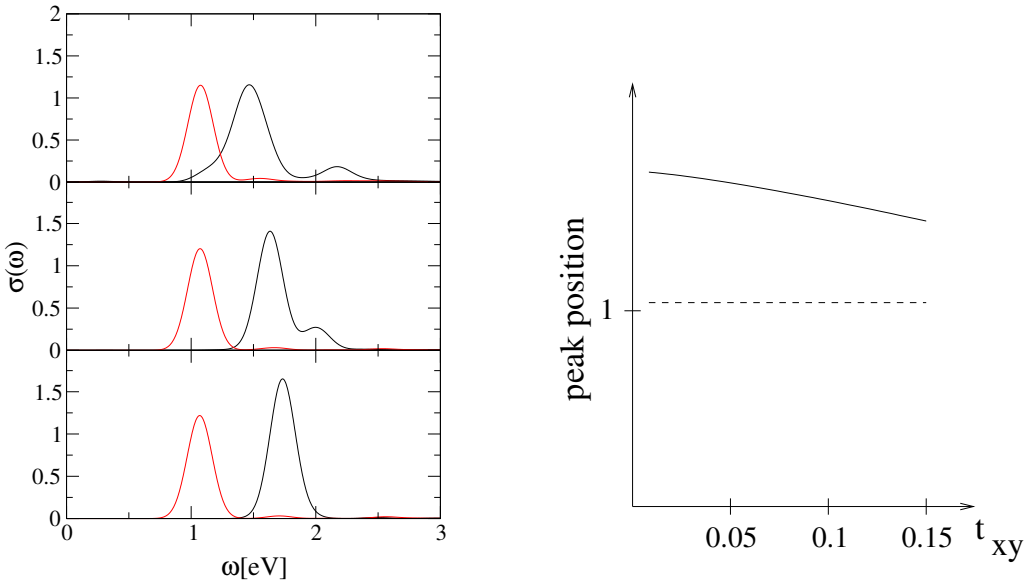

Figure 4.14: Left panel: Optical conductivity in a (black line) and b direction (red line). Parameters are $t_a = 0.4$, $t_b = 0.2$, $V_a = V_b = 0.8$, $V_{xy} = 0$ at $T = 0\,\mathrm{K}$. From bottom to top: $t_{xy} = 0.015, 0.07, 0.15$. Right panel: Peak position of the peaks in a (solid line) and b direction (dashed line).

Table 4.1: Density correlation function $\langle n_1 n_i \rangle$ for $t_a = 0.4$, $t_b = 0.2$, $t_{xy} = 0$ and $V_a = V_b = 0.8$ at $T = 0\,\mathrm{K}$. For the meaning of the indices see figure 4.12.

	$\langle n_1 n_2 \rangle$	$\langle n_1 n_3 \rangle$	$\langle n_1 n_4 \rangle$	$\langle n_1 n_5 \rangle$	$\langle n_1 n_6 \rangle$
$V_{xy} = 0.0$	0.031	0.102	0.381	0.370	0.129
$V_{xy} = 0.8$	0.037	0.128	0.355	0.336	0.164
$V_{xy} = 1.2$	0.027	0.181	0.303	0.262	0.238

in order to explain the dependence of the spectra on V_{xy}. Later on we will find by considering the Ising model in a transverse field, that the system is close to its quantum critical point, where the transition from the ordered to the disordered phase takes place. From the values of the parameter one can easily see that this point is at $\frac{2t_a}{V_b} = 1$ and not at $\frac{2t_a}{V_b} = 2$ as shown in the mean field phase diagram 4.11.

In a next step we want to determine the influence of the interladder hopping t_{xy} on the charge order. In order to separate this effects from the interladder coulomb interaction we set V_{xy} to zero. The results are shown in figure 4.14. One can see that there is a slight downward shift of the peak in a direction of about 0.3 eV. In this case we cannot explain this shift by assuming the same

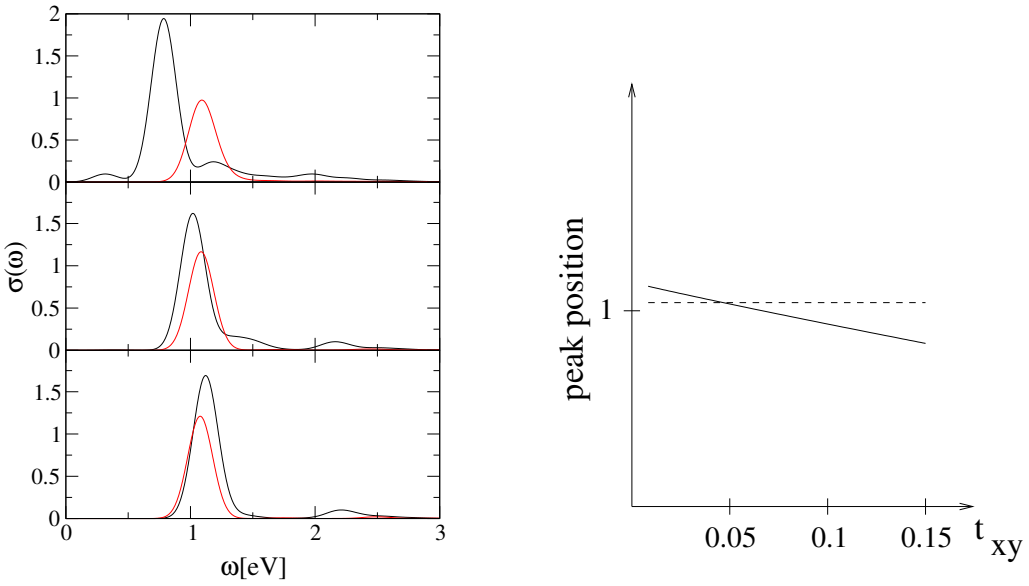

Figure 4.15: Left panel: Optical conductivity in a (black line) and b direction (red line). Parameters are $t_a = 0.4$, $t_b = 0.2$, $V_a = V_b = 0.8$, $V_{xy} = 0.9$ at $T = 0\,\mathrm{K}$. From bottom to top: $t_{xy} = 0.015, 0.07, 0.15$. Right panel: Peak position of the peaks in a (solid line) and b direction (dashed line).

defects as above, i.e. where there is one electron on the rung but on the wrong position, because V_{xy} was set to zero and these defects don't give raise to any shift of the peak. But there is another kind of defect that could explain the shifting in this case. The interladder hopping allows the electrons to hop from one ladder to a neighboring one. Therefore there is a small possibility to find states with a doubly occupied rung and an empty rung in the neighboring ladder. These defects can cause now a slight downward shift of the peak in a direction, because the excitation energy is not $2V_b$ any more but a bit smaller. The position of the peak in b direction is again not influenced by these defects (doubly occupied rung $\leftrightarrow$ empty rung), as one can see from figure 4.14, too.

In order to check our assumptions we calculated the optical conductivity for the same values of t_{xy} as in figure 4.14 but for a finite interladder coulomb interaction $V_{xy} = 0.9$. Figure 4.15 shows again the slight downward shift of the peak in a direction of about 0.3 eV, which is another hint that the defects produced by finite t_{xy} couple mainly to V_b and not to V_{xy}.

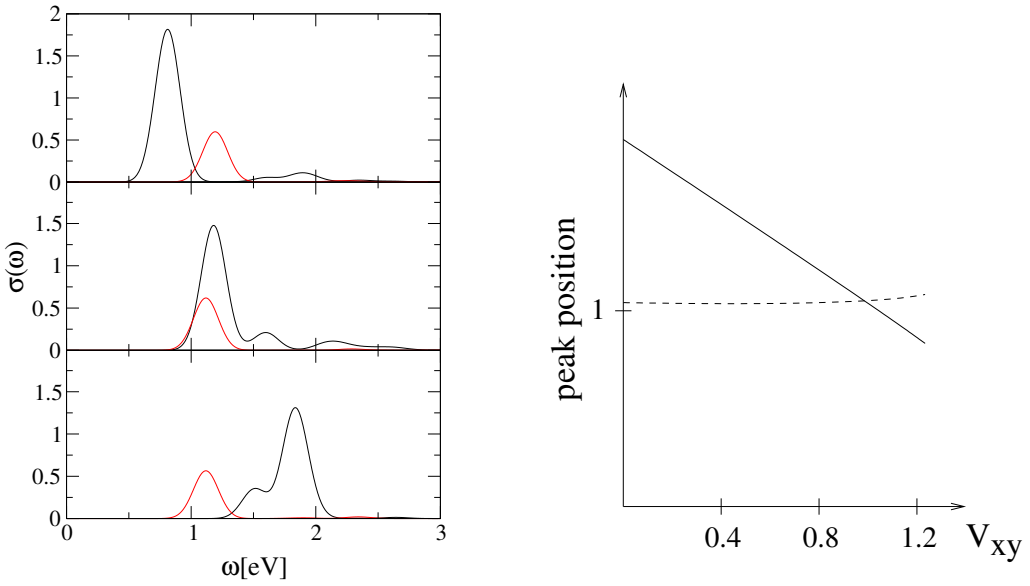

Figure 4.16: Left panel: Optical conductivity in a (black line) and b direction (red line). Parameters are $t_a = 0.375$, $t_b = 0.08$, $t_d = 0.095$, $t_{xy} = 0$, $V_a = V_b = 0.8$ at $T = 0\,\mathrm{K}$. From bottom to top: $V_{xy} = 0.0$, 0.8, 1.2. Right panel: Peak position of the main peaks in a (solid line) and b direction (dashed line).

4.4.2 Including Diagonal Hopping

In the previous section the optical conductivity was calculated using only three hopping matrix elements t_a, t_b and t_{xy}. Density functional calculations show, that there are in fact more matrix elements that should be taken into account, above all the diagonal hopping within the single ladders. This hopping, from now on called t_d, connects the sites 1 and 4, 2 and 3 and so on (see figure 4.12). In order to get the same LDA band structure as without diagonal hopping one has to choose a smaller value for the interladder hopping matrix element t_b, whereas all other parameters remain the same. For our calculations we took the values for the parameters from reference [22]: $t_a = 0.375$, $t_b = 0.08$ and $t_d = 0.095$. The parameter values for the coulomb interaction are as before $V_a = V_b = 0.8$. We again vary t_{xy} and V_{xy} to study their influence.

To begin with we set t_{xy} equal to zero and vary V_{xy} between 0 and 1.2. In figure 4.16 one can see that the main message is the same in both cases, i.e. with and without diagonal hopping. Again we have an immense downward shift of the main peak in a direction, whereas the position of the peak in

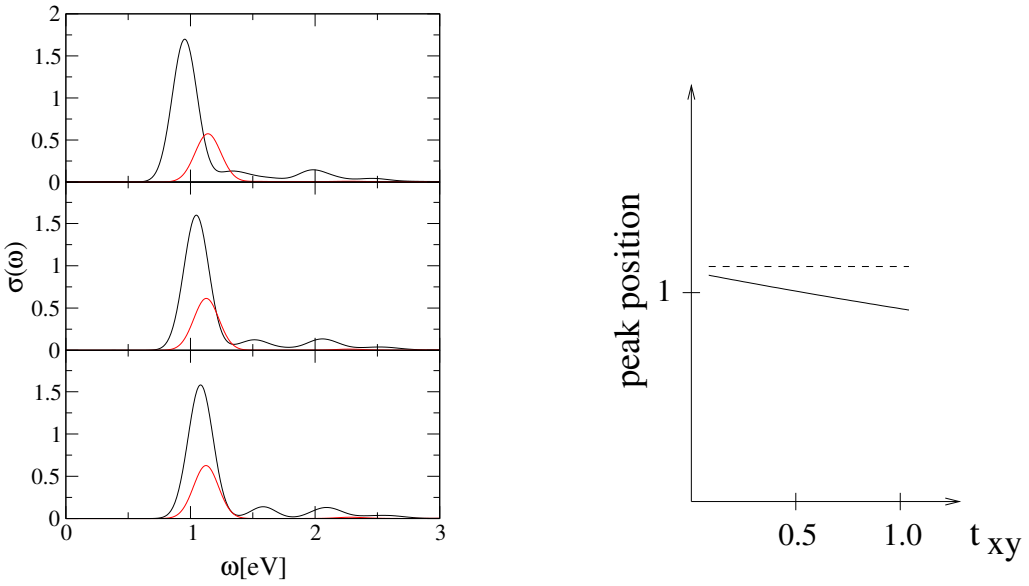

Figure 4.17: Left panel: Optical conductivity in a (black line) and b direction (red line). Parameters are $t_a = 0.375$, $t_b = 0.08$, $t_d = 0.095$, $V_a = V_b = 0.8$ $V_{xy} = 0.9$ at $T = 0\,\mathrm{K}$. From bottom to top: $t_{xy} = 0.01, 0.05, 0.1$. Right panel: Peak position of the main peaks in a (solid line) and b direction (dashed line).

b-direction is not influenced by V_{xy}. One difference is the occurrence of additional excitations in a direction above 1.5 eV. One could try to attribute these excitations to elementary excitations caused by the diagonal hopping t_d. In this case the diagonal hopping should contribute to both a and b direction in the same way, but in b direction no additional excitations are observed. Therefore the additional excitations in a direction could be some bonding-antibonding transitions within a rung turned on by the diagonal hopping. We again calculated the density correlation function $\langle n_1 n_i \rangle$ indicating zig-zag charge order and many defects as in the case without diagonal hopping (see table 4.2).

Table 4.2: Density correlation function $\langle n_1 n_i \rangle$ for $t_a = 0.375$, $t_b = 0.08$, $t_d = 0.095$, $t_{xy} = 0$ and $V_a = V_b = 0.8$ at $T = 0\,\mathrm{K}$. For the meaning of the indices see figure 4.12.

	$\langle n_1 n_2 \rangle$	$\langle n_1 n_3 \rangle$	$\langle n_1 n_4 \rangle$	$\langle n_1 n_5 \rangle$	$\langle n_1 n_6 \rangle$
$V_{xy} = 0.0$	0.017	0.094	0.396	0.386	0.114
$V_{xy} = 0.8$	0.018	0.123	0.365	0.347	0.152
$V_{xy} = 1.2$	0.018	0.187	0.302	0.256	0.243

When setting $V_{xy} = 0.9$ and varying t_{xy} the picture is again very similar to that without diagonal hopping, i.e. the b peak does not depend on the interladder hopping, whereas there is a slight downward shift of the peak in a direction (see figure 4.17). In this case we did the calculations for $t_{xy} = 0.01$, 0.05 and 0.1, which means the range of variation of t_{xy} is smaller than in the previous section. Therefore it is not astonishing, that the downward shift of the a peak is a bit smaller, too.

One difference between the two cases $t_d = 0$ and $t_d \neq 0$ should be mentioned. The ratio between the spectral weight of the peaks in a and b direction, which means the optical conductivity integrated from 0.6 to 2 eV, lies between 1.5 and 2 in the case $t_d = 0$, which is noticeably larger than in the case $t_d \neq 0$, where this ratio lies between 3 and 3.3. The loss of spectral weight in b direction is due to the reduced value for t_b, because this hopping contributes most to the optical conductivity in b direction. The experimental value for this ratio is 2.2, which gives raise to the assumption that including t_d in the calculation does not lead to an improvement of the results. One could now argue that by including even more longer ranging hopping matrix elements the results could be improved again. The problem is that our calculations are done on a small cluster of 16 sites, where the inclusion of long ranging hopping terms is not reasonable.

In conclusion one can say that the inclusion of the diagonal hopping t_d in the calculation gives the same dependence on the parameters V_{xy} and t_{xy} as before, which gives raise to the assumption that the charge order is very similar for $t_d = 0$ and $t_d \neq 0$, resp, which can also be seen by comparing tables 4.1 and 4.2.

4.4.3 Results for Finite Temperature

In this section we want to compare the numerical results for the optical conductivity in the frame of the t-J-V model with the numerical results in the frame of the t-U-V model. The calculations were performed using the finite temperature Lanczos method (see section 3.4). Figure 4.18 shows the results for $T = 100\,\mathrm{K}$. For the t-U-V model the peak in a direction is considerably larger than for the t-J-V model, whereas the spectral weight of the peak is almost the same in both models, because for the t-J-V model the peak is broader. Experimental data (see figures 5.1 and 5.2) at $T = 100\,\mathrm{K}$ shows the same ratio of the peak heights as the results from the t-U-V model. From figure 4.19 one can see that for higher temperatures (in this case $T = 700\,\mathrm{K}$) this discrepancy nearly disappears and the spectra are very similar. The

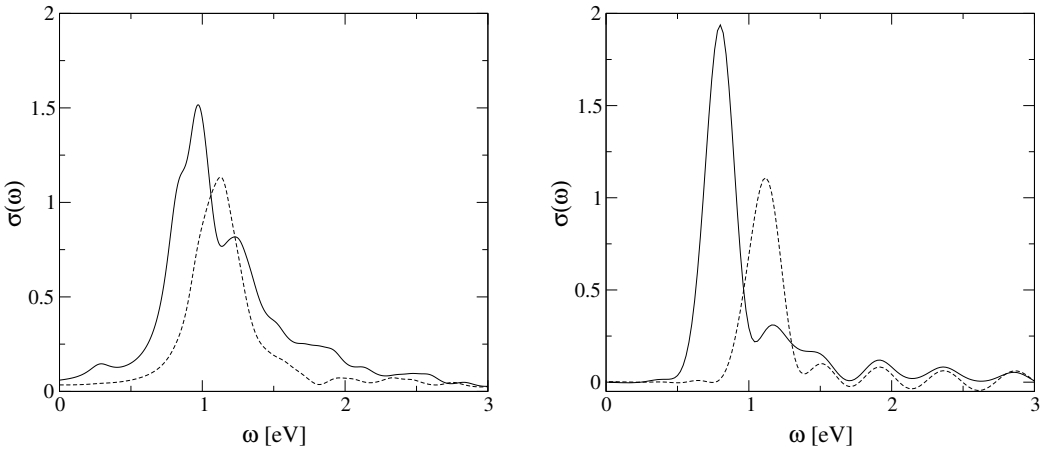

Figure 4.18: Optical conductivity for a (full line) and b direction (dashed line) at $T = 100$ K. Parameters are $t_a = 0.4$, $t_b = 0.2$, $t_{xy} = 0.15$, $V_a = V_b = 0.8$ and $V_{xy} = 0.9$. Left panel: t-J-V model. Right panel: t-U-V model.

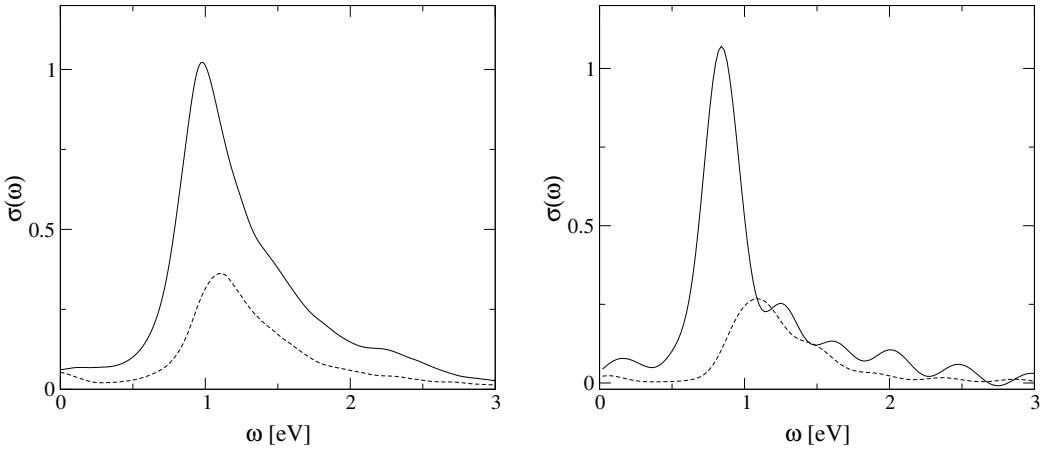

Figure 4.19: Optical conductivity for a (full line) and b direction (dashed line) at $T = 700$ K. Parameters are $t_a = 0.4$, $t_b = 0.2$, $t_{xy} = 0.15$, $V_a = V_b = 0.8$ and $V_{xy} = 0.9$. Left panel: t-J-V model. Right panel: t-U-V model.

oscillations that appear at high frequencies in the spectra calculated in the frame of the t-U-V model occur due to our implementation that is not very efficient at low temperatures.

We used for our calculation the parameter set used by Cuoco et al. [23], for which they found the best agreement of calculations in the frame of the t-J-V model with experimental results at room temperature [24, 25, 26]. From figures 4.18 and 4.19 one can see that the peaks of the conductivity in b direction are the same for the t-J-V and the t-U-V model, whereas the peak in a direction is for the t-U-V model at lower energies than in the t-J-V model. One can overcome this difference by choosing a lower value for t_{xy} for the t-U-V model (see figure 4.15), which is consistent with literature. If one chooses for example $t_{xy} = 0.08$ then the peak is a bit below 1 eV as observed in experiments.

A few words should be added regarding computational details. The Hilbert space for the t-U-V model is much larger than for the t-J-V model, because in the latter case no double occupancies are allowed. The computational effort when applying the FTLM to the t-U-V model is therefore larger. On this account we use the t-J-V model for the further calculations.

Chapter 5

Temperature Dependence of Optical Spectra of α'-NaV_2O_5

In this chapter we want to investigate the temperature dependence of the integrated optical conductivity (IOC). In order to describe the experimental results of Presura *et al.* [27]. We calculated the IOC by FTLM (see section 3.4 for details) for several temperatures and found quite similar behaviour, namely that spectral weight of the 1 eV peak decreases when temperature raises. The reason for the decrease will be analyzed in detail in the sequel.

5.1 Experimental Results

Presura *et al.* measured the dielectric function and the optical conductivity of NaV_2O_5 for different temperatures by ellipsometric measurements of the (001) surfaces of the crystals both with the plane of incidence of the light along the a and the b axis [27]. The results of these measurements are shown in figure 5.1 and 5.2. The 0.9-eV peak in $\sigma_a(\omega)$ corresponds to bonding-antibonding transitions within a rung, whereas the peak at 1.1 eV in $\sigma_b(\omega)$ is attributed to transitions between neighbouring rungs along the ladder. The peak at 3.3 eV in $\sigma_a(\omega)$ was attributed to the transition from the $2p$ orbital of oxygen to the antibonding level within the same V_2O_5 cluster.

Let us now turn to the discussion of the temperature dependence of the spectra. As one can see from figures 5.1 and 5.2 the position of the peaks is temperature independent, which suggests that the valence of the vanadium ions above and below the phase transition at $T_c = 34K$ is almost the same.

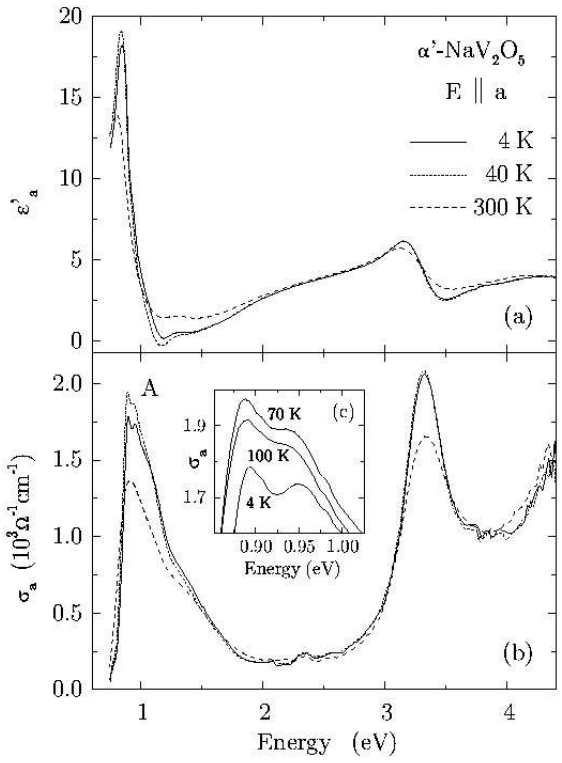

Figure 5.1: Real part $\epsilon'(\omega)$ of the dielectric function (a) and optical conductivity $\sigma(\omega)$ (b) for $E \parallel a$. Figure taken from reference.

Presura *et al.* claimed that the changes in the valences of the V atoms are smaller than $0.06e$. If the changes were larger, then the equilibrium positions of the V ions in the V_2O_5 pyramids and therefore the onsite energies would be changed [19]. This rapid change of the onsite energy would shift the peaks to lower energies, which has not been observed.

Although the peaks remain on the same position the intensity decreases dramatically with increasing temperature. The spectral weight of the B peak seems to be transferred to energies up to and above 4 eV. The spectral weight of the A peak is transferred to even higher energies of about 4.5 eV. Let us now take a look at the temperature dependence of the integrated spectral weight of the 1 eV peaks. For this purpose Presura *et al.* integrated the optical conductivity from 0.75 eV up to 2.25 eV, results are shown in figure 5.3. A non-linear fit with the formula $I(T) = I(0)(1 - fe^{-E_0/T})$ gave $f = 0.35$ and $E_0 = 286$ K for the a direction and $f = 0.47$ and $E_0 = 370$ K for the b direction. That means that the activation energy E_0 is about 25 meV, which is very small regarding the rather large optical gap of ap-

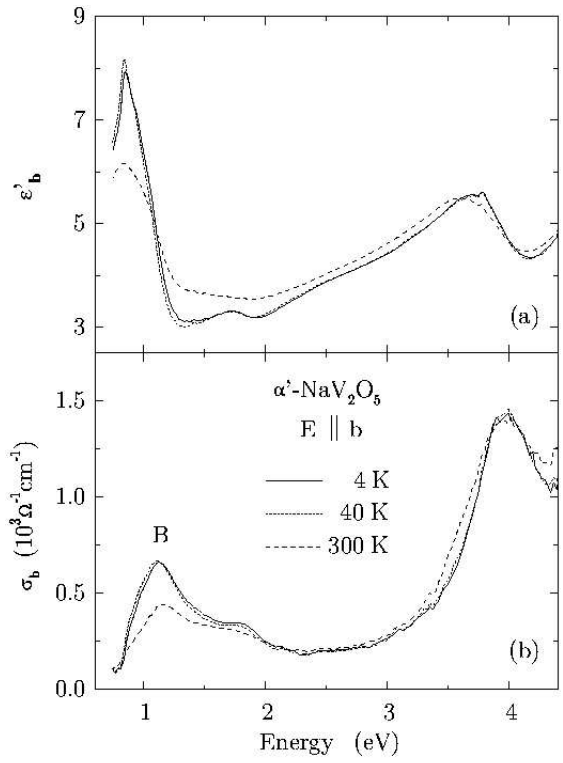

Figure 5.2: Real part $\epsilon'(\omega)$ of the dielectric function (a) and optical conductivity $\sigma(\omega)$ (b) for $E \parallel b$. Figure taken from reference.

proximately 0.9 eV. Presura *et al.* claimed, that this low-energy scale results from collective motions of the charge, which can actually be much lower in energy than a single-particle excitation. Such a soft charge excitation can be found in zig-zag charge ordering for momentum k at the boundary of the Brillouin zone $k = (\pi, \pi)$. These modes could only appear indirectly in the optical conductivity, which is by definition restricted to $k = 0$, by charge-phonon or spin-phonon coupling. But before discussing this assumption in a later section, let us first consider some numerical results for the temperature dependence of the optical conductivity of NaV_2O_5.

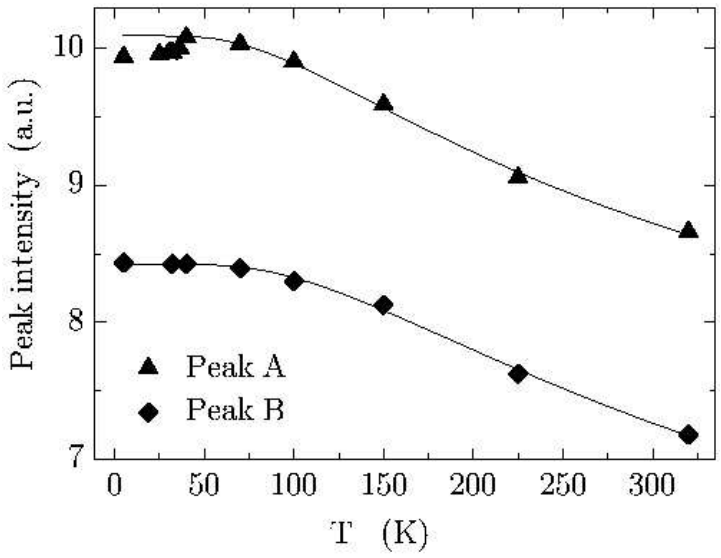

Figure 5.3: Integrated optical conductivity from 0.75 eV to 2.25 eV for a and b direction. Solid line are fits to the formula $I(T) = I(0)(1 - fe^{-E_0/T})$.

5.2 Numerical Results for the Optical Conductivity

For our numerical calculations we started from the t-J-V hamiltonian (4.2) introduced in section 4.2. For the parameters we chose the values used in figure 4.18 which gave the best agreement with experiments:

- hopping matrix elements: $t_a = 0.4$, $t_b = 0.2$, $t_{xy} = 0.15$
- coulomb interactions: $V_a = 0.8$, $V_b = 0.8$, $V_{xy} = 0.9$
- intrasite Hubbard repulsion: $U = 4.0$

We calculated the optical conductivity for both directions for several temperatures. Temperatures below 100 K could not be handled properly, because in this region the stochastic evaluation of the trace (see section 3.4) yields significant statistical errors. With the present implementation we cannot address the phase transition at $T_c = 34$ K, which also leads to a decrease of spectral weight in a direction, shown in figure 5.3.

The results of our calculations are shown in figure 5.4. The spectral weight of the 1 eV peak in both directions decreases with increasing temperature

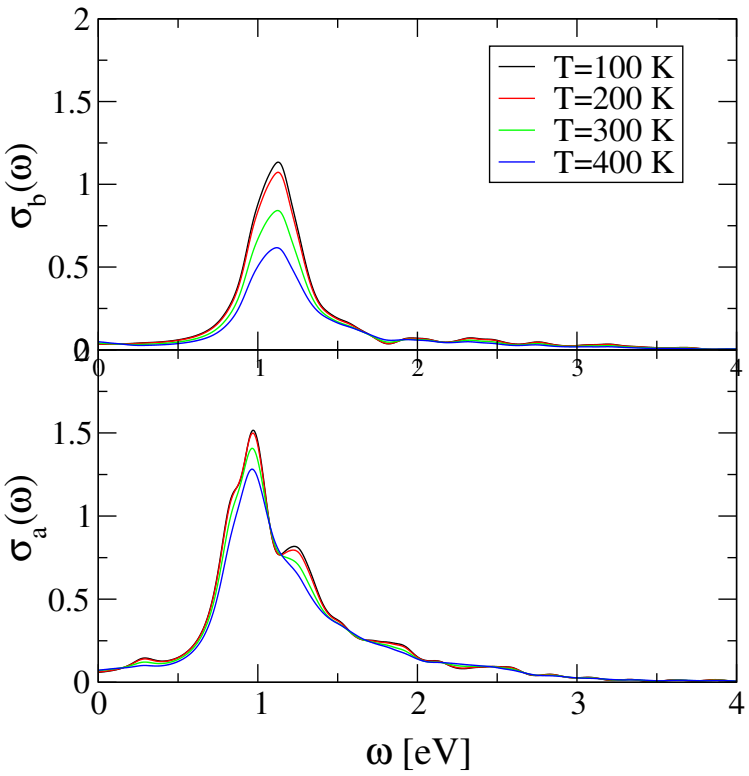

Figure 5.4: Optical conductivity calculated by FTLM for a and b direction for several temperatures. Parameters as in figure 4.18.

in agreement with the experimental spectra. But in our calculations the decrease in b direction is much larger than the decrease in a direction. In order to analyze the parameter dependence we calculated the optical conductivity and the IOC, integrated from 0 to 2.5 eV, in the wide temperature region of $k_BT = 0\,\text{eV}$ to $k_BT = 10\,\text{eV}$ for several sets of parameters. The IOC's of these calculations are shown in figure 5.5. One can see that for the standard parameter set with $t_b = 0.2$ the temperature dependence is almost the same for $t_{xy} = 0$ and $t_{xy} = 0.15$. The IOC shows qualitatively the same behavior, constant value for low temperatures and the same onset of the decrease, with only slight discrepancies, and at high temperatures the same tendency to zero.

When choosing a lower value for t_b the situation is different. In the case $t_{xy} = 0$ the behavior of the IOC is at least comparable to the results for $t_b = 0.2$. The temperature region where the IOC is constant is about a factor 4 smaller and after the decrease there is no constant region as in the case $t_b = 0.2$ but the IOC increases again slightly. For high temperatures $k_BT > 0.5\,\text{eV}$ the

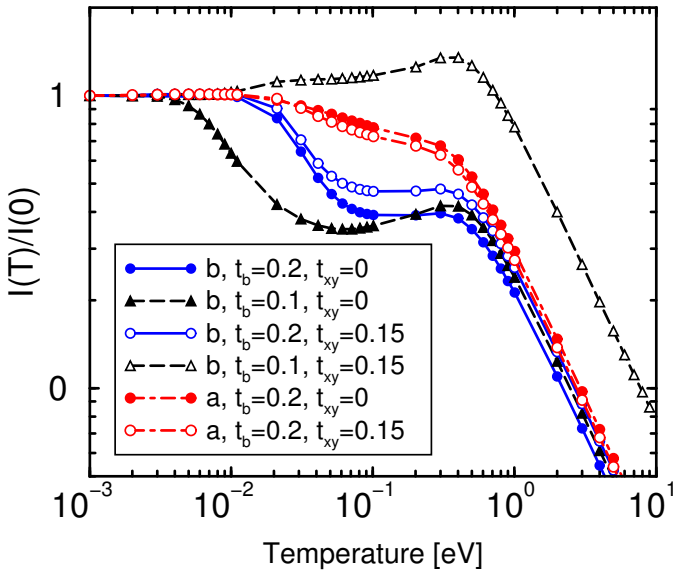

Figure 5.5: IOC for a (dot-dashed) and b direction (solid and dashed lines). Results are given for both $t_{xy} = 0.15$ (open) and $t_{xy} = 0$ (filled symbols). The set $t_b = 0.2$ and $t_{xy} = 0.15$ corresponds to the spectra shown in figure 5.4.

IOC (and therefore the kinetic energy) decreases exponentially to zero, a behavior observed for all parameter sets.

In the case $t_b = 0.1$ and $t_{xy} = 0.15$ the IOC shows a quite different temperature dependence. Here the constant region (up to ≈ 0.01 eV) is followed by a slight increase up to $k_B T \approx 0.5$ eV, beyond which the IOC decreases again exponentially to zero. We assumed, that in cases when the intraladder hopping t_b is smaller than the interladder hopping t_{xy}, the excitations are determined by interladder hopping, which is not valid for NaV_2O_5, as we argued above. Restricted to the case $t_b > t_{xy}$ one can see from figure 5.5, that the interladder hopping has no significant influence on the temperature dependence of the IOC, which is consistent with the assumption stated in section 4.4, that the coupling between two ladders in NaV_2O_5 is mainly determined by V_{xy} and not by t_{xy}.

We also calculated the charge and spin correlation function of the system for the standard parameter set $t_b = 0.2$ and $t_{xy} = 0.15$ (see figure 5.6). The charge correlations reveal that the system is in zig-zag charge order up to a temperature of about $T = 0.4\,\mathrm{eV}$, which is the same temperature where the high temperature decrease of the IOC sets in. One is therefore prompted to assume that the break down of charge correlations causes the decrease of the

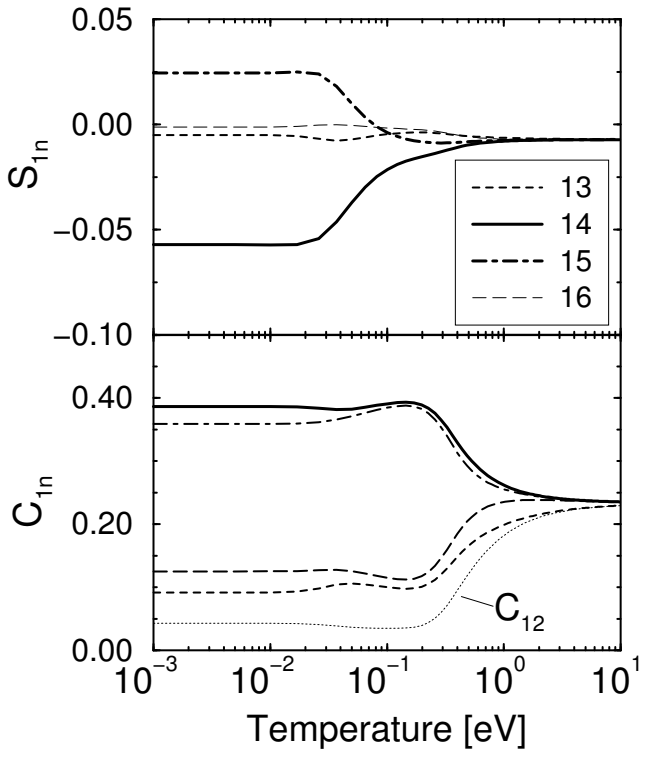

Figure 5.6: Spin (top) and charge correlations (bottom) $S_{1n} = \langle S_1^z S_n^z \rangle$ and $C_{in} = \langle n_1 n_n \rangle$ as function of temperature with the standard parameter set. For the meaning of the indices see figure 4.12.

IOC at high temperatures, which will be analyzed in the next section.

The spin correlations, which actually show antiferromagnetic order, break down at an even lower temperature of about $k_B T = 0.03\,\mathrm{eV}$ which could be the reason for the decrease of the IOC at this temperature. But let us first concentrate on the charge correlations and their influence on the IOC. The influence of the spin correlations will be discussed later on.

5.3 Ising Model in a Transverse Field (IMTF)

In order to understand the influence of the charge correlations on the IOC we turn to a different representation of the low energy degrees of freedom. For large U and V_a the relevant subspace of our Hilbert space is the one with one electron per rung. These states can be represented by eigenstates of spin $\mathbf{S}$ and pseudo-spin $\mathbf{T}$ operators, where the configuration with $T^z = \pm\frac{1}{2}$

corresponds to the left/right position of the electron within a rung. In figure 5.6 one can see, that for low temperatures the charge correlation function C_{12}, which gives the amount of double occupancies of a rung, is very small and the assumption that there is only one electron per rung is valid. It is now possible to project out the high energy states, which yields a spin-pseudospin Hamiltonian [28, 29]. For a single ladder it is given by

$$\begin{aligned}\mathcal{H}_{ladder} = &- 2t_a \sum_l T_l^x + \left(2V_b + \frac{2t_b^2}{\Delta}\right) \sum_l T_l^z T_{l+1}^z \\ &+ \frac{8t_b^2}{\Delta} \sum_l \left(\mathbf{S}_l \cdot \mathbf{S}_{l+1} - \frac{1}{4}\right) \left(T_l^+ T_{l+1}^- + \text{h.c.}\right) \end{aligned} \tag{5.1}$$

where l stands for a rung consisting of two vanadium sites. The hopping t_a acts as a transverse field, while the coulomb interaction between electrons on neighbor rungs l and $l+1$ in the ladder corresponds to the zz-coupling in the Ising model. The third term is due to exchange between electrons in different rungs along the b direction. The energy Δ scales between $V_a + V_b$ and $2t_a$ depending on which value is larger.

The coupling between neighboring ladders is given by

$$\begin{aligned}\mathcal{H}_{interladder} = &- V_{xy} \sum_{\langle l,m \rangle} \left(T_l^z - \frac{1}{2}\right) \left(T_m^z + \frac{1}{2}\right) \\ &+ \frac{4t_{xy}^2}{\Delta_1} \sum_{\langle l,m \rangle} \left(\mathbf{S}_l \cdot \mathbf{S}_m - \frac{1}{4}\right) \left(T_l^z T_m^z + \frac{1}{4}\right) \end{aligned} \tag{5.2}$$

where $\langle l, m \rangle$ connects two next-neighbor rungs on neighboring ladders and $\Delta_1 = 2V_b + V_a - V_{xy}$. In order to simplify this Hamiltonian we do the following approximations:

- The system should be in zig-zag charge order, this means, that the interladder coulomb interaction V_{xy} does not have big influence on the ground state and on the spectral weights of the 1 eV peaks of the optical conductivity (see figure 4.13). Therefore we set $V_{xy} = 0$.

- The ground state is mainly determined by configurations with one electron on a rung. We now assume, that the interrung hopping t_b can be neglected, i.e. we neglect all second order corrections $\propto t_b^2$. The interladder hopping t_{xy} can be set to zero, because its influence is very small (see figure 5.5).

These assumptions lead to a simpler Hamiltonian only consisting of the transverse field t_a and the zz coupling constant V_b, which has the form of an Ising model in a transverse field (IMTF) [30, 31, 32, 33].

5.3.1 Hamiltonian of the IMTF

Starting point of our calculation is the Hamiltonian

$$\mathcal{H} = -2t_a \sum_l T_l^x + 2V_b \sum_l T_l^z T_{l+1}^z, \tag{5.3}$$

where we have chosen periodic boundary conditions $T_{N+1}^\alpha = T_1^\alpha$. The eigenvalues of the pseudo-spin operators $T_l^z = \pm\frac{1}{2}$ correspond to the left/right position of the electron within a rung. This Hamiltonian can be rewritten by setting $\tilde{\mathcal{H}} := \mathcal{H}/V_b$ and $h := 2t_a/V_b$

$$\tilde{\mathcal{H}} = -h \sum_l T_l^x + 2 \sum_l T_l^z T_{l+1}^z. \tag{5.4}$$

If we rotate the coordinate system around the y-axis, i.e. $z \to x, \quad x \to -z$ we get

$$\tilde{\mathcal{H}} = h \sum_l T_l^z + 2 \sum_l T_l^x T_{l+1}^x \tag{5.5}$$

It is now useful to introduce the raising and lowering operators

$$T_l^+ = T_l^x + iT_l^y \tag{5.6a}$$
$$T_l^- = T_l^x - iT_l^y \tag{5.6b}$$

With these two operators the product $T_l^x T_{l+1}^x$ in the Hamiltonian can be rewritten and leads to

$$\tilde{\mathcal{H}} = h \sum_l T_l^z + \frac{1}{2} \sum_l \left(T_l^+ T_{l+1}^+ + T_l^+ T_{l+1}^- + T_l^- T_{l+1}^+ + T_l^- T_{l+1}^- \right) \tag{5.7}$$

Let us now consider the behavior of the operators T_l^+ and T_l^-. Directly from the definition one can obtain the commutation relations

$$[T_l^+, T_j^-] = 2T_l^z \delta_{lj} \tag{5.8a}$$
$$[T_l^z, T_j^+] = T_l^+ \delta_{lj} \tag{5.8b}$$
$$[T_l^z, T_j^-] = -T_l^- \delta_{lj} \tag{5.8c}$$

where we have used the well known commutation relations for spin one-half operators [2]

$$[T_l^x, T_j^y] = iT_l^z \delta_{lj} \tag{5.9a}$$
$$[T_l^y, T_j^z] = iT_l^x \delta_{lj} \tag{5.9b}$$
$$[T_l^z, T_j^x] = iT_l^y \delta_{lj} \tag{5.9c}$$

If one looks at the commutation relation (5.8) for different sites, i.e. $l \neq j$, one finds that the raising and lowering operators obey a bosonic commutation relation

$$[T_l^+, T_j^-] = 0, \qquad l \neq j. \tag{5.10}$$

For the same site, i.e. $l = j$, there is no such bosonic commutation relation, which means on the right hand side of equations (5.8) stands an operator and no complex number. Instead we find for $l = j$

$$\begin{aligned} T_j^+ T_j^- + T_j^- T_j^+ &= 2\left[\left(T_j^x\right)^2 + \left(T_j^y\right)^2\right] = 2\left[\mathbf{T}\cdot\mathbf{T} - \left(T_j^z\right)^2\right] \\ &= 2\left[T(T+1) - \left(T_j^z\right)^2\right] \end{aligned} \tag{5.11}$$

For spin one-half we have to use $T = 1/2$ and $(T_j^z)^2 = 1/4$, which leads to the anticommutation relation

$$\left\{T_j^+, T_j^-\right\} = 2\left[\frac{1}{2}\left(\frac{3}{2}\right) - \frac{1}{4}\right] = 1 \tag{5.12}$$

Thus we have found that the spin one-half operators behave like fermions on the same site and like bosons on different sites. Because of that they are sometimes called hard-core bosons, which means that one cannot create two bosons of the same type on the same site.

This peculiar behavior of the spin operators causes severe difficulties when dealing with Heisenberg-like Hamiltonians.

5.3.2 Jordan-Wigner Transformation

When treating spin problems one is facing severe difficulties because of the fact that the spins are neither bosons nor fermions. In one dimension, however, there is a famous way to overcome these problems, because it is possible to map the spin operators exactly into fermion operators [2]. This transformation was introduced by Jordan and Wigner (1928).

In one dimension the spins are located along a chain. We define new operators by multiplying the spin operators by a phase factor depending on the spin site:

$$c_l = e^{i\pi\phi_l} T_l^- \tag{5.13a}$$

$$c_l^\dagger = e^{-i\pi\phi_l} T_l^+ \tag{5.13b}$$

The phase ϕ_l counts the number of spin-up sites to the left of position l

$$\phi_l = \sum_{k=1}^{l-1} \left(\frac{1}{2} + T_k^z \right), \qquad l > 1. \tag{5.14}$$

This definition implies that in the Jordan-Wigner transformation (5.13) the phase factors commute with the spin operators, because the ϕ_l do not depend on the spin at site l itself. Therefore the phases can be put either in front of the spin operators or behind.

From equations (5.13) we obtain for the density $n_l = c_l^\dagger c_l$

$$n_l = c_l^\dagger c_l = T_l^+ T_l^- = T(T+1) - (T_l^z)^2 + T_l^z = \frac{1}{2} + T_l^z \tag{5.15}$$

This implies that the density n_l measures the number of spin up at site l.

Our claim is that the operators defined by (5.13) are fermion operators. On the same site we get the anticommutation relation quite simple, because the phase factors cancel each other:

$$\left\{ c_l, c_l^\dagger \right\} = \left\{ T_l^-, T_l^+ \right\} = 1, \tag{5.16}$$

where we have used the fermionic behavior of spins at the same site. At different sites we have to calculate the anticommutator explicitly:

$$\left\{ c_l, c_j^\dagger \right\} = e^{i\pi\phi_l} T_l^- e^{-i\pi\phi_j} T_j^+ + e^{-i\pi\phi_j} T_j^+ e^{i\pi\phi_l} T_l^-$$

Without loss of generality we may assume that $l > j$. Consequently we can split the phase factor ϕ_l into two terms, one with $l = j$ and one with $l \neq j$:

$$\phi_l = \underbrace{\left(\frac{1}{2} + T_j^z \right)}_{n_j} + \sum_{\substack{k=1 \\ k \neq j}}^{l-1} \underbrace{\left(\frac{1}{2} + T_k^z \right)}_{n_k}$$

Thus we get for the anticommutator

$$\left\{ c_l, c_j^\dagger \right\} = e^{i\pi(\phi_l - \phi_j)} \left(T_l^- T_j^+ + e^{-i\pi n_j} T_j^+ e^{i\pi n_j} T_l^- \right) \tag{5.17}$$

Let us now focus on the second term of the right hand side of above equation. The operator T_j^+ must raise the magnetic quantum number. This implies that n_j to the right of this operator has to be zero, while to the left it is equal to one, i.e.

$$e^{-i\pi n_j} T_j^+ e^{i\pi n_j} = e^{-i\pi} T_j^+ = -T_j^+$$

Inserting this result into (5.17) we obtain for the anticommutator

$$\left\{ c_l, c_j^\dagger \right\} = e^{i\pi(\phi_l - \phi_j)} \left[T_l^-, T_j^+ \right] = 0, \tag{5.18}$$

because spin operators commute on different site. In other words, $c_l^\dagger$ and c_l are fermion creators and annihilators, resp.

Summarizing all our results we have shown that the Jordan-Wigner transformation (5.13) leads to a fermionic formulation of one-dimensional spin problems.

5.3.3 Application to the IMTF

In order to solve the eigenvalue problem of the IMTF we apply the Jordan-Wigner transformation to the Hamiltonian (5.7) [30]. In order to do this we rewrite equations (5.13) in the form

$$T_l^- = e^{-i\pi \sum_{k=1}^{l-1} n_k} c_l \tag{5.19a}$$

$$T_l^+ = e^{i\pi \sum_{k=1}^{l-1} n_k} c_l^\dagger \tag{5.19b}$$

To begin with we transform the first term of Hamiltonian (5.7) into Jordan-Wigner fermions, which is rather simple:

$$\sum_l T_l^z = \sum_l \left(c_l^\dagger c_l - \frac{1}{2} \right) = -\frac{N}{2} + \sum_l c_l^\dagger c_l, \tag{5.20}$$

where N denotes the number of sites. In the next step we transform the interaction part of (5.7). For the first term we obtain

$$\begin{aligned} T_l^+ T_{l+1}^+ &= e^{i\pi \sum_{k=1}^{l-1} n_k} c_l^\dagger e^{i\pi \sum_{k=1}^{l} n_k} c_{l+1}^\dagger \\ &= e^{2i\pi \sum_{k=1}^{l-1} n_k} c_l^\dagger e^{i\pi n_l} c_{l+1}^\dagger \\ &= c_l^\dagger c_{l+1}^\dagger \end{aligned}$$

In the last step we used that $\sum_{k=1}^{l-1} n_k$ is an integer and n_l has to be zero, because it stands right of a creation operator.

Similar one can calculate the other terms of the interaction part leading to

$$\begin{aligned} T_l^+ T_{l+1}^- &= c_l^\dagger c_{l+1} \\ T_l^- T_{l+1}^+ &= -c_l c_{l+1}^\dagger \\ T_l^- T_{l+1}^- &= -c_l c_{l+1} \end{aligned}$$

At last we have to look at the periodic boundary conditions, which are defined by $T_{N+1}^\alpha = T_1^\alpha$. Applying the Jordan-Wigner transformation to the first term of the interaction part leads to

$$\begin{aligned} T_N^+ T_{N+1}^+ = T_N^+ T_1^+ &= e^{i\pi \sum_{k=1}^{N-1} n_k} c_N^\dagger c_1^\dagger \\ &= e^{i\pi n_N} e^{-i\pi n_N} e^{i\pi \sum_{k=1}^{N-1} n_k} c_N^\dagger c_1^\dagger \\ &= -e^{i\pi \sum_{k=1}^{N} n_k} c_N^\dagger c_1^\dagger \end{aligned}$$

where $n_N = 1$ because of the creation operator $c_N^\dagger$. Similarly one gets for the other terms

$$\begin{aligned} T_N^+ T_{N+1}^- &= -e^{i\pi \sum_{k=1}^{N} n_k} c_N^\dagger c_1 \\ T_N^- T_{N+1}^+ &= e^{i\pi \sum_{k=1}^{N} n_k} c_N c_1^\dagger \\ T_N^- T_{N+1}^- &= e^{i\pi \sum_{k=1}^{N} n_k} c_N c_1 \end{aligned}$$

We now define a constant L as number of Jordan-Wigner fermions in the whole chain, which is equivalent to the number of spin up,

$$L = \sum_{k=1}^{N} n_k$$

Finally we can write the Hamiltonian (5.7) in terms of Jordan-Wigner fermions

$$\begin{aligned} \tilde{\mathcal{H}} = -\frac{hN}{2} + h \sum_{l=1}^{N} c_l^\dagger c_l + \frac{1}{2} \sum_{l=1}^{N} \left(c_l^\dagger - c_l \right) \left(c_{l+1}^\dagger + c_{l+1} \right) \\ - \frac{1}{2} \left(c_N^\dagger - c_N \right) \left(c_1^\dagger + c_1 \right) \left(e^{i\pi L} + 1 \right) \end{aligned} \tag{5.21}$$

One must mention here that the number of fermions L within the chain is no constant of motion, but its parity is conserved and therefore $\exp(i\pi L)$ is a constant of motion which is equal to $+1$ or -1 for an even or odd number of fermions, resp. Hence we have to choose antiperiodic boundary conditions for an even number of fermions and periodic boundary conditions for an odd number.

If the number of fermions L is odd then the last term of (5.21), which is the correction term due to the periodic boundary conditions, equals zero. But if L is even, then it gives corrections of the order $1/N$, which can be neglected in large systems. In addition we will drop the constant term in the Hamiltonian (5.21) in the following calculation, because it gives only a shift in the energy. The Hamiltonian that we have to diagonalise is

$$\tilde{\mathcal{H}} = h \sum_{l=1}^{N} c_l^\dagger c_l + \frac{1}{2} \sum_{l=1}^{N} \left(c_l^\dagger - c_l \right) \left(c_{l+1}^\dagger + c_{l+1} \right) \tag{5.22}$$

This Hamiltonian is quadratic in the fermion creators/annihilators and therefore diagonalizable. This can be done using the Bogoliubov-Transformation [30].

5.3.4 Bogoliubov Transformation

The Bogoliubov transformation is a general way to diagonalise Hamiltonian which are quadratic in the fermion operators. The main idea is to rewrite the Hamiltonian in a diagonal form using new fermion operators constructed by a linear transformation of the old ones.

First we write the Hamiltonian in the general quadratic form

$$\tilde{\mathcal{H}} = \sum_{ij} c_i^\dagger A_{ij} c_j + \frac{1}{2} \sum_{ij} \left(c_i^\dagger B_{ij} c_j^\dagger + \text{h.c.} \right) \tag{5.23}$$

$\mathcal{H}$ has to be hermitian, which means in this case that A has to be symmetric and B has to be antisymmetric.

Our aim is to rewrite the Hamiltonian using variables $\eta_q^\dagger$ and η_q in the diagonal form

$$\tilde{\mathcal{H}} = \sum_{q} \omega_q \eta_q^\dagger \eta_q + \text{const}, \tag{5.24}$$

where ω_q are one fermion energies. The $\eta_q^\dagger$ and η_q are obtained via a linear transformation

$$\eta_q = \sum_i \left(g_{qi} c_i + h_{qi} c_i^\dagger \right) \tag{5.25a}$$

$$\eta_q^\dagger = \sum_i \left(g_{qi} c_i^\dagger + h_{qi} c_i \right) \tag{5.25b}$$

If the Hamiltonian exists in the form (5.24) then one can calculate the following anticommutator

$$\{\eta_q, \mathcal{H}\} = \omega_q \eta_q \tag{5.26}$$

We insert now the definitions (5.25) and the quadratic Hamiltonian (5.23) into equation (5.26) and find

$$\omega_q g_{qi} = \sum_j \left(g_{qj} A_{ji} - h_{qj} B_{ji}\right)$$
$$\omega_q h_{qi} = \sum_j \left(g_{qj} B_{ji} - h_{qj} A_{ji}\right).$$

These are two coupled equations to determine ω_q, g_{qi} and h_{qi}. One can rewrite these equations by adding them or by subtracting the second one from the first one in order to get

$$\Phi_q(A - B) = \omega_q \Psi_q \tag{5.27a}$$
$$\Psi_q(A + B) = \omega_q \Phi_q \tag{5.27b}$$

The $2N$ components of the vectors Φ_q and Ψ_q are given by

$$(\Phi_q)_i = g_{qi} + h_{qi}$$
$$(\Psi_q)_i = g_{qi} - h_{qi}$$

If one inserts the first equation of (5.27) into the second one and vice versa one gets

$$\Phi_q(A - B)(A + B) = \omega_q^2 \Phi_q \tag{5.28a}$$
$$\Psi_q(A + B)(A - B) = \omega_q^2 \Psi_q \tag{5.28b}$$

There are now two possibilities: Either one solves the first equation to get Φ_q and calculates Ψ_q from equations(5.27) or the other way round. The quasiparticle dispersion relation ω_q is obtained both times.

We apply this results now to our original problem, namely diagonalising (5.22). For this Hamiltonian the matrices A and B are given by

$$A_{ii} = h, \quad A_{i,i+1} = A_{i+1,i} = \frac{1}{2}$$
$$B_{i,i+1} = \frac{1}{2}, \quad B_{i+1,i} = -\frac{1}{2}$$

We need the sum and the difference of these two matrices. But because A is symmetric, which means $A = A^T$, and B is antisymmetric, which means

$B = -B^T$, the relation $(A - B) = (A + B)^T$ holds and we have to calculate only $(A + B)$ explicitly. Finally we get

$$(A-B)(A+B) = \begin{pmatrix} 1+h^2 & h & \cdot & \cdot & h \\ h & 1+h^2 & h & \cdot & \cdot \\ \cdot & h & 1+h^2 & \ddots & \cdot \\ \cdot & \cdot & \ddots & \ddots & h \\ h & \cdot & \cdot & h & 1+h^2 \end{pmatrix} \tag{5.29}$$

where the dots indicate zeros. For this matrix we can solve the eigenvalue equation (5.28) using the ansatz $\Phi_q = e^{iqj}$. The quasiparticle dispersion relation is given by

$$\omega_q^2 = 1 + h^2 + 2h\cos q \tag{5.30}$$

where the wave vectors are $q = \frac{2\pi m}{N}$ with

$$m = \begin{cases} -\frac{N}{2}, \ldots, 0, \ldots, \frac{N}{2} - 1 & \text{N even} \\ -\frac{N-1}{2}, \ldots, 0, \ldots, \frac{N-1}{2} & \text{N odd} \end{cases}$$

and the eigenvectors, which can be chosen to be real and orthogonal, are

$$\Phi_{qj} = \begin{cases} \sqrt{\frac{2}{N}} \sin qj & q > 0 \\ \sqrt{\frac{2}{N}} \cos qj & q \leq 0 \end{cases} \tag{5.31}$$

The second set of vectors Ψ_q can now be obtained from equation (5.27a). The left hand side gives for $q > 0$

$$\begin{aligned} \Phi_{qj}(A-B)_{jn} &= \sqrt{\frac{2}{N}} (\sin q, \sin 2q, \cdots, \sin Nq) \begin{pmatrix} h & \cdot & \cdot & 1 \\ 1 & h & \cdot & \cdot \\ \cdot & \ddots & \ddots & \cdot \\ \cdot & \cdot & 1 & h \end{pmatrix} \\ &= \sqrt{\frac{2}{N}} (\cdots, h\sin nq + \sin(n+1)q, \cdots) \\ &= \sqrt{\frac{2}{N}} (\cdots, (h + \cos q)\sin nq + \sin q \cos(-nq), \cdots) \end{aligned}$$

Similar one can calculate Ψ_q for $q \leq 0$ which leads to

$$\Psi_{qj} = \sqrt{\frac{2}{N}} (\cdots, (h + \cos q)\cos(nq) + \sin q \sin(-nq), \cdots)$$

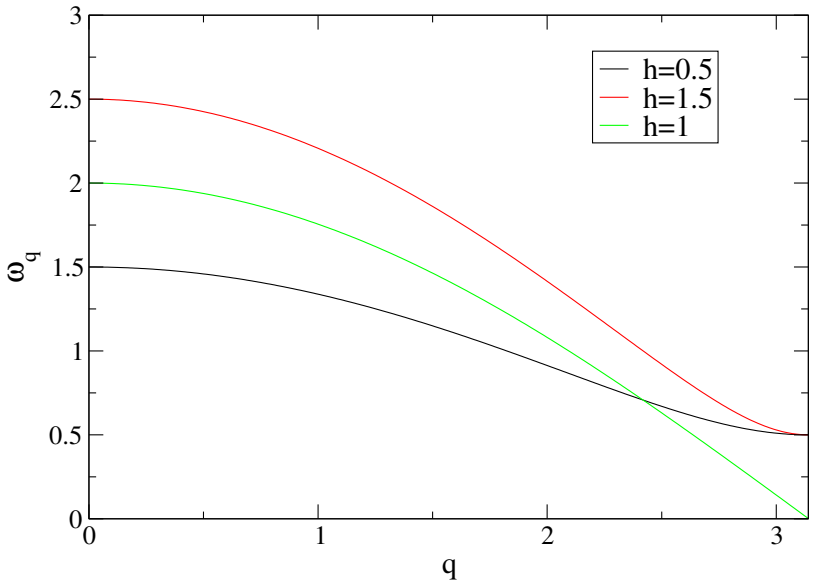

Figure 5.7: Elementary excitation energy as function of momentum q for different h.

Adding the two parts of the vector Ψ_q one can write

$$\Psi_{qj} = \frac{1}{\omega_q}\left[(h + \cos q)\Phi_{qj} + \sin q\, \Phi_{-qj}\right] \tag{5.32}$$

In conclusion we diagonalised the original Hamiltonian (5.3) which reads in its diagonalised form as

$$\mathcal{H} = V_b \sum_q \omega_q \eta_q^\dagger \eta_q + \text{const.} \tag{5.33}$$

where the one-fermion energies are given by

$$\omega_q = \sqrt{1 + h^2 + 2h\cos q} \tag{5.34}$$

The energy of elementary excitations is shown in figure 5.7. As one can see there is a energy gap in the spectrum that goes to zero at $q = \pi$ for $h = h_c = 1$ as $\Delta(h) = V_b|1 - h| = |2t_a - V_b|$.

5.3.5 Magnetization and Kinetic Energy

In order to apply the f-sum rule (2.17) we calculate now the kinetic energy of the system. In the formulation of the IMTF the kinetic part of the Hamil-

tonian is

$$\mathcal{H}_{kin} = -2t_a \sum_l T_l^x = -V_b h \sum_l T_l^z, \tag{5.35}$$

where we have again introduced the parameter $h = 2t_a/V_b$ and additionally we rotated the coordinate system as in section 5.3.1. One can see that one gets the kinetic energy by calculating the transverse magnetization of the IMTF

$$E_{kin} = \frac{1}{N}\langle \mathcal{H}_{kin} \rangle_\beta = -hV_b M^z \tag{5.36}$$

where we have defined the magnetization as

$$M^z = \left\langle \frac{1}{N} \sum_l T_l^z \right\rangle_\beta \tag{5.37}$$

and $\langle \cdot \rangle_\beta$ means the thermodynamic expectation value. We use again the Jordan-Wigner transformation (5.15) to express this term in fermion operators

$$\begin{aligned} M^z &= \left\langle \frac{1}{N} \sum_l T_l^z \right\rangle_\beta = \frac{1}{N} \sum_l \langle T_l^z \rangle_\beta = \\ &= \frac{1}{N} \sum_l \left\langle c_l^\dagger c_l - \frac{1}{2} \right\rangle_\beta = \frac{1}{2N} \sum_l \left\langle \left(c_l^\dagger - c_l \right) \left(c_l^\dagger + c_l \right) \right\rangle_\beta \end{aligned} \tag{5.38}$$

In order to evaluate this expectation value we apply the inverse Bogoliubov transformation (5.25) to get an expression written by the fermion operators $\eta_q^\dagger$ and η_q, because for this representation we know already the one fermion energies ω_q. We express the g_{qj} and h_{qj} by the vectors Φ_{qj} and Ψ_{qj}. Because of the orthogonality of these vectors the inverse transformation is simply given by

$$c_l^\dagger = \sum_q \frac{(\Phi_{qj} + \Psi_{qj})}{2} \eta_q^\dagger + \sum_q \frac{(\Phi_{qj} - \Psi_{qj})}{2} \eta_q \tag{5.39a}$$

$$c_l = \sum_q \frac{(\Phi_{qj} - \Psi_{qj})}{2} \eta_q^\dagger + \sum_q \frac{(\Phi_{qj} + \Psi_{qj})}{2} \eta_q \tag{5.39b}$$

Using this inverse transformation in (5.38) we get

$$\begin{aligned} M^z &= \frac{1}{2N}\sum_l \left\langle \sum_{qq'} \Psi_{ql}\Phi_{q'l}\left(\eta_q^\dagger - \eta_q\right)\left(\eta_{q'}^\dagger + \eta_{q'}\right)\right\rangle_\beta \\ &= \frac{1}{2N}\sum_l \sum_{qq'} \Psi_{ql}\Phi_{q'l}\left\langle \left(\eta_q^\dagger - \eta_q\right)\left(\eta_{q'}^\dagger + \eta_{q'}\right)\right\rangle_\beta \\ &= \frac{1}{2N}\sum_l \sum_{q} \Psi_{qj}\Phi_{qj}\left(\left\langle \eta_q^\dagger\eta_q\right\rangle_\beta - \left\langle \eta_q\eta_q^\dagger\right\rangle_\beta\right) \end{aligned}$$

The expectation values in this formula can now be calculated directly using the well known fermion distribution function of statistical physics

$$\begin{aligned} \left\langle \eta_q^\dagger\eta_q\right\rangle_\beta - \left\langle \eta_q\eta_q^\dagger\right\rangle_\beta &= \left\langle \eta_q^\dagger\eta_q\right\rangle_\beta - \left\langle 1 - \eta_q^\dagger\eta_q\right\rangle_\beta \\ &= 2\left\langle \eta_q^\dagger\eta_q\right\rangle_\beta - 1 \\ &= 2\left(e^{\beta V_b\omega_q}+1\right)^{-1} - 1 \\ &= -\tanh\left(\frac{1}{2}\beta V_b\omega_q\right) \end{aligned}$$

This is a quite simple equation which contains all the temperature dependence of the system. All other terms, that have to be calculated in the sequel, are temperature independent. Thus we can write for the thermodynamic expectation value of the magnetization

$$M^z = -\frac{1}{2N}\sum_{l,q}\Psi_{ql}\Phi_{ql}\tanh\left(\frac{1}{2}\beta V_b\omega_q\right) \tag{5.40}$$

To evaluate the sum over the momentums q we assume that our system is very large and we can therefore replace the sum by an integral over q

$$\frac{1}{N}\sum_q \quad\longrightarrow\quad \frac{1}{2\pi}\int_{-\pi}^{\pi} dq$$

In order to insert the expression for Φ_{ql} (5.31) and Ψ_{ql} (5.32) we split the interval of integration $[-\pi,\pi]$ into the intervals $[-\pi,0)$ and $[0,\pi]$. The resulting expression is independent of l and the sum over l is equal to N. In the end we find for the magnetization

$$M^z = -\frac{1}{2\pi}\int_0^\pi dq\frac{h+\cos q}{\omega_q}\tanh\left(\frac{1}{2}\beta V_b\omega_q\right) \tag{5.41}$$

From equation (5.36) we get with equation (5.41) for the expectation value of the kinetic energy

$$E_{kin} = V_b \frac{h}{2\pi} \int_0^{\pi} dq \frac{h + \cos q}{\omega_q} \tanh\left(\frac{1}{2}\beta V_b \omega_q\right) \tag{5.42}$$

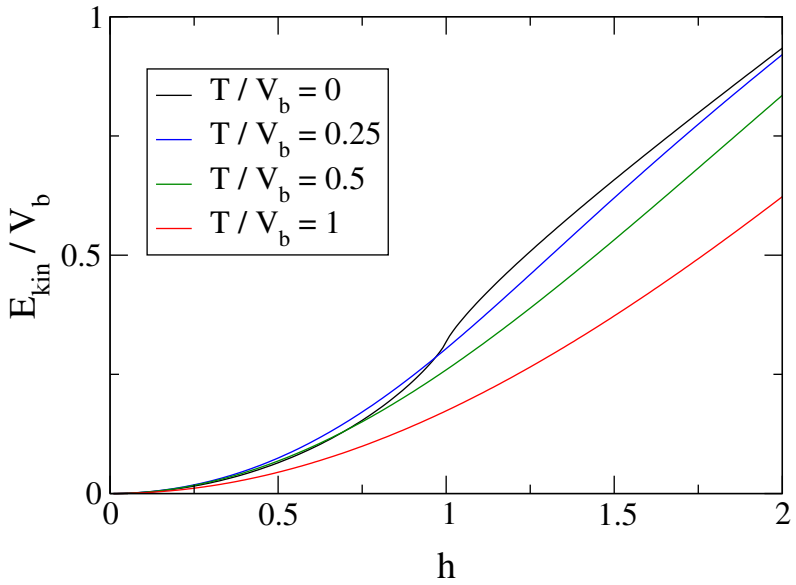

Figure 5.8: Kinetic energy as function of parameter $h = 2t_a/V_b$ for different temperatures.

Figure 5.9 shows the temperature dependence of the kinetic energy from equation (5.42). Obviously, the temperature dependence of E_{kin} is dictated by the coulomb interaction V_b, provided $t_a \not\gg V_b$, or in other words, $h \not\gg 1$. If h increases the argument of the hyperbolic tangent in equation (5.42) becomes $\frac{1}{2}\beta V_b \omega_q \approx \frac{1}{2}\beta(2t_a)$, which shows that for $h \gg 1$ the relevant energy scale is twice the hopping matrix element within a rung t_a. In the high temperature limit ($\beta \ll 1$) one can approximate the hyperbolic tangent by its argument. The integration can now be done analytically and one finds $E_{kin} \sim h/T$.

There is one peculiar behavior of the kinetic energy which should be mentioned. For $h < 1$ the transverse magnetization and therefore the kinetic energy is not strictly monotonic. One possible explanation is that for $h < 1$ the leading term in the Hamiltonian is the interaction term and not the transverse field. Therefore at low temperature there are rather large z-correlations.

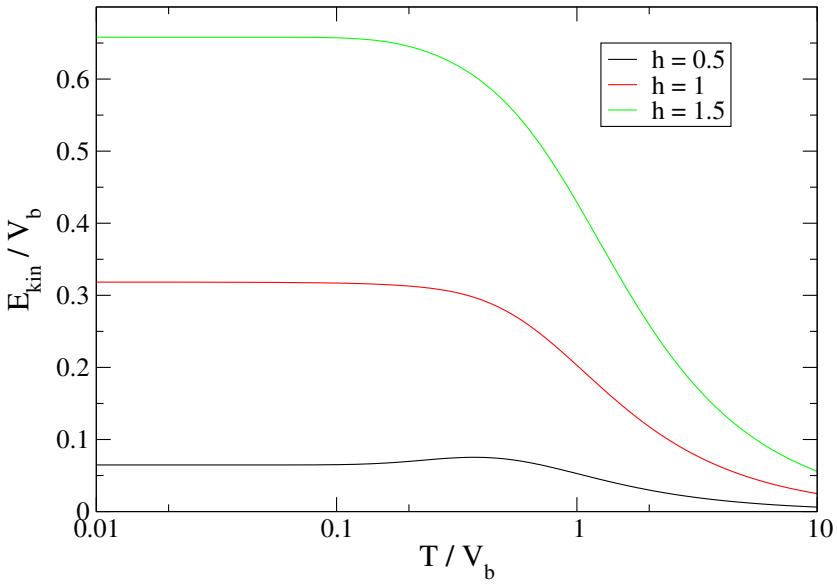

Figure 5.9: Kinetic energy as function of temperature for different values of h.

When temperature increases this correlations get weaker and weaker and the transverse field can produce more correlation in x-direction. At high temperature the magnetization drops again, as it should. For larger h the leading term in the Hamiltonian is already the transverse field, which means that it cannot profit of the weaker z-correlations when temperature increases.

Let us now compare our results from the IMTF and the results obtained by the numerical calculations for the t-J-V model (see section 5.2). We have to compare one of the red curves for $t_b = 0.2$ in figure 5.5 and the red curve for $h = 1$ in figure 5.9. If the assumption of Presura is correct and the decrease of spectral weight with characteristic energy of about 30 meV is driven by charge excitations then the two curves should show at least qualitatively the same temperature behavior, because the IMTF represents the charge degrees of freedom of the system. When considering very high temperatures above 0.3 eV, which actually cannot be investigated experimentally, we find almost the same behavior. There is a huge decrease of the spectral weight starting at about 0.4 eV both in the IMTF and in the results from exact diagonalisation. But the decrease of the integrated optical conductivity in figure 5.5 starting at about 0.03 eV cannot be found in the analytical result of the IMTF in figure 5.9. Therefore we concluded that the low energy charge excitations of the IMTF at the boundary of the Brioullin zone have nothing to do with the decrease of the spectral weight with characteristic energy of about 30 meV,

as Presura argued. Obviously the reason is, that this low energy excitations cannot couple directly to the optical conductivity because of the different values of momentum vector **q**. In the end we can say that charge degrees of freedom alone cannot describe the behavior of the IOC properly.

5.3.6 Correlation Functions

In order to investigate the electronic structure of the ladder system we are going to calculate the correlation functions for the pseudo-spin operator T_i^z. If this correlations are mainly antiferromagnetic then the groundstate is zig-zag ordered. Because we have rotated our coordinate system we have to calculate the correlation function

$$C_{ij}^x = \langle T_i^x T_j^x \rangle_\beta, \tag{5.43}$$

where $\langle \cdot \rangle_\beta$ again denotes the thermodynamic expectation value. Inserting the ladder operators (5.6) one can write

$$C_{ij}^x = \frac{1}{4} \left\langle \left(T_i^+ + T_i^-\right) \left(T_j^+ + T_j^-\right) \right\rangle_\beta$$

In terms of Jordan-Wigner fermions this expression can be rewritten as

$$C_{ij}^x = \frac{1}{4} \left\langle \left(c_i^\dagger + c_i\right) \exp\left(-i\pi \sum_{l=i}^{j-1} c_l^\dagger c_l\right) \left(c_j^\dagger + c_j\right) \right\rangle_\beta ,$$

provided $i < j$. The exponential function can be evaluated using a representation where $c_i^\dagger c_i$ is diagonal, because in this representation one can verify that

$$\exp\left(-i\pi c_l^\dagger c_l\right) = (c_l^\dagger + c_l)(c_l^\dagger - c_l)$$

Using this identity the correlation function reads as

$$C_{ij}^x = \frac{1}{4} \left\langle (c_i^\dagger + c_i)(c_i^\dagger + c_i)(c_i^\dagger - c_i)(c_{i+1}^\dagger + c_{i+1}) \cdots (c_{j-1}^\dagger - c_{j-1})(c_j^\dagger + c_j) \right\rangle_\beta$$

We define now the abbreviations $A_i = c_i^\dagger + c_i$ and $B_i = c_i^\dagger - c_i$. It is easy to check that $A_i^2 = 1$ holds. Therefore we get for the correlation function

$$C_{ij}^x = \frac{1}{4} \langle B_i A_{i+1} B_{i+1} \cdots B_{j-1} A_j \rangle_\beta$$

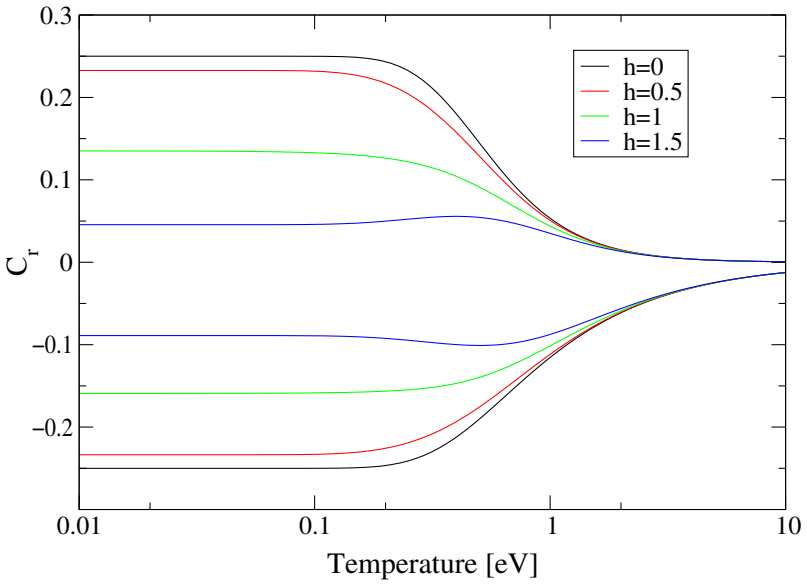

Figure 5.10: Temperature dependence of the longitudinal correlation function of the IMTF given by equation (5.44). Negative curves are for $r = 1$, positive for $r = 2$.

This complicated expression can be simplified using Wick's theorem. We first calculate the contractions

$$\langle A_i A_j \rangle_\beta = \langle \delta_{ij} - c_j^\dagger c_i + c_i^\dagger c_j \rangle_\beta = \delta_{ij}$$
$$\langle B_i B_j \rangle_\beta = \langle -\delta_{ij} + c_j^\dagger c_i - c_i^\dagger c_j \rangle_\beta = -\delta_{ij}$$

Because these two contraction are always equal to zero provided $i \neq j$ the only contractions which contribute are $\langle B_i A_j \rangle_\beta$ and $\langle A_j B_i \rangle_\beta$. Defining now $G_{j-i} := \langle B_i A_j \rangle_\beta = -\langle A_j B_i \rangle_\beta$ one can write the correlation function as determinant of the form

$$C^x_{i,i+n} = \frac{1}{4} \det \begin{pmatrix} G_1 & G_0 & \cdots & G_{2-n} \\ G_2 & G_1 & & G_{3-n} \\ \vdots & & \ddots & \vdots \\ G_n & G_{n-1} & \cdots & G_1 \end{pmatrix} \tag{5.44}$$

The contractions G_{j-i} can be calculated using the same method as in section 5.3.5, i.e. applying the inverse Bogoliubov transformation. Denoting the

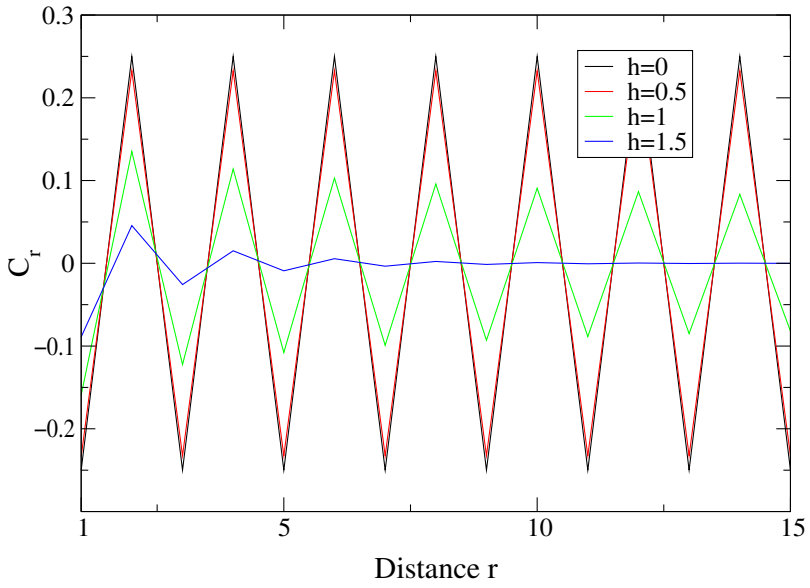

Figure 5.11: Longitudinal correlation function for different transverse fields at $T = 0\,\mathrm{eV}$.

distance between two sites i and j by $r = j - i$ this leads to

$$\begin{aligned} G_r &= \langle B_i A_j \rangle_\beta = \langle (c_i^\dagger - c_i)(c_j^\dagger + c_j) \rangle_\beta \\ &= \cdots = -\sum_q \Psi_{qi} \Phi_{qj} \tanh\left(\frac{1}{2}\beta V_b \omega_q\right) \end{aligned}$$

with Ψ_{qi} and Φ_{qj} from equations (5.32) and (5.31). After replacing the sum by the integral and inserting equations (5.31) and (5.32) we get for the contraction

$$G_r = -\frac{1}{\pi} \int_0^\pi dq \frac{1}{\omega_q} \left[h \cos qr + \cos q(r-1)\right] \tanh\left(\frac{1}{2}\beta V_b \omega_q\right) \tag{5.45}$$

Let us now consider first the pure Ising model, that means $h = 0$. In this case the quasiparticle dispersion relation (5.30) gives $\omega_q \equiv 1$ and the integration in (5.45) can be done analytically. Thus we have

$$\begin{aligned} G_r &= -\frac{1}{\pi} \tanh\left(\frac{1}{2}\beta V_b\right) \int_0^\pi dq \cos q(r-1) \\ &= \begin{cases} -\tanh\left(\frac{1}{2}\beta V_b\right) & r = 1 \\ 0 & r \neq 1 \end{cases} \end{aligned} \tag{5.46}$$

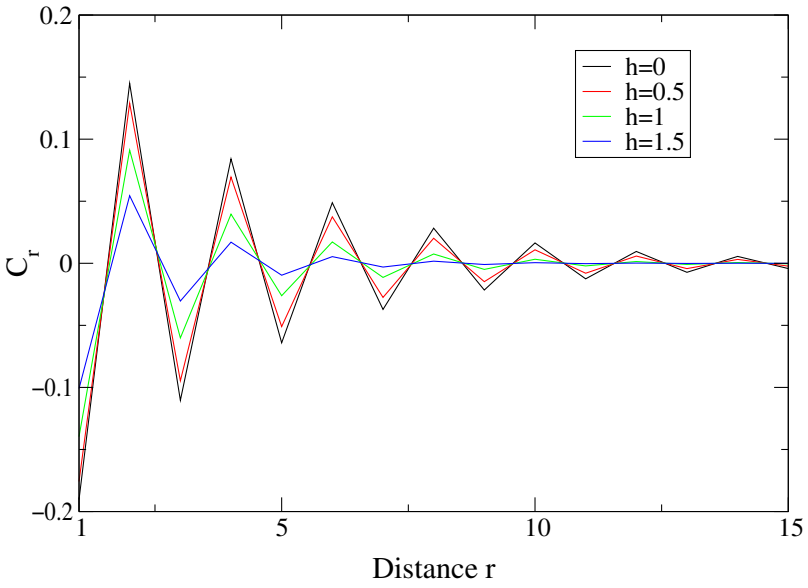

Figure 5.12: Longitudinal correlation function for different transverse fields at $T = 0.5\,\mathrm{eV}$.

This result is quite satisfactory, because all off-diagonal matrix elements in (5.44) are equal to zero and the determinant is therefore simply the product of the diagonal elements, which are actually G_1. The longitudinal correlation function for the pure Ising model ($h = 0$) reads therefore

$$\begin{aligned} C_r^x &= \frac{1}{4}(-1)^r \tanh^r\left(\frac{1}{2}\beta V_b\right) \\ &= \frac{(-1)^r}{4} \exp\left(r \ln\tanh\left(\frac{1}{2}\beta V_b\right)\right) \end{aligned} \tag{5.47}$$

For finite temperature the hyperbolic tangent lies between zero and one and the logarithm is therefore negative. We can now define $\alpha = |\ln\tanh\left(\frac{1}{2}\beta V_b\right)|$ and write

$$C_r^x = \frac{(-1)^n}{4} e^{-r\alpha}$$

This means that the longitudinal correlation is controlled by an exponential decrease and no long range order can be expected in the case of the pure Ising model. At $T = 0$ the situation is different. In this case the hyperbolic tangent is equal to one and therefore we have $\alpha = \infty$, i.e. long range order.

When the transverse field is present ($h > 0$) one has to distinguish whether the system is in the ordered phase ($h < 1$) or in the disordered phase ($h > 1$).

In these two regions one can find for the longitudinal correlation function at $T = 0$ [34]

$$\lim_{r\to\infty} C_r^x = \begin{cases} \frac{1}{4}(1-h^2)^{1/4} & h < 1 \\ 0 & h > 1 \end{cases}$$

indicating the absence of long range order for $h > 1$ and long range order for $h < 1$. The only thing left is the behavior at the transition point $h = 1$. In this case one finds at $T = 0$ [34]

$$C_r^x = \frac{1}{4}\left(\frac{2}{\pi}\right)^r 2^{2r(r-1)}\frac{H(r)^4}{H(2r)}$$

where $H(r) = 1^{r-1}2^{r-2}\cdots(r-1)$. Therefore there is no long range order at $T = 0$ and $h = 1$ as shown in figure 5.11.

At finite temperature there is no long range order, because our model is one-dimensional and there is no phase transition in such models at finite temperature (see figure 5.12).

Let us now discuss the results of these analytical calculations. In figure 5.10 the temperature behavior of the nearest neighbor ($r = 1$) and next nearest neighbor ($r = 2$) pseudo-spin correlation function is shown. In order to compare these results with the numerical results in section 5.2 we need the relation that connects the correlation functions. Let us denote the correlation function of the IMTF by C_r and the correlation function calculated by exact diagonalisation in section 5.2 by $\tilde{C}_{1r}$. If one assumes that there is one single electron on a rung one can derive the very simple relation

$$C_r = \tilde{C}_{1,2r+1} - \frac{1}{4}. \tag{5.48}$$

In other words the nearest neighbor correlation function for $h = 1$ in figure 5.10 should be equal to $\tilde{C}_{13} - \frac{1}{4}$ in figure 5.6, whereas the next nearest neighbor correlation function should be equal to $\tilde{C}_{15} - \frac{1}{4}$. Keeping this relations in mind one can see that figure 5.10 shows the same temperature behavior as figure 5.6, which means zig-zag charge order up to a temperature of about 1 eV and tendency to zero at higher temperatures.

Summarizing our results in the previous two sections one can say that the IMTF gives a quite good description of the charge degrees of freedom of the system. But the experimentally found decrease of the spectral weight with characteristic energy of about 30 meV can not be explained by these charge excitations.

5.4 Influence of Spin Correlations

In the previous section we found that charge degrees cannot explain the decrease of the spectral weight experimentally observed by Presura. By comparing the integrated optical conductivity 5.5 and the spin correlation function in figure 5.6 one can see quite clearly, that the low temperature decrease in the spectral weight is due to the loss of short range antiferromagnetic spin correlation. Thus the characteristic energy for this decrease should be controlled by the magnetic super-exchange parameter J. In order to investigate the influence of spin correlations we use a very simple approach similar to the approach by Horsch and Mack [15]. They explained the insulating behavior of NaV_2O_5 by assuming that the basic elements of this compound are two sites connected by hopping t_a which form a rung. All other hoppings, i.e. hopping along the ladders and between different ladders can be taken as virtual excitations.

5.4.1 Two Rung Model

As mentioned above we use a very simple approach to understand the low temperature behavior of the IOC. Figure 5.6 shows that there are no long range spin correlations but only short ones. Therefore it should be possible to get the main information about these short range spin correlations by considering a very small system. Horsch and Mack treated the problem by second order perturbation theory but without coulomb interactions. For our purpose this ansatz is not very useful because we want to calculate the optical conductivity, for which we need to know all eigenstates and eigenenergies of the system.

As Hamiltonian we use the t-U-V model, but we do not include doubly occupied states in our calculation, because the system is at quarter filling and the magnetism is therefore controlled by the nearest neighbor coulomb interaction. We also neglect interladder couplings t_{xy} and V_{xy}. It should now be possible to separate a singlet and a triplet channel in our two rung system, whose energy splitting E_{st} gives the magnetic super exchange constant J. In figure 5.13 the possible states in our two rung model are shown. The second and third row results from the first row by hopping due to t_a and t_b, resp.

We define now bonding/anti-bonding operators, that create one electron in

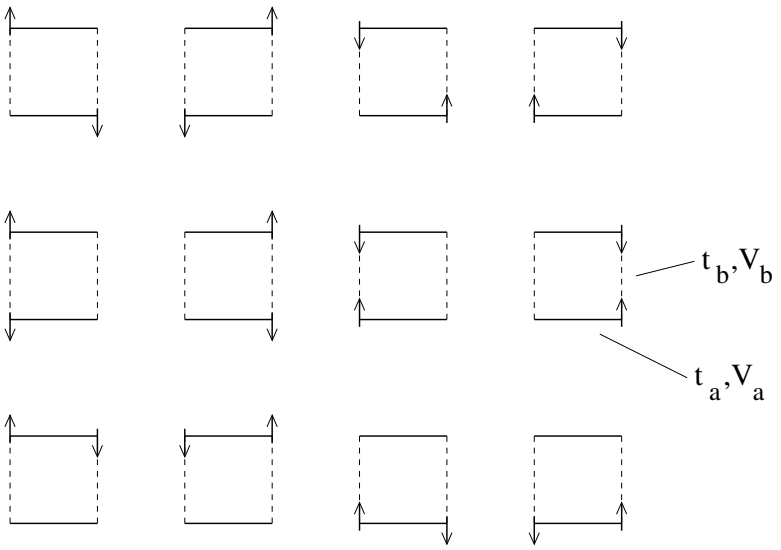

Figure 5.13: Possible two electron states with $S_z = 0$ in our two rung model. Doubly occupied states are not taken into account. Up and down arrows indicate spin up and spin down electrons, resp.

a bonding/anti-bonding orbital on a rung.

$$b^\dagger_{i\sigma} = \frac{1}{\sqrt{2}}(c^\dagger_{il\sigma} + c^\dagger_{ir\sigma}) \qquad \text{bonding operator} \tag{5.49a}$$

$$a^\dagger_{i\sigma} = \frac{1}{\sqrt{2}}(c^\dagger_{il\sigma} - c^\dagger_{ir\sigma}) \qquad \text{anti-bonding operator} \tag{5.49b}$$

The index i denotes the rung, l and r denotes the left and right position in the rung, resp. Using this definition one can define an operator, which creates a singlet state of the two electrons on different rungs by

$$D^\dagger_S = \frac{1}{\sqrt{2}}(b^\dagger_{i\uparrow} b^\dagger_{j\downarrow} - b^\dagger_{i\downarrow} b^\dagger_{j\uparrow})$$

Inserting the definition (5.49a) and expanding the brackets one gets

$$\begin{aligned} D^\dagger_S = \frac{1}{2\sqrt{2}}(&c^\dagger_{il\uparrow} c^\dagger_{jl\downarrow} + c^\dagger_{ir\uparrow} c^\dagger_{jr\downarrow} - c^\dagger_{il\downarrow} c^\dagger_{jl\uparrow} - c^\dagger_{ir\downarrow} c^\dagger_{jr\uparrow} \\ &+ c^\dagger_{il\uparrow} c^\dagger_{jr\downarrow} + c^\dagger_{ir\uparrow} c^\dagger_{jl\downarrow} - c^\dagger_{il\downarrow} c^\dagger_{jr\uparrow} - c^\dagger_{ir\downarrow} c^\dagger_{jl\uparrow}) \end{aligned} \tag{5.50}$$

For the further calculation it is convenient to split the above equation into two parts, in other words we split the operator $D^\dagger_S$ into two new singlet operators

$S^\dagger_{++1}$ and $S^\dagger_{++2}$, where $S^\dagger_{++1}$ is given by the second row and $S^\dagger_{++2}$ by the first row of above equation. The indices $(++1)$ can be understood as follows: The first plus sign indicates, that this operator creates a state with even parity in a direction, whereas the second one indicates even parity in b direction. The additional numbers 1 and 2 enumerates the creation operators. One can easily see that the operator $S^\dagger_{++1}$ is a linear combination of the states in the first row of figure 5.13, whereas $S^\dagger_{++2}$ is a linear combination of the states in the second row. These two new operators create zig-zag ($S^\dagger_{++1}$) and inline charge order ($S^\dagger_{++2}$), resp. Motivated by the definition of these two symmetrized states we define a third state with parity $(++)$ as linear combination of the states in the third row of figure 5.13. It is given by

$$S^\dagger_{++3} = \frac{1}{2}(c^\dagger_{il\uparrow}c^\dagger_{ir\downarrow} + c^\dagger_{jl\uparrow}c^\dagger_{jr\downarrow} - c^\dagger_{il\downarrow}c^\dagger_{ir\uparrow} - c^\dagger_{jl\downarrow}c^\dagger_{jr\uparrow}).$$

So far we have considered only states with parity $(++)$. In order to expand the full Hilbert space, that is of dimension 12, we have to define additional three singlet states. We choose again linear combinations of the states in the rows of figure 5.13, but now with parities $(--)$, $(-+)$ and $(+-)$. The corresponding singlet creation operators are $S^\dagger_{--}$, $S^\dagger_{-+}$ and $S^\dagger_{+-}$. An additional index that enumerates the operators is in this case not necessary, because we have only one operator per parity.

So far we have only taken into account singlet states. The same considerations as above can be done starting with the operator

$$D^\dagger_T = \frac{1}{\sqrt{2}}(b^\dagger_{i\uparrow}b^\dagger_{j\downarrow} + b^\dagger_{i\downarrow}b^\dagger_{j\uparrow}),$$

which creates a triplet state of two electrons on different rungs. One difference between singlet and triplet states is that there is no triplet state with parity $(++)$ because of the Pauli principle. Thus we get the symmetrized triplet creation operators $T^\dagger_{+-1}$, $T^\dagger_{+-2}$, $T^\dagger_{-+1}$, $T^\dagger_{-+2}$, $T^\dagger_{--1}$, $T^\dagger_{--2}$. Summing up we got 12 symmetrized states, 6 in the singlet channel and 6 in the triplet channel. These states are given in table 5.1. It is easy to check that all these states are orthonormal. The Hamiltonian that we have to diagonalise is given by

$$\begin{aligned}\mathcal{H} = &- t_a \sum_{\beta\sigma}(c^\dagger_{\beta l\sigma}c_{\beta r\sigma} + \text{h.c.}) - t_b \sum_{\alpha\sigma}(c^\dagger_{i\alpha\sigma}c_{j\alpha\sigma} + \text{h.c.}) \\ &+ V_a \sum_\beta n_{\beta l}n_{\beta r} + V_b \sum_\alpha n_{i\alpha}n_{j\alpha} \end{aligned} \tag{5.51}$$

Because of the introduction of symmetrized states the Hamilton matrix decouples into several blocks and the diagonalisation can be done analytically

Table 5.1: Symmetrized creation operators in the two rung problem.

$$
\begin{aligned}
S^\dagger_{++1} &= \tfrac{1}{2}(c^\dagger_{il\uparrow}c^\dagger_{jr\downarrow} + c^\dagger_{ir\uparrow}c^\dagger_{jl\downarrow} - c^\dagger_{il\downarrow}c^\dagger_{jr\uparrow} - c^\dagger_{ir\downarrow}c^\dagger_{jl\uparrow}) \\
S^\dagger_{++2} &= \tfrac{1}{2}(c^\dagger_{il\uparrow}c^\dagger_{jl\downarrow} + c^\dagger_{ir\uparrow}c^\dagger_{jr\downarrow} - c^\dagger_{il\downarrow}c^\dagger_{jl\uparrow} - c^\dagger_{ir\downarrow}c^\dagger_{jr\uparrow}) \\
S^\dagger_{++3} &= \tfrac{1}{2}(c^\dagger_{il\uparrow}c^\dagger_{ir\downarrow} + c^\dagger_{jl\uparrow}c^\dagger_{jr\downarrow} - c^\dagger_{il\downarrow}c^\dagger_{ir\uparrow} - c^\dagger_{jl\downarrow}c^\dagger_{jr\uparrow}) \\
S^\dagger_{--} &= \tfrac{1}{2}(c^\dagger_{il\uparrow}c^\dagger_{jr\downarrow} - c^\dagger_{ir\uparrow}c^\dagger_{jl\downarrow} - c^\dagger_{il\downarrow}c^\dagger_{jr\uparrow} + c^\dagger_{ir\downarrow}c^\dagger_{jl\uparrow}) \\
S^\dagger_{-+} &= \tfrac{1}{2}(c^\dagger_{il\uparrow}c^\dagger_{jl\downarrow} - c^\dagger_{ir\uparrow}c^\dagger_{jr\downarrow} - c^\dagger_{il\downarrow}c^\dagger_{jl\uparrow} + c^\dagger_{ir\downarrow}c^\dagger_{jr\uparrow}) \\
S^\dagger_{+-} &= \tfrac{1}{2}(c^\dagger_{il\uparrow}c^\dagger_{ir\downarrow} - c^\dagger_{jl\uparrow}c^\dagger_{jr\downarrow} - c^\dagger_{il\downarrow}c^\dagger_{ir\uparrow} + c^\dagger_{jl\downarrow}c^\dagger_{jr\uparrow}) \\
T^\dagger_{+-1} &= \tfrac{1}{2}(c^\dagger_{il\uparrow}c^\dagger_{jr\downarrow} + c^\dagger_{ir\uparrow}c^\dagger_{jl\downarrow} + c^\dagger_{il\downarrow}c^\dagger_{jr\uparrow} + c^\dagger_{ir\downarrow}c^\dagger_{jl\uparrow}) \\
T^\dagger_{+-2} &= \tfrac{1}{2}(c^\dagger_{il\uparrow}c^\dagger_{jl\downarrow} + c^\dagger_{ir\uparrow}c^\dagger_{jr\downarrow} + c^\dagger_{il\downarrow}c^\dagger_{jl\uparrow} + c^\dagger_{ir\downarrow}c^\dagger_{jr\uparrow}) \\
T^\dagger_{-+1} &= \tfrac{1}{2}(c^\dagger_{il\uparrow}c^\dagger_{ir\downarrow} + c^\dagger_{jl\uparrow}c^\dagger_{jr\downarrow} + c^\dagger_{il\downarrow}c^\dagger_{ir\uparrow} + c^\dagger_{jl\downarrow}c^\dagger_{jr\uparrow}) \\
T^\dagger_{-+2} &= \tfrac{1}{2}(c^\dagger_{il\uparrow}c^\dagger_{jr\downarrow} - c^\dagger_{ir\uparrow}c^\dagger_{jl\downarrow} + c^\dagger_{il\downarrow}c^\dagger_{jr\uparrow} - c^\dagger_{ir\downarrow}c^\dagger_{jl\uparrow}) \\
T^\dagger_{--1} &= \tfrac{1}{2}(c^\dagger_{il\uparrow}c^\dagger_{jl\downarrow} - c^\dagger_{ir\uparrow}c^\dagger_{jr\downarrow} + c^\dagger_{il\downarrow}c^\dagger_{jl\uparrow} - c^\dagger_{ir\downarrow}c^\dagger_{jr\uparrow}) \\
T^\dagger_{--2} &= \tfrac{1}{2}(c^\dagger_{il\uparrow}c^\dagger_{ir\downarrow} - c^\dagger_{jl\uparrow}c^\dagger_{jr\downarrow} + c^\dagger_{il\downarrow}c^\dagger_{ir\uparrow} - c^\dagger_{jl\downarrow}c^\dagger_{jr\uparrow})
\end{aligned}
$$

except of one case. We define the basis states of our Hilbert space for singlet and triplet channel in the following order:

$$
\begin{aligned}
\{|\phi^S_i\rangle\} &= \left\{S^\dagger_{++1}|0\rangle, S^\dagger_{++2}|0\rangle, S^\dagger_{++3}|0\rangle, S^\dagger_{--}|0\rangle, S^\dagger_{-+}|0\rangle, S^\dagger_{+-}|0\rangle\right\} \\
\{|\phi^T_i\rangle\} &= \left\{T^\dagger_{+-1}|0\rangle, T^\dagger_{+-2}|0\rangle, T^\dagger_{-+1}|0\rangle, T^\dagger_{-+2}|0\rangle, T^\dagger_{--1}|0\rangle, T^\dagger_{--2}|0\rangle\right\}
\end{aligned}
$$

With this basis we can calculate the matrix elements very easily, because there is hardly any mixing of states. In the singlet channel the Hamilton matrix is given by

$$
\mathcal{H}_S = \begin{pmatrix}
0 & -2t_a & -2t_b & 0 & 0 & 0 \\
-2t_a & V_b & 0 & 0 & 0 & 0 \\
-2t_b & 0 & V_a & 0 & 0 & 0 \\
0 & 0 & 0 & 0 & 0 & 0 \\
0 & 0 & 0 & 0 & V_b & 0 \\
0 & 0 & 0 & 0 & 0 & V_a
\end{pmatrix} \tag{5.52}
$$

One can see that this matrix has a 3×3 block, whereas all other matrix elements are diagonal elements and therefore eigenvalues of the Hamiltonian.

The diagonalisation of this 3×3 block can be done analytically, but it is not possible to give a simple equation for the eigenvalues. In the triplet channel the situation is a bit different. The Hamilton matrix is given by

$$\mathcal{H}_T = \begin{pmatrix} 0 & -2t_a & 0 & 0 & 0 & 0 \\ -2t_a & V_b & 0 & 0 & 0 & 0 \\ 0 & 0 & V_a & -2t_b & 0 & 0 \\ 0 & 0 & -2t_b & 0 & 0 & 0 \\ 0 & 0 & 0 & 0 & V_b & 0 \\ 0 & 0 & 0 & 0 & 0 & V_a \end{pmatrix} \tag{5.53}$$

In this case we have two blocks of dimension 2×2 which can be diagonalised analytically very easily, and two diagonal elements that are already eigenvalues of the Hamiltonian. We derived this Hamiltonian for the triplet channel in the case $S_z = 0$, in other words for one spin up and one spin down electron. If we start with $S_z = 1$, i.e. two spin up electrons, and define the symmetrized states in the same order of parity as in the case $S_z = 0$ we get the same Hamilton matrix for the triplet channel. Thus it is possible to do all calculations with $S_z = 0$ and multiply the triplet channel by 3 in order to take account of the threefold degeneracy of the triplet channel. One can see from equations (5.52) and (5.53) that the Hamiltonian conserves the parity of the states. Except of the block with $(++)$ parity in the singlet channel we can give analytic expressions for the eigenvalues:

$$E^S_{++} = EV \begin{pmatrix} 0 & -2t_a & -2t_b \\ -2t_a & V_b & 0 \\ -2t_b & 0 & V_a \end{pmatrix} \tag{5.54a}$$

$$E^S_{--} = 0 \tag{5.54b}$$

$$E^S_{-+} = V_b \tag{5.54c}$$

$$E^S_{+-} = V_a \tag{5.54d}$$

$$E^T_{+-} = \frac{1}{2}\left(V_b \pm \sqrt{16t_a^2 + V_b^2}\right) \tag{5.54e}$$

$$E^T_{-+} = \frac{1}{2}\left(V_a \pm \sqrt{16t_b^2 + V_a^2}\right) \tag{5.54f}$$

$$E^T_{--1} = V_a \tag{5.54g}$$

$$E^T_{--2} = V_b \tag{5.54h}$$

where $EV(\cdot)$ stands for the calculation of the eigenvalues of the matrix $(\cdot)$ and E^S and E^T are eigenvalues in the singlet and triplet channel, resp. The level system for different parameter values is shown in figure 5.14. Next we want

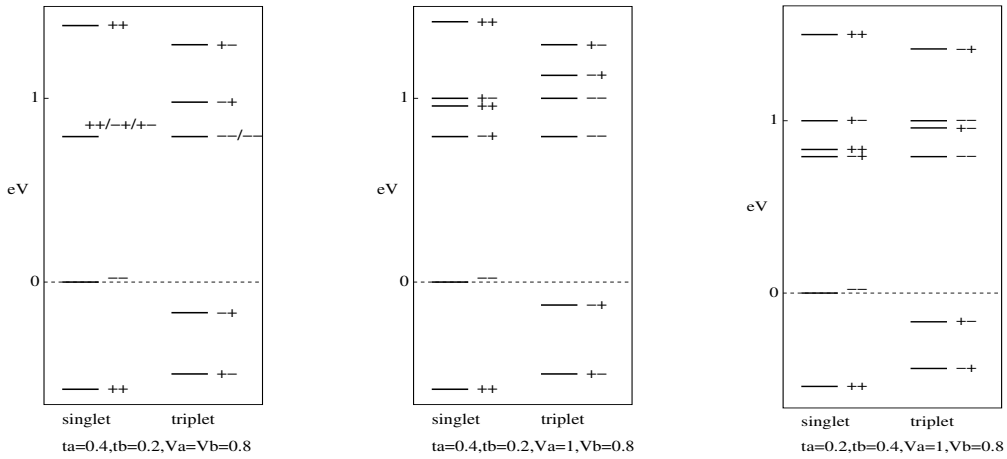

Figure 5.14: Level system of the two rung problem for different parameter values. + and − indicates the parity of the level (see equations (5.54)).

to investigate the singlet-triplet splitting in this two rung cluster. For this purpose we need to know the lowest singlet and triplet state of the system, which are actually given by the lowest eigenvalues of equations (5.54a) and (5.54e), because t_a is greater than t_b. To get an analytical approximation we make the assumption $V_a = V_b = V$ which is in fact not far away from reality because so far we set $V_a = V_b = 0.8$ in this work. Thus we get for the singlet and triplet eigenvalues

$$E^S = \frac{V}{2}\left(1 - \sqrt{\frac{16t_a^2}{V^2} + \frac{16t_b^2}{V^2} + 1}\right) \tag{5.55a}$$

$$E^T = \frac{V}{2}\left(1 - \sqrt{\frac{16t_a^2}{V^2} + 1}\right). \tag{5.55b}$$

Because t_b is a small quantity in our calculations we do a Taylor series expansion around $t_b^2 = 0$ and cut the series after the linear term. Thus the singlet energy reads

$$E^S = \frac{V}{2}\left(1 - \sqrt{\frac{16t_a^2}{V^2} + 1} - \frac{1}{2\sqrt{\frac{16t_a^2}{V^2} + 1}}\frac{16t_b^2}{V^2} + O(t_b^4)\right) \tag{5.56}$$

When calculating the singlet-triplet splitting $E^T - E^S$ one can see that the first two terms of equation (5.56) cancel with equation (5.55b). Therefore we

can write for the singlet-triplet splitting

$$E_{st} := E^T - E^S = \frac{4t_b^2}{V} \frac{1}{\sqrt{\frac{16t_a^2}{V^2} + 1}}. \tag{5.57}$$

Now we replace again the parameter V in the above equation in the following way: In the fraction where t_b occurs we set $V = V_a$ and in the fraction with t_a we set $V = V_b$, because the relevant parameters are $\frac{t_b^2}{V_a}$ and $\frac{t_a^2}{V_b}$, resp. In a next step we expand the formula from the small two rung cluster to a whole ladder. Considering an extended ladder hopping from the left to the right position in the rung (a direction) causes an excitation energy of $2V_b$ and not V_b as in the two rung cluster. Similarly hopping from one rung to the neighboring one (b direction) causes an excitation energy of $V_a + V_b$ and not V_a. Therefore we have to set $V_a \to V_a + V_b$ and $V_b \to 2V_b$ in order to get the correct excitation energies. Finally we get the formula for the singlet-triplet splitting for a single ladder

$$E_{st} = \frac{4t_b^2}{(V_a + V_b)} \frac{1}{\sqrt{\frac{4t_a^2}{V_b^2} + 1}}. \tag{5.58}$$

With parameter values of $t_a = 0.4$, $t_b = 0.2$ and $V_a = V_b = 0.8$ we obtain $E_{st} \approx 70$ meV. As mentioned at the beginning of this section this energy E_{st} is in this small system equal to the magnetic super-exchange constant J. We conjecture that in extended systems the optical excitations are governed by these local singlet-triplet excitation energies.

5.4.2 Optical Conductivity

In our small system we can calculate the optical conductivity analytically. This enables us to determine the relevant states that contribute most. Starting point of the calculation is the spectral representation of the optical conductivity (2.16). After integration over ω we get for the IOC

$$I_\mu(T) = \pi \frac{e^2}{\Omega} \frac{1}{Z} \sum_{n,m} \frac{1 - e^{-\beta(E_m - E_n)}}{E_m - E_n} e^{-\beta E_n} |\langle m|j_\mu|n\rangle|^2. \tag{5.59}$$

For evaluating the IOC we have to calculate the matrix elements $\langle m|j_\mu|n\rangle$, where the current operator is given by equation (2.6). From figure 5.14 one can see, that at low temperatures only the lowest singlet and triplet

level is populated, whereas the thermal population of all other levels can be neglected. These two states are given by

$$|n^S\rangle = \left(k_1^S S_{++1}^\dagger + k_2^S S_{++2}^\dagger + k_3^S S_{++3}^\dagger\right)|0\rangle \tag{5.60a}$$

$$|n^T\rangle = \left(k_1^T T_{+-1}^\dagger + k_2^T T_{+-2}^\dagger\right)|0\rangle, \tag{5.60b}$$

which follows from diagonalisation of the Hamilton matrices (5.52) and (5.53). The energies of these two states are denoted by E^S and E^T. We use now the definition of the symmetrized creation operators in table 5.1 and calculate the matrix elements of the current operator for the relevant initial states $S_{++1}^\dagger|0\rangle$, $S_{++2}^\dagger|0\rangle$, $S_{++3}^\dagger|0\rangle$, $T_{+-1}^\dagger|0\rangle$ and $T_{+-2}^\dagger|0\rangle$. We find that there are only three non zero matrix elements whereas all others vanish, i.e.

$$\langle 0|S_{-+}j_a S_{++1}^\dagger|0\rangle = 2it_a \tag{5.61a}$$

$$\langle 0|T_{--1}j_a T_{+-1}^\dagger|0\rangle = 2it_a \tag{5.61b}$$

$$\langle 0|S_{+-}j_b S_{++1}^\dagger|0\rangle = 2it_b \tag{5.61c}$$

There is one big difference between the conductivity in a and b direction. As one can see from above equations there is a matrix element from the singlet and the triplet channel in a direction, whereas in b direction only the singlet channel contributes. The reason for that can be found by considering the effect of the current operator on the parity of the states. It does not change the total spin, which means that there is no mixing of the singlet and the triplet channel. But the current operator changes the parity of the states in the direction of the current, in other words the operator j_a changes for instance $(++)$ to $(-+)$. When the operator j_a acts now on the lowest lying triplet state with parity $(+-)$ it changes the parity to $(--)$, but in b direction the operator j_b wants to change the parity to $(++)$, which is actually forbidden for a state with total spin $S = 1$. With the matrix elements (5.61) we can now evaluate equation (5.59). Denoting the excitation energy $E_{+-}^S - E^S$ by ΔE^S we get for b direction

$$I_b(T) = \pi \frac{e^2}{\Omega}\frac{1}{Z}\frac{1-e^{-\beta\Delta E^S}}{\Delta E^S} e^{-\beta E^S} 4\left|k_1^S\right|^2 t_b^2,$$

where $|k_1^S|^2$ comes from the initial state $|n^S\rangle$. The partition function Z can be calculated straight forward and yields

$$\begin{aligned} Z &= \sum_n \langle n|e^{-\beta\mathcal{H}}|n\rangle = \langle n^S|e^{-\beta\mathcal{H}}|n^S\rangle + 3\langle n^T|e^{-\beta\mathcal{H}}|n^T\rangle \\ &= e^{-\beta E^S} + 3e^{-\beta E^T} \end{aligned} \tag{5.62}$$

where we inserted the factor 3 due to the threefold degeneracy of the triplet states. With this result the IOC $I_b(T)$ can be written as

$$\begin{aligned} I_b(T) &= \pi 4 \left|k_1^S\right|^2 t_b^2 \frac{e^2}{\Omega} \left[\frac{1-e^{-\beta\Delta E^S}}{\Delta E^S} \frac{e^{-\beta E^S}}{e^{-\beta E^S}+3e^{-\beta E^T}}\right] \\ &= \pi 4 \left|k_1^S\right|^2 t_b^2 \frac{e^2}{\Omega} \left[\frac{1-e^{-\beta\Delta E^S}}{\Delta E^S} \frac{1}{1+3e^{-\beta E_{st}}}\right], \end{aligned} \tag{5.63}$$

with $E_{st} = E^T - E^S$ the singlet triplet splitting. In a direction the sum over the initial states $|n\rangle$ consists of two terms, $|n^S\rangle$ and $|n^T\rangle$. Denoting the triplet excitation energy $E^T_{--} - E^T$ by ΔE^T and using the same definitions as above we get (Z is the same as in b direction)

$$\begin{aligned} I_a(T) = \pi 4 t_a^2 \frac{e^2}{\Omega} \Bigg[&\left|k_1^S\right|^2 \frac{1-e^{-\beta\Delta E^S}}{\Delta E^S} \frac{e^{-\beta E^S}}{e^{-\beta E^S}+3e^{-\beta E^T}} \\ &+ \left|k_1^T\right|^2 \frac{1-e^{-\beta\Delta E^T}}{\Delta E^T} \frac{e^{-\beta E^T}}{e^{-\beta E^S}+3e^{-\beta E^T}}\Bigg] \end{aligned} \tag{5.64}$$

We can now divide the last fraction in the first row by $e^{-\beta E^S}$ and the last fraction in the second row by $e^{-\beta E^T}$. Additionally we set $\kappa = (k_1^T/k_1^S)^2$. Thus we get

$$\begin{aligned} I_a(T) = \pi 4 t_a^2 \left|k_1^S\right|^2 \frac{e^2}{\Omega} \Bigg[&\frac{1-e^{-\beta\Delta E^S}}{\Delta E^S} \frac{1}{1+3e^{-\beta E_{st}}} \\ &+3\kappa \frac{1-e^{-\beta\Delta E^T}}{\Delta E^T} \frac{1}{3+e^{\beta E_{st}}}\Bigg]. \end{aligned} \tag{5.65}$$

The factor 3 in the second row comes again from the threefold degeneracy of the triplet states. By comparing equations (5.63) and (5.65) and can see, that the additional contribution of the triplet states to $\sigma_a(\omega)$ is the reason for the smaller decrease of the IOC that we found in our numerical calculations (see figure 5.5).

The aim of these calculations was to explain the decrease of the IOC at low temperatures found both in experiments and numerical calculations. Assuming that we have no long range spin correlations and the excitations are governed by local singlet triplet excitations we can use equations (5.63) and (5.65) to investigate the extended system. Because we are not interested in the high temperature regime we can do the following approximation. The excitation energies ΔE^S and ΔE^T are at energies of about 1 eV, which is

much larger than the onset of the decrease of the IOC which we are interested in. We argue that for this low temperature decrease the characteristic energy is given by E_{st} which is at energies of about 70 meV. Therefore we set the fractions consisting of terms of $\Delta E^{S/T}$ constant. Moreover we normalize equations (5.63) and (5.65) to one because of convenience. Taking account of all these assumptions we get formulas for the IOC in a and b direction depending only on two parameters E_{st} and κ:

$$\tilde{I}_a(T) = \frac{1}{1+3e^{-\beta E_{st}}} + 3\kappa \frac{1}{3+e^{\beta E_{st}}} \tag{5.66a}$$

$$\tilde{I}_b(T) = \frac{1}{1+3e^{-\beta E_{st}}} \tag{5.66b}$$

with $\tilde{I}_\alpha(T) = I_\alpha(T)/I_\alpha(0)$. We can test the validity of these formulas by fitting our numerical data in the low temperature region of 0 to 0.6 eV by using the parameters E_{st} and κ as fit parameters. The result of this fit is shown in figure 5.15. One can see that there is reasonable agreement of the solid lines with the numerical data for the t-J-V model. For a direction we get $\kappa = 0.54$ and $E_{st} = 76$ meV, and for b direction $E_{st} = 61$ meV. Moreover the value for the singlet-triplet splitting of about 70 meV calculated in the previous section coincides very well with the fitted data.

The final test for our formulas is now the comparison to the experiment. We tried to fit the experimental data of Presura in the temperature region 0 K to 300 K. The results are shown in figure 5.16. The fit for a direction could be done quite easy and lead to a characteristic energy $J \approx 39\,\text{meV}$ and $\kappa = 0.68$. For b direction we had to include another fit parameter in order to have good agreement with the experimental data. For this purpose we replaced the factor 3 in the denominator of equation (5.66b) by a parameter α. With this formula we got $J \approx 34\,\text{meV}$ and $\alpha = 0.6$. This modification could be justified by restricting ourselves to $S_z = 0$, where we havo no degeneracy of the triplet channel. Fitting the data for a direction with formula (5.66a) modified in the same way leads to $J \approx 35\,\text{meV}$, $\kappa = 0.41$ and $\alpha = 1$. The values for the characteristic energy J coincide again very well for both directions and are consistent with other experiments, i.e. $J \approx 48.2$ [11] and $J \approx 37.9\,\text{meV}$ [35, 36]. Considering our formula for the singlet triplet splitting (5.58) one could now argue, that the value for hopping along the ladders t_b should rather be 0.15 like in [15] than 0.2 used in this work.

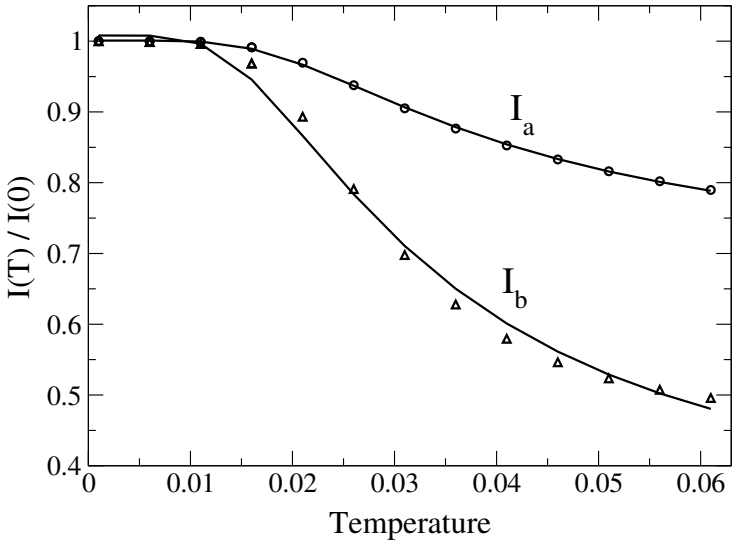

Figure 5.15: IOC in a and b direction. The circles and triangles indicate numerical data (see figure 5.5). Solid lines are fits to the formulas (5.66). Parameters are $t_b = 0.2$ and $t_{xy} = 0.15$.

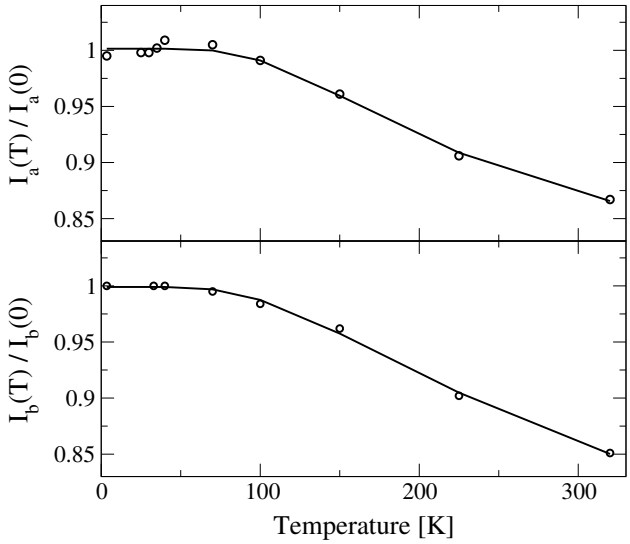

Figure 5.16: Experimental data for the IOC for a and b direction, see figure 5.3. Solid lines are fits to the formulas (5.66).

Chapter 6

Conclusion

The aim of this work was to investigate the charge order and to explain the temperature dependence of the integrated optical conductivity of the low dimensional transition metal oxide α'-NaV_2O_5. For this purpose we applied both analytical and numerical methods.

By mean field calculations we were able to construct a phase diagram, that indicates that the charge order should be rather of zig-zag type and not of inline type. Results from exact diagonalisation in the frame of a t-J-V and a t-U-V model showed tendency to zig-zag charge order, too. In addition we found that α'-NaV_2O_5 is near to the quantum critical point where the transition from zig-zag charge order to disorder takes place. Modifying our model by including diagonal hopping matrix elements yielded very similar results, but the peak in b-direction is considerably smaller than without diagonal hopping. The charge order, however, is not influenced by this modification.

For the temperature dependence we found good agreement between experiment and numerical calculations in the frame of the t-J-V model. In order to explain the behavior of the integrated optical conductivity we studied the effective Ising model in a transverse field, which describes the charge degrees of freedom of the system. Our calculations showed that this model cannot explain the decrease of the spectral weights at low temperature observed in experiments. By investigating the short range spin correlations we could attribute this behavior to the destruction of short range antiferromagnetic spin correlations. Hence the characteristic energy of this decrease is given by the super exchange constant J. In addition we derived a fit formula which enabled us to calculate J from the experimental data for the integrated optical conductivity. This value for J is in good agreement with values obtained by other methods.

Acknowledgements

It is a pleasure to thank the group members of the group of Walter Metzner at the Max Planck Institute for solid state physics in Stuttgart, especially Dr. Peter Horsch. Without him this work would have never been finished. In addition I would like to thank Dr. Wolfgang von der Linden for his support. A special thank goes to Dipl. Ing. Maria Daghofer for her help when my algorithms didn't work. And last but not least I would like to thank my parents, Josef and Marianne Aichhorn, for their encouragement all over the last few years.

Bibliography

[1] M. Aichhorn, P. Horsch, W. von der Linden and M. Cuoco, Phys. Rev. B **65**, 201101R (2002).

[2] G. D. Mahan, *Many-Particle Physics* (Kluwer Academic/Plenum Publishers, New York, 2000), 3rd ed.

[3] W. von der Linden, *Fundamentale Effekte stark korrelierter Vielteilchensysteme*, Lecture notes, Technische Universität Graz, 1999.

[4] A. Hübsch, Ph.D. thesis, Technische Universität Dresden (2001).

[5] D. Baeriswyl, J. Carmelo and A. Luther, Phys. Rev. B **33**, 7247 (1986).

[6] D. Baeriswyl, C. Gros and T. M. Rice, Phys. Rev. B **35**, 8391 (1987).

[7] M. Daghofer, Master's thesis, Technische Universität Graz (2001).

[8] W. von der Linden, *Numerische Behandlung von Vielteilchenproblemen*, Lecture notes, Technische Universität Graz, 2000.

[9] J. Jaklič and P. Prelovšek, Phys. Rev. B **49**, 5065 (1994).

[10] A. Carpy and J. Galy, Acta Crystallogr., Sect. B: Struct. Crystallogr. Cryst. Chem. **31**, 1481 (1975).

[11] M. Isobe and Y. Ueda, J. Phys. Soc. Jpn. **65**, 1178 (1996).

[12] H. G. Schnering et al., Z. Kristallogr. **213**, 246 (1998).

[13] H. Smolinsk et al., Phys. Rev. Lett. **80**, 5164 (1998).

[14] A. Meetsma et al., Acta Crystallogr., Sect. C: Cryst. Struct. Commun. **54**, 1558 (1998).

[15] P. Horsch and F. Mack, Eur. Phys. J. B **5**, 367 (1998).

[16] T. Ohama et al., Phys. Rev. B **59**, 3299 (1998).

[17] J. Lüdecke et al., Phys. Rev. Lett. **82**, 3663 (1999).

[18] H. Sawa et al., cond-mat/0109164.

[19] E. Y. Sherman, M. Fischer, P. Lemmens, P. H. M. van Loodsrecht and G. Güntherodt, Europhys. Lett. **48**, 648 (1999).

[20] M. Fischer et al., Phys. Rev. B **60**, 7284 (1999).

[21] S. Atzkern et al., Phys. Rev. B **63**, 165113 (2001).

[22] R. Valenti, T. Saha-Dasgupta, J.V. Alvarez, K. Požgajčić and C. Gros, cond-mat/0101282.

[23] M. Cuoco, P. Horsch and F. Mack, Phys. Rev. B **60**, R8438 (1999).

[24] M. J. Konstantinović et al., Phys. Rev. B **63**, 121102(R) (2001).

[25] A. Damscelli et al., Phys. Rev. Lett. **81**, 918 (1998).

[26] S. A. Golubchik et al., J. Phys. Soc. Jpn. **66**, 4042 (1997).

[27] C. Presura, D. van der Marel, A. Damscelli and R. K. Kremer, Phys. Rev. B **61**, 15762 (2000).

[28] M. V. Mostovoy and D. I. Khomskii, Solid State Commun. **113**, 159 (2000).

[29] M. V. Mostovoy, J. Knoester and D. I. Khomskii, cond-mat/0009464.

[30] B. K. Chakrabarti, A. Dutta and P. Sen, *Quantum Ising Phases and Transitions in Transverse Ising Models* (Springer Verlag, Berlin Heidelberg, 1996).

[31] E. Lieb, T. Schultz and D. Mattis, Ann. Phys. **16**, 407 (1961).

[32] T. H. Niemeijer, Physica **36**, 377 (1967).

[33] P. Pfeuty, Ann. Phys. **57**, 79 (1970).

[34] B. M. McCoy, Phys. Rev. **173**, 531 (1968).

[35] M. Weiden et al., Z. Phys. B **103**, 1 (1997).

[36] T. Yosihama et al., J. Phys. Soc. Jpn. **67**, 744 (1998).